วัสดุเรืองแสงที่มีไพรีนและคาร์บาโซลสำหรับไดโอดอินทรีย์เปล่งแสง

นาย ตระกูล ค้ำชู

วิทยานิพนธ์นี้เป็นส่วนหนึ่งของการศึกษาตามหลักสูตรปริญญาวิทยาศาสตรมหาบัณฑิต
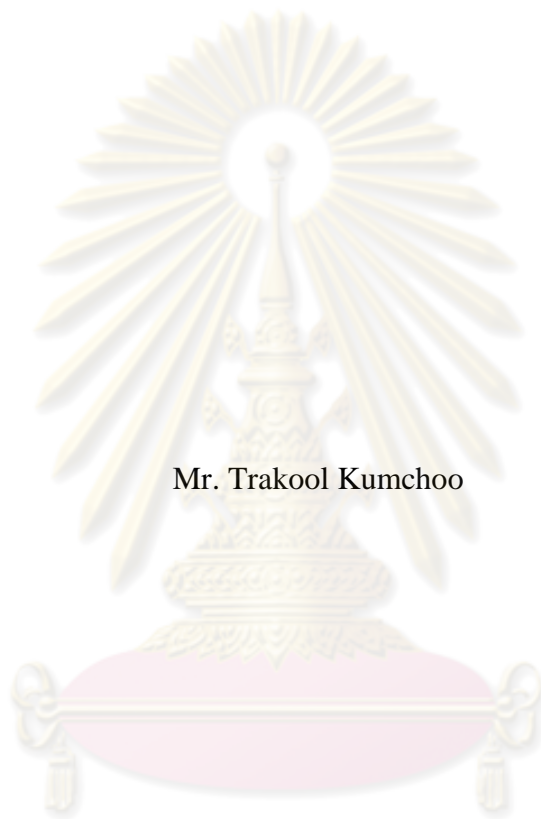สาขาวิชาปิโตรเคมีและวิทยาศาสตร์พอลิเมอร์
คณะวิทยาศาสตร์ จุฬาลงกรณ์มหาวิทยาลัย
ปีการศึกษา 2552
ลิขสิทธิ์ของจุฬาลงกรณ์มหาวิทยาลัย

LUMINESCENT MATERIALS CONTAINING PYRENE AND CARBAZOLE FOR
ORGANIC LIGHT-EMITTING DIODE

Mr. Trakool Kumchoo

A Thesis Submitted in Partial Fulfillment of the Requirements
for the Degree of Master of Science Program in Petrochemistry and Polymer Science
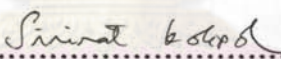Faculty of Science
Chulalongkorn University
Academic Year 2009
Copyright of Chulalongkorn University

Thesis Title	LUMINESCENT MATERIALS CONTAINING PYRENE AND CARBAZOLE FOR ORGANIC LIGHT-EMITTING DIODE
By	Mr. Trakool Kumchoo
Field of Study	Petrochemistry and Polymer Science
Thesis Advisor	Assistant Professor Paitoon Rashatasakhon, Ph.D.
Thesis Co-Advisor	Associate Professor Mongkol Sukwattanasinitt, Ph.D.

Accepted by the Faculty of Science, Chulalongkorn University in Partial Fulfillment of the Requirements for the Master's Degree
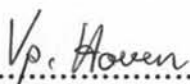
.... Dean of the Faculty of Science

(Professor Supot Hannongbua, Dr.rer.nat)

THESIS COMMITTEE

.... Chairman

(Associate Professor Sirirat Kokpol, Ph.D.)

.... Thesis Advisor

(Assistant Professor Paitoon Rashatasakhon, Ph.D.)

.... Thesis Co-Advisor

(Associate Professor Mongkol Sukwattanasinitt, Ph.D.)

.... Examiner

(Associate Professor Voravee Hoven, Ph.D.)

.... External Examiner

(Pittaya Takolpuckdee, Ph.D.)

ตระกูล ค้ำชู : วัสดุเรืองแสงที่มีไพรีนและคาร์บาโซลสำหรับไดโอดอินทรีย์เปล่งแสง. (LUMINESCENT MATERIALS CONTAINING PYRENE AND CARBAZOLE FOR ORGANIC LIGHT-EMITTING DIODE) อ. ที่ปรึกษาวิทยานิพนธ์หลัก : ผศ. ดร. ไพฑูรย์ รัชตะสาคร, อ. ที่ปรึกษาวิทยานิพนธ์ร่วม : รศ. ดร. มงคล สุขวัฒนาสินิทธิ์, 78 หน้า.

อนุพันธ์ของ 3,6-ไดไพรีนิลคาร์บาโซล จำนวนสามชนิด (2PCT, 4P2C และ 2PCP) ได้ถูก สังเคราะห์และใช้เป็นวัสดุเรืองแสงสีน้ำเงินหรือวัสดุส่งผ่านประจุบวกสำหรับไดโอดอินทรีย์เรือง แสง ในสารละลายเมทิลีนคลอไรด์ หมู่แทนที่แบบ 4-(ไดเฟนิลอะมิโน)เฟนิล จะเพิ่มอิเล็กโทรนิกส์- ไวเบรชั่น คัปปลิงในสถานะกระตุ้น แต่หมู่แทนจะไม่มีผลต่อสมบัติทางกายภาพเชิงแสงในสถานะ ของแข็งแบบฟิล์มบาง หมู่แทนที่จำพวกโทลูอิล และ4-(ไดเฟนิลอะมิโน)เฟนิล สามารถทำให้เกิด อิเล็กโทร-ออกซิเดทีฟ คัปปลิงในสารละลายของ 2PCT หรือ 2PCP อนุพันธ์ทุกชนิดมีความเสถียร ทางความร้อนที่สูงและสามารถใช้เป็นสารเรืองแสงและวัสดุส่งผ่านประจุบวกใน OLED ได้ ซึ่ง 2PCP มีสมบัติด้านออปโทอิเล็กโทรนิกส์ที่ดีโดยมีค่าศักย์ไฟฟ้าเริ่มต้น 3.8 โวลต์ ให้ค่าความสว่าง สูงสุดได้ 1,600 แคนเดลาต่อตารางเมตร ที่ 8.8 โวลต์

สาขาวิชา ปิโตรเคมีและวิทยาศาสตร์พอลิเมอร์	ลายมือชื่อนิสิต
ปีการศึกษา 2552	ลายมือชื่อ อ.ที่ปรึกษาวิทยานิพนธ์หลัก
	ลายมือชื่อ อ.ที่ปรึกษาวิทยานิพนธ์ร่วม

5072276123 : MAJOR PETROCHEMISTRY AND POLYMER SCIENCE

KEYWORDS : PYRENE / CARBAZOLE / OLED

TRAKOOL KUMCHOO : LUMINESCENT MATERIALS CONTAINING PYRENE AND CARBAZOLE FOR ORGANIC LIGHT-EMITTING DIODE. THESIS ADVISOR : ASST. PROF. PAITOON RASHATASAKHON, Ph.D., THESIS CO-ADVISOR : ASSOC. PROF. MONGKOL SUKWATTANASINITT, Ph.D., 78 pp.

Three N-substituted 3,6-dipyrenylcarbazole derivatives (**2PCT**, **4P2C** and **2PCP**) were synthesized and applied as blue light-emitting or hole-transporting materials in organic light-emitting diode (OLED). In CH_2Cl_2 solution, the 4-(diphenylamino)phenyl substituent increases electronic-vibration coupling in the excited state whereas the substituents have no effect on the photophysical properties of the compounds in solid state thin film. Toluyl and 4-(diphenylamino)phenyl substitutents promote electro-oxidative coupling of **2PCT** and **2PCP** in solution. All derivatives show high thermal stability and can be used as both emitting and hole-transporting materials in OLED. **2PCP** exhibits the most promising optoelectronic properties as it gives the highest maximum luminance of 1,600 cd/m^2 at 8.8 V with the lowest turn-on voltage of 3.8 V.

ศูนย์วิทยทรัพยากร
จุฬาลงกรณ์มหาวิทยาลัย

Field of Study : Petrochemistry and Polymer Science   Student's Signature _____

Academic Year : 2009   Advisor's Signature _____

Co-Advisor's Signature _____

ACKNOWLEDGEMENTS

CONTENTS

Page

LIST OF TABLES

LIST OF FIGURES

Page

Page

ศูนย์วิทยทรัพยากร
จุฬาลงกรณ์มหาวิทยาลัย

LIST OF ABBREVIATIONS

A	Ampere
Å	Angstrom
Alq_3	Tris(8-hydroxyquinoline)aluminium
Al	Aluminium
^oC	Degree of celsius
cm^2	Square centimeter
Ca	Calcium
cd	Candela
$CDCl_3$	Dueterated chloroform
CH_2Cl_2	Methylene chloride
CRT	Cathode ray tube
Cu	Copper
CV	Cyclic voltammetry
d	Doublet
dd	Doublet of doublet
DMSO	Dimethyl sulfoxide
DMSO-*d*6	Deuterated dimethyl sulfoxide
DSC	Differential scanning colorimeter
EMMs	Emitting materials
EL	Electroluminescent
EML	Emitting layer
ETL	Electron-transporting layer
EtOAc	Ethyl acetate
eV	Electron volt
g	Gram (s)
h	Hour
HOMO	Highest occupied molecular orbital
HRMS	High resolution mass spectroscopy
H_2SO_4	Sulfuric acid
HTL	Hole-transporting layer

HTMs	Hole-transporting materials
Hz	Hertz
ITO	Indium tin oxide
J	Coupling constant
K_2CO_3	Potassium carbonate
KI	Potassium iodide
KIO_3	Potassium iodate
LCD	Liquid crystal display
LED	Light-emitting diode
lm	Lumen
LiF	Lithium fluoride
LUMO	Lowest unoccupied molecular orbital
Mg	Magnesium
m^2	Square meter
m	Multiplet
mg	Milligram (s)
$MgSO_4$	Magnesium sulfate
min	Minute (s)
mL	Milliliter (s)
mmol	Millimole
M	Molar
MS	Mass spectroscopy
m.p.	Melting point
nm	Nanometer (s)
NMR	Nuclear magnetic resonance
OLED	Organic light-emitting diode
$Pd(PPh_3)_4$	Tetrakis(triphenylphosphine)palladium
ppm	Parts per million
PL	Photoluminescent
s	Singlet
t	Triplet
T_g	Glass transition temperature

TGA	Thermo gravimetric analysis
THF	Tetrahydrofuran
TLC	Thin layer chromatography
V	Volt
W	Watt
%	Percent
δ	Chemical shift
ε	Molar absorptivity
λ	Wavelength
Φ	Fluorescence quantum yield

CHAPTER I
INTRODUCTION

1.1 Introduction

Novel optical devices have recently been developed and improved by advanced technology in order to achieve lightweight and flexible displays with high brightness and excellent resolution. In addition, wide viewing angles, low power consumptions and low manufacturing costs are also desirable qualifications. Conventional cathode ray tube (CRT) displays which are heavy and bulky have been replaced by slimmer and flatter liquid crystal display (LCD). LCD also has some advantages over CRT; for examples, they generally create less eye-strain and light flickering, and most importantly, they consume much lower electrical power. However, LCD technology still has some disadvantages such as the LCD cannot emit light by itself and must be illuminated reflectively or by background light source.

To date, the development of electroluminescent devices has been one of the most active research themes, especially for the organic light-emitting diode (OLED) which have a potential application in full-color flat panel displays. For comparison purposes, pictures of CRT, LCD and OLED displays are shown in **Figure 1.1**.

Figure 1.1 CRT (Top), LCD (bottom-left) and OLED (bottom-right) displays in computer monitors [1].

1.2 Introduction to OLED

OLED is the electrically driven emission of light based on the fluorescent properties of organic material. They have recently received a great deal of attention because of their application for wide range of display applications as well as from the standpoint of scientific interest. They are attractive because of their low driving voltage, high brightness, capability of multicolor emission by the selection of emitting materials and ease in fabrication on large-area and super-thin design.

Organic electroluminescence was first discovered by Pope *et al.* in 1963 [2]. They observed luminescence when a voltage of about 400 V was applied to an anthracene crystal. However the development of devices based on organic electroluminescence was very slow, mainly because this type of device requires high electrical voltage but usually provides low efficiency. In 1987, Ching W. Tang and Steve Van Slyke of the Eastman Kodak Company developed a novel electroluminescent device, which is considered the first organic light-emitting diode [3]. The device was fabricated by vapor deposition using Alq_3 **(Figure 1.2-1)** and diamine **(Figure 1.2-2)** in a double layer structure. This structure makes the electron and hole recombination effective: the device has a 1% external quantum efficiency, 1.5 lm/W luminous efficiency, and a brightness of more than 1000 cd/m^2 at a driving voltage of about 10 V. Shortly afterwards, in 1990 the researcher at Cambridge university announced a PPV based LED **(Figure 1.2-3)**, which is called polymer-LED [4]. Since, there have been increasing interests and research activities in this new field and the improvements of color gamut, luminance efficiency and device reliability have progressed enormously.

1, tris(8-hydroxyquinoline) aluminium (Alq_3)

2, 4,4'-(cyclohexane-1,1-diyl) bis(*N*,*N*-di*p*-tolylaniline) (Diamine)

3, Poly(*p*-phenylene vinylene) (PPV)
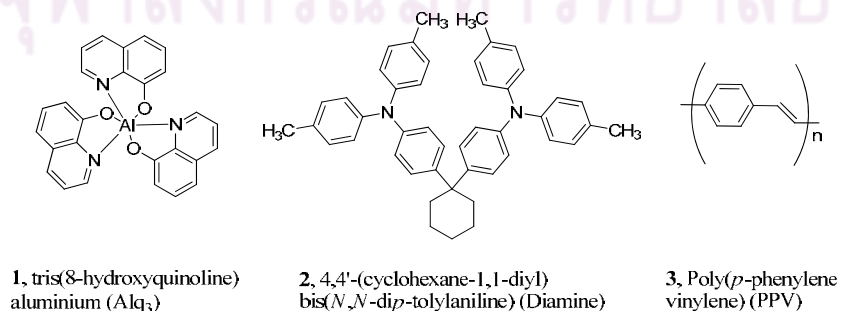
Figure 1.2 Chemical structures of Alq_3, Diamine and PPV.

Emerging as the leading element for next generation flat panel displays, the OLED is now challenging with the present LCD technology. **Figure 1.3** shows a comparison between an LCD with an OLED display. It shows that the OLED display is easier to see at almost every angle with high brightness and contrast which is a significant improvement over the LCD display.
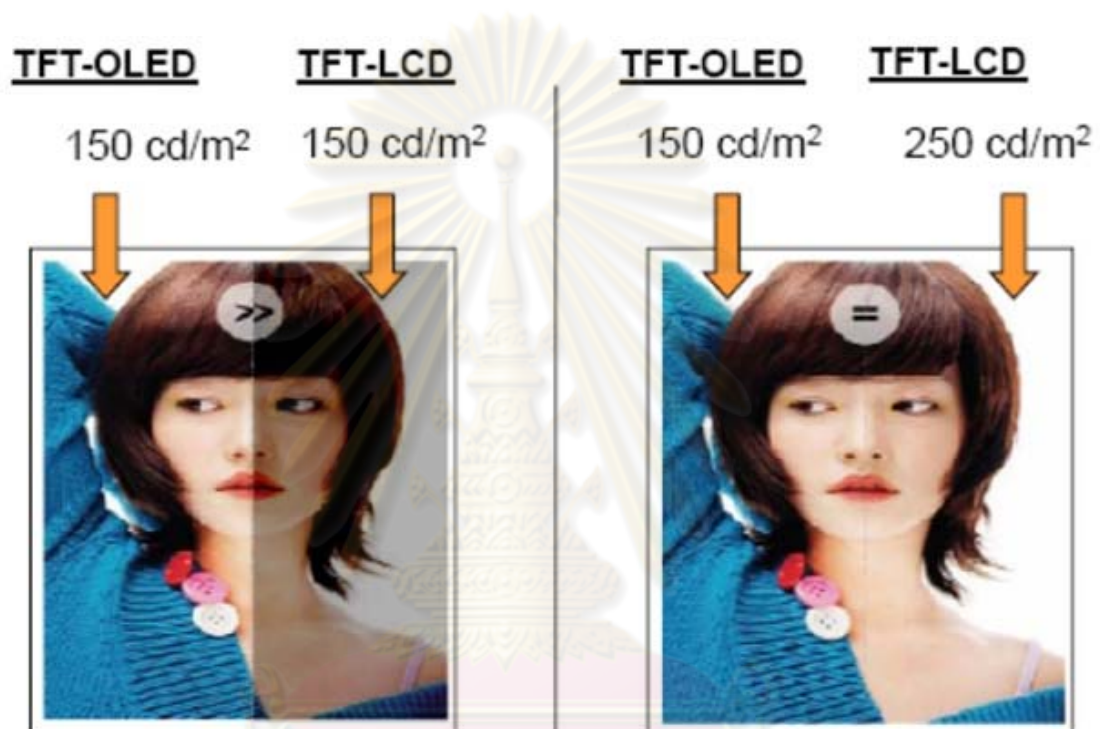
Figure 1.3 OLED and LCD display [5].

1.3 OLED structure and operation [6-9]

The schematic structure and energy level diagrams of single-layer and multi-layer OLED is shown in **Figure 1.4**. The single-layer OLED is the simplest structure used to describe the basic mechanism of OLED device. Multi-layer OLED is the high performance device improved by inserting the other organic layers such as a hole-transporting layer (HTL) and an electron-transporting layer (ETL) between an emitting layer (EML) and an electrode.
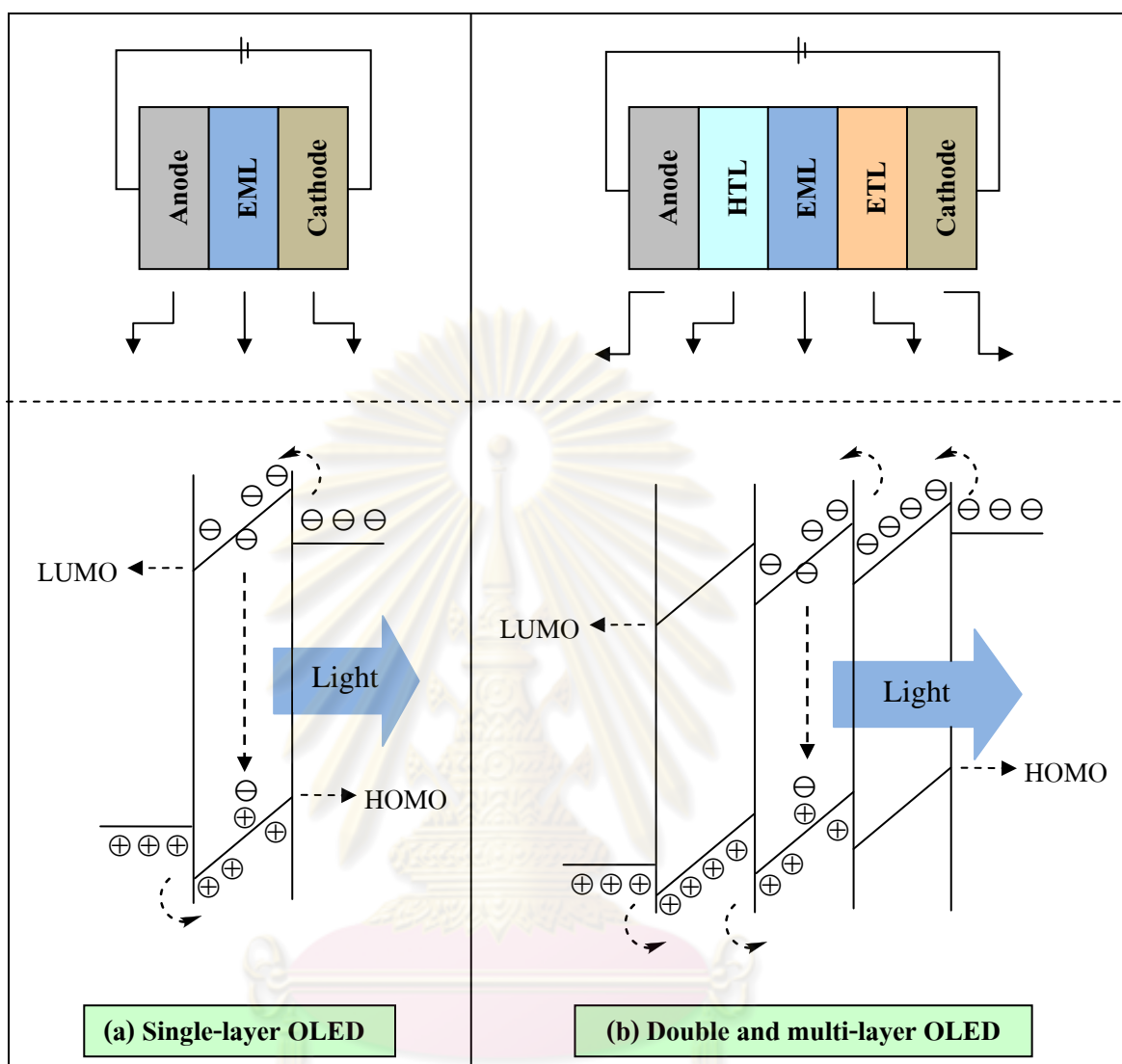
Figure 1.4 Schematic structure (top) and energy level diagram (bottom) of (a) single-layer OLED and (b) Double and multi-layer OLED.

1.3.1 Single-layer OLED

The single-layer OLED consists of a thin film of an organic electroluminescent material that is sandwiched between two conducting electrodes. The cathode electrode supplies electrons to the organic layers. The cathode is a low work function metal. The widely used materials are calcium (Ca) and magnesium (Mg). Aluminum (Al) is often used to cover the electrode to prevent an oxidation. The function of the anode supplied positively charged holes. Indium tin oxide (ITO) is often used as the anode material for hole injection. It has a high work function, to match the

HOMO of the organic material. ITO is also transparent, so that the light can emit from the device. The operation of the device involves injection of holes from anode and electrons from the cathode into HOMO and LUMO of the EML, respectively. The electrons and holes migrate through the EML under the influence of applied electric fields. The recombination of a hole and electron within a single molecule of the EML may then result in electronic excited state species called an exciton. The radiative decay of singlet excitons for fluorescent emitters results in light emission. Therefore, emission color of the devices depends on characteristic of HOMO-LUMO energy gap of the EML.

1.3.2 Double and multi-layer OLED

The key to increase the OLED efficiency is to control the recombination of holes and electrons in the EML in equal quantities. The energy barrier between the electrodes and the organic material must be minimized to enhance the injection of the carriers. Instead of one organic layer in single-layer OLED, one or/and two layers, a HTL or/and an ETL, are placed between two electrodes according to **Figure 1.4(b)**. This reduces the energy barrier for the injection of charge from anode to the EML and also provides a barrier to electrons and holes at the heterojunction between the layers. A resulting better balance in the number of injected holes and electrons promotes a radiative recombination in the EML.

1.4 Organic electroluminescent materials

Electroluminescent (EL) from organic materials was first demonstrated in 1963. Single crystals of anthracene were contacted on opposite faces between two metal electrodes. EL was observed when a DC voltage bias above 400 V was applied [10]. Using asymmetrical liquid electrodes for electron and hole injection, Helfrich and Schneider first demonstrated injection EL from anthracene single crystals in 1965 [11]. In the 20 years following these initial reports, organic EL was mainly studied for scientific curiosity as an interesting phenomenon associated with certain organic semiconductors. The developments of organic EL materials are divided into 2 classes.

1.4.1 Conjugated polymers

The first polymeric light-emitting diode based on a luminescent conjugated polymer was demonstrated in 1990 by Burroughes and co-workers at Cambridge University. The polymer was PPV, which is luminescent but not soluble in organic solvents. The PPV film was prepared from its solution-processable precursor polymer by thermal conversion. Ultra-thin, dense and homogenous film of PPV was formed on a suitable substrate, which had been pre-coated with a transparent bottom electrode. The device was completed by the deposition of a top electrode on top of the PPV film. Substantial charge injection was achieved with a DC voltage bias of just below 14 V, with indium oxide electrode positively biased with respect to the aluminum electrode. However, the quantum efficiency of the PPV devices was only 0.05%, much lower than the estimated photoluminescence (PL) quantum yield of about 8% for PPV. The results of the Cambridge group were quickly confirmed by Braun and Heeger at UC Santa Barbara, with improved material processability and device performance [12,13]. The intensive research and development activity in polymer LEDs mirrored that of organic LEDs in recent years.

1.4.2 Low molecular-weight materials

The work pioneered by Tang and Van Slyke initiates recent improvements of the OLED device efficiency and durability. For the fabrication of highly stable OLED, low molecular weight materials with specific optical and electronic properties such as fluorescence, energy levels, charge mobility, etc., and high morphology and thermally stable are required [14-16]. The thermal stability of materials used in OLED is the one of the significant factors of the device durability. Under thermal stress, most organic materials tend to turn into the thermodynamically stable crystalline state, which leads to device failure [17,18]. A considerable amount of evidence indicates that an amorphous thin film with a high glass transition temperature (T_g) is more stable to heat damage [19-24]. For the organic materials in OLED, high thermal stability, especially high T_g, excellent film formability are essentially needed.

Amorphous molecular materials or molecular glasses are of interest because of the following aspect. They are in a thermodynamically non equilibrium

state and hence may exhibit glass transition phenomena usually associated with amorphous polymers. It is thought that they assume a variety of states such as the amorphous glass, supercooled liquid, and crystal. They may be characterized by the presence of free volume and by the disorder of both intermolecular distance and orientation. They may form uniform, transparent amorphous thin films by thermal evaporation and spin-coating methods.

Therefore, one of the key challenges on the path to developing the next generation of high-performance OLED is the design and synthesis of readily processible and thermally robust emissive and charge transport materials with improved multifunctional properties. In this work, the novel emitting materials (EMMs) and hole-transporting materials (HTMs) consist of 3,6-di(pyren-1-yl)-9-*p*-tolyl-9*H*-carbazole (**2PCT**), ethane-1,2-diyl bis(2-(3,6-di(pyren-1-yl)-9*H*-carbazol-9-yl)acetate) (**4P2C**) and 4-(3,6-di(pyren-1-yl)-9*H*-carbazol-9-yl)-*N*,*N*-diphenylaniline (**2PCP**) was synthesized. Our design of the new materials is motivated by the high thermal stability and hole-transporting ability of carbazole together with the high quantum efficiency of pyrene. A combination of both pyrenes and carbazoles should result in electroluminescent materials with desirable physical, optical, and electronic properties. Thus, to evaluate the performance of these materials, the OLED based on these materials has been fabricated in this work.

1.5 Hole-transporting materials (HTMs)

The HTMs provide a hole-conductive pathway for positive charge carrier to migrate from the anode into the EML. On the basis of this requirement, HTMs are usually easily oxidized and are fairly stable in the radical cationic form. By far, one of the widely used HTMs in OLED are still *N*,*N*′-diphenyl-*N*,*N*′-bis(3-methylphenyl)-1,1′-biphenyl-4,4′-diamine (TPD) [25-28] and 4,4′-bis-[*N*-(1-naphthyl)-*N*-phenyl-amino]-biphenyl (NPD) [29-35]. The chemical structure of TPD and NPD are shown in **Figure 1.5**. Furthermore, the NPD is used as the blue-emitting materials (blue-EMMs) [19, 40]. The reasons for its popularity are because sublimed TPD and NPD could be manufactured readily and are thus abundantly available even though its glass transition temperature (T_g) at 70 ^{o}C and 98 ^{o}C, respectively, are a little low which may affect its morphological stability at high operating temperature.
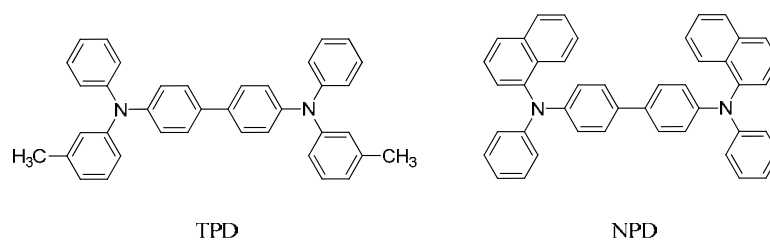
Figure 1.5 Chemical structures of TPD and NPD.

1.6 Emitting materials (EMMs)

Organic fluorescence compounds are used as the emitter in OLED device. The fluorescence principles are described by the Jablonski diagram in **Figure 1.6**.
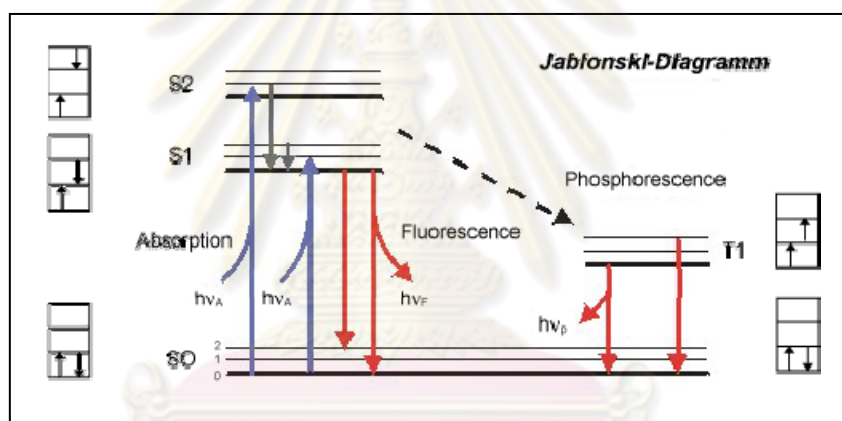
Figure 1.6 Jablonski diagram.

The examples of emitting materials are a red emitter 4-(dicyanomethylene)-2-methyl-6-[4-(dimethyl-aminostyryl)-4H-pyran] (DCM) [36] (**Figure 1.7**), a green emitter tris(8-hydroxyl-quinoline) aluminum (Alq$_3$) [37,38,39] and blue emitters NPD and polyfluorene (PF) derivatives (**Figure 1.7**) [40,41]. Among these compounds, Alq$_3$ is the most frequently used substance due to its thermal and morphological stabilities (T_g ~172 ^{o}C) which are essential factors for the synthesis, purification, evaporating process into thin films [42,43]. Moreover, the Alq$_3$ is used as the electron-transporting material (ETM) [44-46].

In principle, it is possible to obtain a variety of colors by using a combination of red, green and blue color light. Thus, the most important materials required for the full-color OLED display technology are red, green and blue emitters.
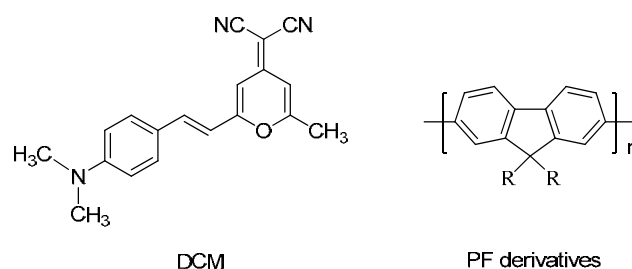
Figure 1.7 Chemical structures of DCM and PF derivatives.

To assemble a full-color OLED display, highly efficient red-, green-, and blue-emitting materials and devices are required. However, only the red and the green materials and devices with sufficient efficiencies and lifetimes of commercial value have been described, while high-efficient, pure blue light still remains a challenge. Consequently, a great number of blue-emitting materials, such as anthracene [47], triphenylfluoranthene [48], oligoquinoline [49], triarylamines [50], fluorine [51], and pyrene [52] have been developed. However, most of these materials are still not satisfactory due to their large energy gaps and low electron affinities leading to inefficient electron injection into the blue emitters [64].

In summary, the objectives of this work are following:

(1) To synthesized the 3,6-dipyrenylcarbazole derivatives as both blue-emitting and hole-transporting materials for OLED.

(2) To characterize and study the electronic, photophysical, electrochemical and thermal properties of the target molecules.

(3) To investigate their potential application as both blue-emitting and hole-transporting materials for OLED.

1.7 Literature reviews

This section will survey the applications of carbazole and pyrene derivatives as the HTMs and EMMs for OLED.

Many carbazole derivatives have been extensively studied for different applications due to the nitrogen atom in the carbazole ring bestows an electron-donating ability, and possess high morphology stable. Carbazole has strong absorption in the near-UV region and a low redox potential. The electrochemical and

spectroscopic properties of carbazole and its derivatives have been extensively investigated [24]. Chemically, carbazole can be easily functionalized at its 3-, 6- or 9-positions and covalently linked to other molecular moieties [53,54]. Due to its unique optical, electrical, and chemical properties, carbazole has been used widely as a functional building block or substituent in the construction of organic molecules for use as light-emitting and hole-transporting layers in OLED devices [55-57], as host materials for electrophosphorescent applications [58] and as active components in solar cells [59]. Moreover, the thermal stability and glassy state durability of the organic molecules were found to be significantly improved upon incorporation of a carbazole moiety into the structure [60].

For the pyrene derivatives, they exhibited a strong fluorescence signal with high fluorescence quantum yield and usually used as fluorescence dye for DNA and RNA probe or metal sensors [61-63]. Recently, some pyrene derivatives have been used in OLED in order to improve hole-transporting ability because of its electron rich property, yet the performance of those OLED is still not satisfactory in terms of brightness and efficiency. However, there have been an increasing interest in the use of pyrenyl ring in the synthesis of emissive and charge transport materials for OLED.

In 2010, S. Lengvinaite and coworker [65] synthesized an Indolo[3,2-b]carbazole-based functional derivatives **4-6** (**Figure 1.8**) for use as hole-transporting materials for OLED. Compounds **4-6** exhibited maximum emission wavelength at ~ 427-462 nm. Their glass transition temperature (T_g) were observed at 155 ^{o}C, 123 ^{o}C and 172 ^{o}C, respectively. The hole-transporting property of **4-6** were tested by using device structure of ITO / Compound **4-6** / Alq$_3$ / LiF:Al. These devices exhibited turn-on voltages of 5-8 V and a maximum brightness of 1090-5670 cd/m^2 (at 13-17 V). The current efficiencies of the OLED range from 2.21 to 3.64 cd/A. Among these devices, the OLED using compound **6** as the HTM exhibited the best overall performance, i.e. a turn-on voltage of 5 V and maximal photometric efficiency of 3.64 cd/A.
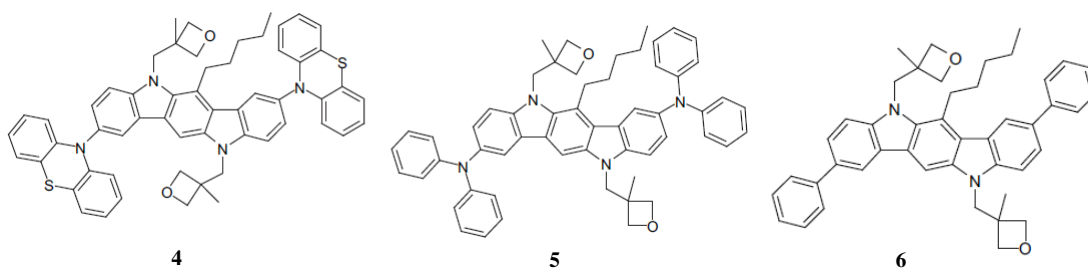
Figure 1.8 Chemical structures of compounds **4-6** [65].

In 2008, V. Promarak and coworker [66] synthesized a hole-transporting materials based on carbazole compounds (G2CB and G2CC) (**Figure 1.9**). G2CB and G2CC exhibited identical emission shapes in bluish-purple region with the maxima at 382 and 390 nm, respectively. G2CB and G2CC that containing carbazole moieties showed high T_g at 206 ^{o}C and 245 ^{o}C, respectively. The electrochemical properties of the G2CB and G2CC were investigated by cyclic voltammetry (CV) analysis. HOMO levels of G2CB and G2CC are 5.46 and 5.44 eV, respectively. LUMO levels of G2CB and G2CC were 2.18 and 2.23 eV, respectively. OLED devices with the structure of ITO/HTL(50 nm)/Alq₃(50 nm)/LiF(0.5 nm):Al(200 nm) were fabricated using compounds G2CB and G2CC as the HTL. The device with G2CC as an HTL has much better performance in terms of brightness, current and turn-on voltage than that with G2CB. In the case of ITO / G2CC / Alq₃ / LiF:Al device, its maximum luminance is about 8900 cd/m^2 at 14 V with a turn-on voltage of 3.5 V. The ITO/G2CB/Alq₃/LiF:Al device shows the maximum luminance at 3000 cd/m^2 at 15 V with a turn-on voltage of 7.5 V.
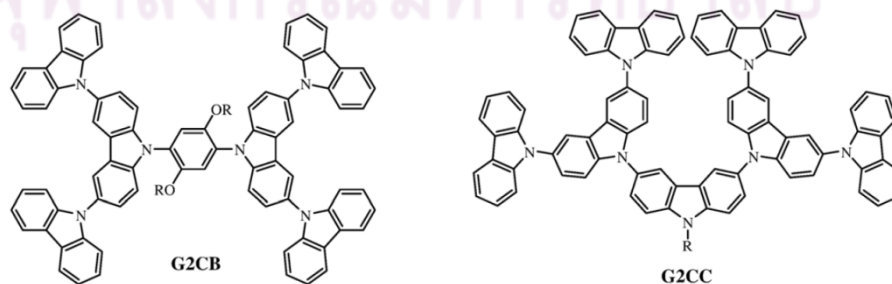
Figure 1.9 Chemical structures of G2CB and G2CC [66].

In 2007, C.-H. Yang and coworker [67] synthesized a greenish blue-emitting organic diodes based on pyrene derivatives (DP and DPB) (**Figure 1.10**). DP and DPB exhibited maximum emission wavelength at 430 and 426 nm. The T_g of DPB was observed at 145.5 ^{o}C. The electrochemical properties of the DP and DPB were investigated by cyclic voltammetry (CV) analysis. HOMO levels of DP and DPB are 5.40 and 5.70 eV, respectively. LUMO levels of DP and DPB are 2.26 and 2.50 eV, respectively. OLED devices with the structure of ITO / NBP(50 nm) / DP and DPB(30 nm) / BCP (10 nm) / Alq$_3$ (30 nm) / LiF (1nm) / Al were fabricated. The power efficiency of the DPB device was 5.18 lm/W at a voltage, current density, and luminance of 5.2 V, 20 mA/cm^2, and 1714 cd/m^2, respectively. For the DP device the power efficiency was 4.09 lm/W at a voltage, current density, and luminance of 5.6 V, 20 mA/cm^2, and 1459 cd/m^2, respectively.
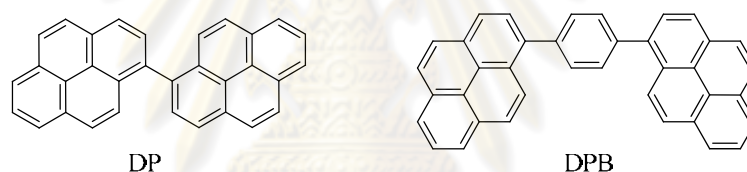
Figure 1.10 Chemical structures of DP and DPB [67].

CHAPTER II
EXPERIMENTAL

2.1 Synthesis

2.1.1 Instruments and Equipment

Thin layer chromatography (TLC) was performed on aluminium sheets precoated with silica gel (Merck Kiesegel 60 F_{254}) (Merck KgaA, Darmstadt, Germany). Column chromatography was performed on silica gel (Merck Kieselgel 60G) (Merck KGaA, Darmstadt, Germany). All ^{1}H- and ^{13}C-NMR spectra were obtained on a Varian Mercury NMR spectrometer, which operated at 400 MHz for ^{1}H and 100 MHz for ^{13}C nuclei (Varian Company, CA, USA). Mass spectra were recorded on a Microflex MALDI-TOF mass spectrometer (Bruker Daltonics) using doubly recrystallized α-cyano-4-hydroxy cinnamic acid (CCA) and dithranol as a matrix. Elemental (CHN) analyses were performed on PE 2400 seriesII (Perkin-Elmer, USA). Absorption spectra were measured by a Varian Cary 50 UV-Vis spectrophotometer. Fluorescence spectra were obtained from a Varian Cary Eclipse spectrofluorometer.

The fluorescence quantum yields (Φ) were determined by comparison with a standard of known fluorescence quantum yield according to the following equation [68].

$$\Phi_{X=} \Phi_{ST}\left(\frac{Slope_X}{Slope_{ST}}\right)\left(\frac{\eta_X^2}{\eta_{ST}^2}\right)$$

Where the subscripts X refer to the unknown samples and ST refers to the standard quinine sulfate solution in 0.01 M H_2SO_4, whose fluorescence quantum yield is known to be 0.54 [68], Φ is the fluorescence quantum yield, *Slope* is the slope from the plot of integrated fluorescence intensity versus absorbance, and η is the refractive index of the solvent. The refractive indexes of CH_2Cl_2 and 0.01 M H_2SO_4 were 1.424 and 1.333, respectively.

The electrochemical analysis by cyclic voltametry was performed using an AUTOLAB spectrometer. All measurements were made at room temperature on sample solutions in freshly distilled dichloromethane with 0.1 M tetra-n-butylammonium hexafluorophosphate as electrolyte. Dichloromethane was distilled from calcium hydride and the electrolyte solutions were degassed by nitrogen bubbling. A glassy carbon working electrode, a platinum wire counter electrode, and a Ag/AgCl/NaCl (Sat.) reference electrode were used in all cyclic voltametric experiments.

Thermal experiments with Differential Scanning Calorimeter (DSC) were performed on Mettler Toledo DSC 822^e and Thermogravimetric Analysis (TGA) were studied using Simultaneous Thermal Analyzer Netzsch 409.

2.1.2 Synthetic procedures

3,6-diiodo-*9H*-carbazole (7)

To a stirred solution of carbazole (5.0 g, 29.9 mmol) in acetic acid (50 mL) was added potassium iodide (6.6 g, 39.8 mmol). Then, potassium iodate (9.6 g, 44.9 mmol) was added in small portions over a period of 5 min and the resulting mixture was refluxed for 20 min. The reaction was allowed to cool to room temperature and diluted with EtOAc (50 mL) and water (50 mL). The aqueous layer was separated and extracted with EtOAc (2×50 mL). The combined organic layer was dried over $MgSO_4$, filtered, and concentrated under reduced pressure to give a brown solid residue. The crude product was purified by crystallization from acetone and hexane to yield **7** as light brown crystals. (12.3 g, 98%). ^{1}H NMR (DMSO-*d6*): δ = 11.56 (s, 1H), 8.58 (s, 2H), 7.66 (d, *J* = 8.5 Hz, 2H), 7.35 (d, *J* = 8.5 Hz, 2H) ppm. ^{13}C NMR (DMSO-*d6*): δ = 138.7, 134.0, 129.1, 123.8, 113.5, 81.8 ppm.

3,6-di(pyren-1-yl)-*9H*-carbazole (8)

A mixture of **1** (1.4 g, 3.3 mmol), pyrene-1-boronic acid (2.0 g, 8.1 mmol), Pd(PPh$_3$)$_4$ (94 mg, 0.08 mmol), THF (50 mL) and 2M K$_2$CO$_3$ aqueous solution (15 mL) was heated under refluxing conditions for 24 h. After the reaction was allowed to cool to room temperature, the resulting brown solution was extracted with CH$_2$Cl$_2$ (3×50 mL). The combined organic layer was dried over MgSO$_4$,

filtered, and concentrated under reduce pressure. The crude product was purified by flash chromatography using hexanes:CH_2Cl_2 (3:1) as the eluent. The product **8** was obtained as pale green solid (1.3 g, 67%). ^{1}H NMR (DMSO-*d6*): δ = 11.72 (s, 1H), 8.50 (s, 2H), 8.36 (d, *J* = 7.9 Hz, 2H), 8.12 – 8.30 (m, 14H), 8.06 (t, *J* = 7.6 Hz, 2H), 7.80 (d, *J* = 8.3 Hz, 2H), 7.70 (d, *J* = 8.3 Hz, 2H) ppm. ^{13}C NMR (DMSO-*d6*): δ = 139.5, 138.3, 130.9, 130.9, 130.4, 129.6, 128.3, 128.2, 127.9, 127.3, 127.05, 126.2, 125.1, 124.7, 124.6, 124.2, 124.0, 122.8, 122.2, 111.0 ppm. HRMS calculated for $C_{44}H_{25}N$ (M+H^{+}): 568.2065. Found: 568.1916. Elemental analysis calculated for $C_{44}H_{25}N$: C, 93.09; H, 4.44; N, 2.47; Found: C, 91.52; H, 4.60; N, 2.15.

4-iodotoluene (9)

A solution of *p*-toluidine (5.0 g, 0.05 mol) in 6 M HCl (10 mL), water (10 mL), and acetonitrile (25mL) was heated to 70 °C for a few minutes and then cooled to 5-10 °C in an ice bath. To this stirred suspension was slowly added a solution of $NaNO_2$ (3.5 g, 0.05 mol) in water (25 mL). The mixture was stirred for additional 15 min then slowly added a solution of KI (12.0 g, 0.07 mol) in water (25 mL). After the reaction mixture was stirred for 15 min, the resulting dark brown mixture was extracted with ether (3 × 50 mL). The combined extracts were washed with saturated $Na_2S_2O_3$ and saturated NaCl. The organic phase was dried ($MgSO_4$), filtered, and concentrated under reduced pressure to afford **9** as an brown solid (7.5 g, 73%). ^{1}H NMR (CDCl$_3$): δ = 7.56 (d, *J* = 8.22 Hz, 2H), 6.92 (d, *J* = 8.37 Hz, 2H), 2.29 (s, 3H). ^{13}C NMR (CDCl$_3$): δ = 137.0, 131.1, 20.9.

1,2-bis(chloroacetoxy)ethane (10)

In a two-necked round bottom flask containing chloroacetyl chloride (19.2 mL, 0.24 mol) was slowly added ethylene glycol (2.7 mL, 0.05 mol) over a period of 1 h under refluxing conditions. The mixture was then refluxed for additional 2 h after which time the solution was allowed to cool to room temperature. The product was obtained by distillation under reduced pressure (approximately 0.2 mmHg) at 140 °C to afford colorless liquid (7.5 g, 70%). ^{1}H NMR (CDCl$_3$): δ = 4.43 (s, 4H), 4.10 (s, 4H). ^{13}C NMR (CDCl$_3$): δ = 167.1, 63.3, 40.6.

4-bromo-*N*,*N*-diphenylaniline (11)

A mixture of triphenylamine (1.0 g, 4.08 mmol) and *N*-bromo succinamide (0.7 g, 4.08 mmol) in CCl$_4$ (40 mL) was refluxed for 4 h. Then the mixture was cooled to room temperature the precipitated succinimide was filtered, and the solvent was evaporated from the solution. The remaining grey oil was recrystallized from ethanol to afford white powder (1.1 g, 80%). ^{1}H NMR (CDCl$_3$): δ = 7.35 – 7.20 (m, 6H), 7.11 – 6.99 (m, 6H), 6.97 – 6.90 (m, 2H). ^{13}C NMR (CDCl$_3$): δ = 147.4, 147.0, 132.1, 129.4, 125.1, 124.4, 123.2, 114.8.

3,6-di(pyren-1-yl)-9-*p*-tolyl-9*H*-carbazole (2PCT)

A mixture of **8** (0.43 g, 0.76 mmol), **9** (0.33 g, 1.52 mmol), Cu bronze powder (0.24 g, 3.80 mmol) and K$_2$CO$_3$ (0.32 g, 2.28 mmol) in degassed nitrobenzene (15 mL) was refluxed for 24 h under N$_2$ atmosphere. The resulting brown solution was allowed to cool to room temperature and extracted with CH$_2$Cl$_2$ (3 × 50 mL). The combined organic layer was dried over MgSO$_4$, filtered, and concentrated under reduce pressure. The crude product was purified by recrystallization from CH$_2$Cl$_2$ and ethanol to yield **2PCT** as green solid (0.25 g, 56%). ^{1}H NMR (CDCl$_3$): δ = 8.37 (s, 2H), 8.25 (d, *J* = 9.2 Hz, 2H), 8.18 (d, *J* = 7.6 Hz, 2H), 8.02 – 8.13 (m, 10H), 7.91 – 7.96 (m, 4H), 7.44 (d, *J* = 8.4 Hz, 2H), 7.56 – 7.60 (m, 4H), 7.45 (d, *J* = 8.0 Hz 4H), 2.49 (s, 3H) ppm. The ^{13}C NMR (CDCl$_3$): δ = 140.9, 138.5, 137.7, 133.1, 131.6, 131.1, 130.7, 130.4, 129.0, 128.2, 127.5, 127.4, 127.2, 127.1, 125.9, 125.7, 125.0, 124.7, 124.6, 123.5, 122.4, 120.4, 109.9, 21.3 ppm. MS(MALDI-TOF) calculated for C$_{51}$H$_{31}$N: 657.799 Found: 657.063. Elemental analysis calculated for C$_{51}$H$_{31}$N: C, 93.12; H, 4.75; N, 2.13; Found: C, 89.22; H, 4.87; N, 1.93.

Ethane-1,2-diyl bis(2-(3,6-di(pyren-1-yl)-*9*-*H*-carbazol-9-yl)acetate) (4P2C)

To a mixture of **8** (250 mg, 0.44 mmol) and K$_2$CO$_3$ (60 mg, 0.44 mmol) in DMSO (3 mL) was slowly added a solution of **10** (45 mg, 0.21 mmol) in DMSO (1 mL). The solution was stirred at room temperature for 24 h and the resulting green solution was diluted with EtOAc (50 mL) and water (50 mL). The organic layer was separated and washed with water (25 mL × 2), dried over MgSO$_4$,

and concentrated under reduced pressure. The crude product was purified by recrystallization in CH_2Cl_2 and hexane to yield **4P2C** as a white solid (60 mg, 42%). ^{1}H NMR (CDCl$_3$): δ = 8.38 (s, 4H), 8.10 – 8.14 (m, 8H), 7.88 – 8.00 (m, 24H), 7.73 (d, J = 9.32 Hz, 4H), 7.67 (d, J = 8.36 Hz, 4H), 7.44 (d, J = 8.40 Hz, 4H), 5.11 (s, 4H), 4.55 (s, 4H) ppm. The ^{13}C NMR (CDCl$_3$): δ = 168.5, 140.3, 138.0, 133.2, 131.4, 130.8, 130.2, 129.1, 128.6, 128.0, 127.3, 127.2, 127.1, 125.8, 125.3, 124.8, 124.6, 124.5, 123.6, 122.6, 108.4, 62.9, 44.8 ppm. MS(MALDI-TOF) calculated for $C_{94}H_{56}N_2O_4$: 1277.461. Found: 1277.528. Elemental analysis calculated for $C_{94}H_{56}N_2O_4$: C, 88.38; H, 4.42; N, 2.19; Found: C, 88.58; H, 3.96; N, 2.11.

4-(3,6-di(pyren-1-yl)-9*H*-carbazol-9-yl)-*N*,*N*-diphenylaniline (2PCP)

A mixture of **8** (0.20 g, 0.35 mmol), **11** (0.23 g, 0.70 mmol), Cu(0) (0.11 g, 1.75 mmol) and K_2CO_3 (0.15 g, 1.05 mmol) in degassed nitrobenzene (15 mL) was refluxed for 24 h under N_2 atmosphere. The resulting brown solution was allowed to cool to room temperature and extracted with CH_2Cl_2 (3 × 50 mL). The combined organic layer was dried over MgSO$_4$, filtered, and concentrated under reduce pressure. The crude product was purified by recrystallization in CH_2Cl_2 and ethanol to yield **2PCP** as green solid (0.28 g, 68%). ^{1}H NMR (CDCl$_3$): δ = 8.44 (s, 2H), 8.32 (d, J = 9.1 Hz, 2H), 8.25 (d, J = 7.5 Hz, 2H), 8.22 – 8.06 (m, 10H), 8.06 – 7.96 (m, 4H), 7.73 (dd, J = 22.4, 8.3 Hz, 4H), 7.61 (d, J = 7.7 Hz, 2H), 7.36 (t, J = 7.2 Hz, 6H), 7.27 (d, J = 8.7 Hz, 4H), 7.13 (dd, J = 14.0, 6.9 Hz, 2H) ppm. The ^{13}C NMR (CDCl$_3$): δ = 147.6, 147.4, 141.0, 138.5, 133.2, 131.6, 131.3, 131.1, 130.4, 129.4, 129.0, 128.9, 128.2, 127.9, 127.5, 127.4, 127.2, 126.0, 125.7, 125.1, 125.0, 124.9, 124.7, 124.7, 124.1, 123.6, 122.7, 122.4, 109.9 ppm. MS(MALDI-TOF) calculated for $C_{62}H_{38}N_2$: 810.979. Found: 810.448. Elemental analysis calculated for $C_{62}H_{38}N_2$: C, 91.82; H, 4.72; N, 3.45; Found: C, 90.51 ; H, 4.51 ; N, 3.53 .

2.2 OLED device fabrication section

    2.2.1 Commercially available materials

        The commercial sources and purities of materials used in these experiments are shown in **Table 2.1**. All materials were analytical grade and used without further purification, unless indicated.

Table 2.1 Commercially available materials for OLED device fabrication.

Materials	Purity (%)	Company
$1'' \times 1''$ Indium oxide doped tin oxide (99.3 wt % In_2O_3:0.7 wt % SnO_2)-coated glasses (5-15 ohm/sq)	99.5	Kintec
Poly(3,4-ethylenedioxythiophene)–poly(styrene) (0.5 wt % PEDOT: 0.5 wt % PSS)	1.3	Baytron
Tris(8-hydroxyl-quinoline) aluminum (Alq_3)	98	Sigma-Aldrich
Lithium fluoride (LiF)	99.98	ACROS
Aluminium (Al) wire	99.97	BDH

    2.2.2 Reagents

        The reagents were obtained from various suppliers as shown in **Table 2.2**. All reagents were analytical grade and used without further purification, unless indicated.

Table 2.2 List of reagents.

Reagents	Purity (%)	Company
Hydrochloric acid (HCl) 37%	36.5	Carlo Erba
Nitric acid (HNO_3) 69%	68.5-69.5	BDH
Sodium hydroxide (NaOH)	99.99	Carlo Erba
Acetone	99.5	BDH
Isopropanol	99.5	Carlo Erba

2.2.3 Instruments

The following instruments were used in this study:

(1) Photoluminescence (PL) spectrophotometer (Perkin–Elmer, Model LS 50B)

(2) Spin-coater (Chemat Technology, Model KW-4A)

(3) Thermal evaporator (ANS Technology, Model ES280)

(4) Digital source meter (Keithley, Model 2400)

(5) Multifunction optical meter (Newport, Model 1835-C)

(6) Calibrated photodiode (Newport, Model 818 UVCM)

(7) USB Spectrofluorometer (Ocean Optics, Model USB4000FL)

2.2.4 Organic thin film preparation and characterization

The preparation process of organic thin films is described in **Figure 2.1**.
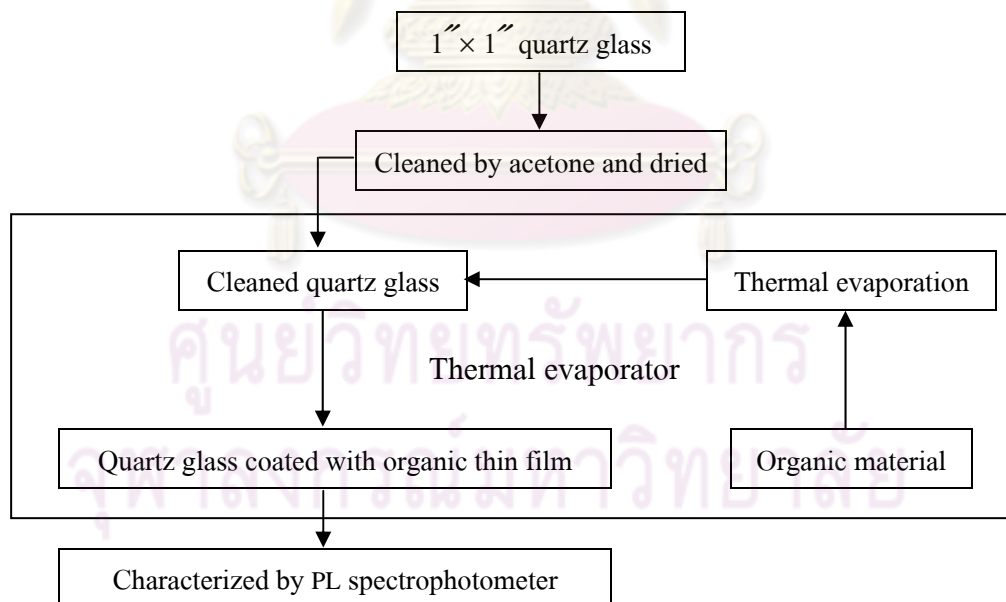
Figure 2.1 Preparation and characterization of organic thin film.

2.2.5 Thermal evaporation of the organic thin films

In order to study the photophysical properties of solid state materials, organic thin films coating on quartz glass substrates ($1'' \times 1''$) were prepared by thermal evaporation. Prior to film deposition, the substrates were cleaned with acetone in ultrasonic bath followed by drying on a hotplate. The clean quartz glass substrate was then placed on a substrate holder and the organic material was loaded into an evaporation source (alumina filament boat) located in the vacuum chamber of the thermal evaporator (see **Figure 2.2** for thermal evaporator and vacuum chamber). The vacuum chamber was evacuated to about 1×10^{-5} mbar by the vacuum pump system (**Figure 2.2b**). The organic material was thermally evaporated to the substrate surface at an evaporation rate of $0.2 - 0.4$ Å/sec controlled by a calibrated quartz crystal oscillator (Maxtek thickness monitor, Model TM-350).

(a)

(b)
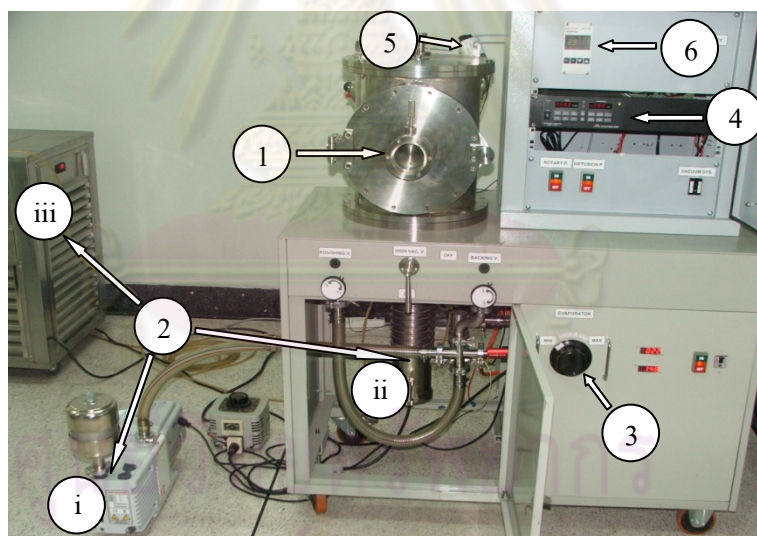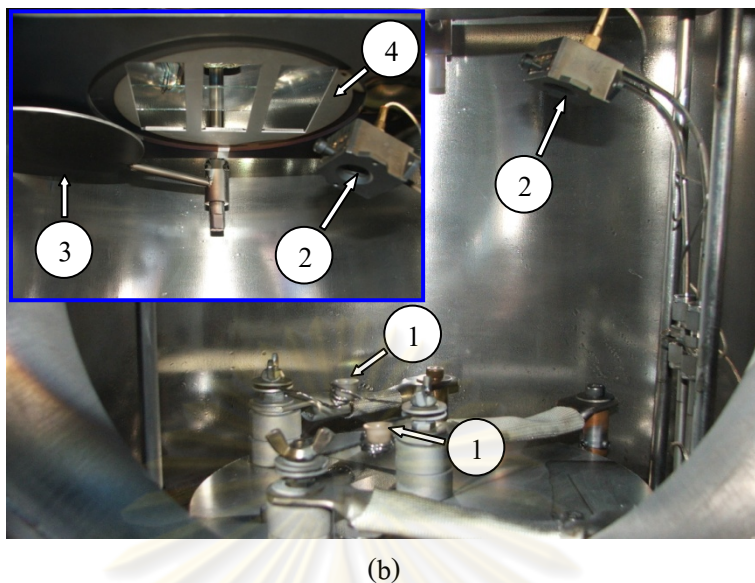
Figure 2.2 (a) A thermal evaporator which consists of (1) vacuum chamber, (2) high vacuum pump system; (i) backing pump, (ii) diffusion pump and (iii) cooler of diffusion pump, (3) volume control of evaporation source heater, (4) thickness monitor of quartz crystal oscillator, (5) vacuum gauge, and (6) vacuum gauge monitor and (b) vacuum chamber consisting of (1) evaporation source heaters (alumina filament bolts), (2) sensor of the quartz crystal oscillator, (3) source shutter, and (4) substrate holder.

2.2.6 OLED device fabrication

The OLEDs fabrication process is described in **Figure 2.3**.
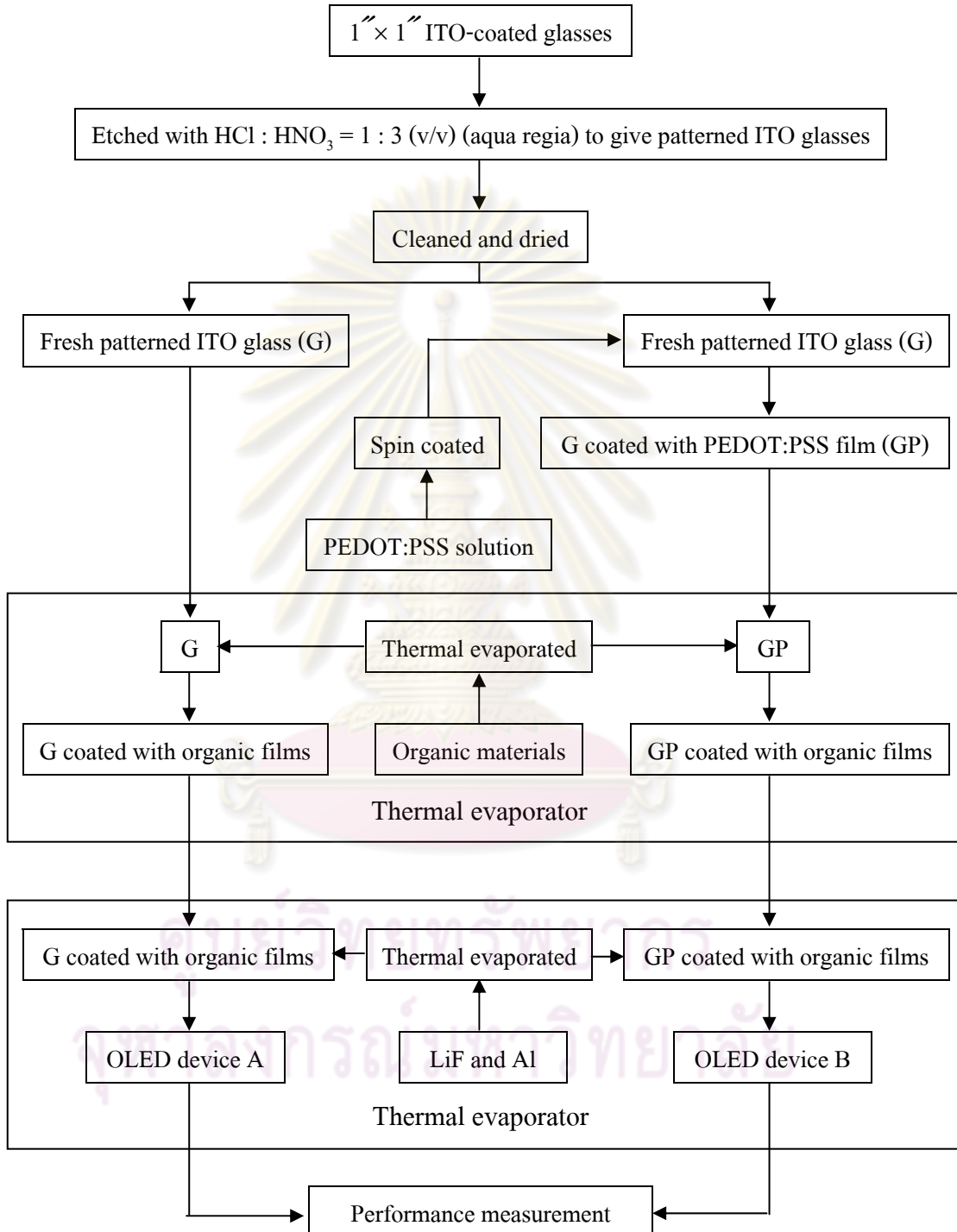
Figure 2.3 Fabrication and measurement of OLED.

2.2.7 Patterning process for ITO-coated glasses

The ITO-coated glasses (**Figure 2.4a**) were firstly etched to give a pattern of ITO sheet on glass. Prior to the patterning process, the ITO sheet on glass was covered with a 2 x 10 mm of negative dry film photo resist (Warf) [69]. The covered ITO glass (**Figure 2.4b**) was immersed in the solution of $HCl:HNO_3$ (1:3 v/v) (aqua regia) for 10 min, with stirring during the etching process. The etched ITO glass was cleaned by thoroughly rinsing with water and subsequently soaking in 0.5 M NaOH for 10 min to remove the negative dry film from an ITO-coated glass surface. Finally, these substrates were thoroughly rinsed with water to give the patterned ITO glasses as shown in **Figure 2.4c**.

(a)   (b)   (c)
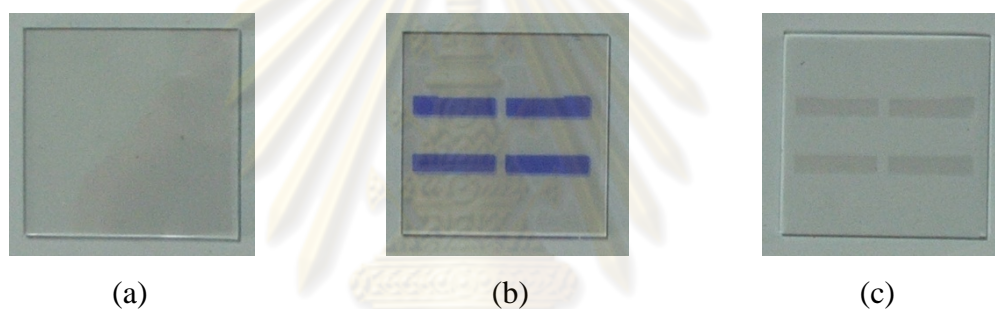
Figure 2.4 (a) ITO-coated glass, (b) ITO-coated glass covered with 2 x 10 mm of negative dry film photo resist and (c) patterned ITO glass.

2.2.8 Cleaning process for the patterned ITO glasses

The cleanliness of the ITO surface was an important factor in the performance of the OLEDs devices. The patterned ITO glasses were cleaned for 10 min with detergent in ultrasonic bath followed by a thorough rinse with de-ionized (DI) water and then subsequently ultra-sonicated in hot acetone and isopropanol for 10 min. Finally, the substrates were dried in vacuum oven at 100 °C to give fresh patterned ITO glasses.

2.2.9 Spin-coating method of PEDOT:PSS

A PEDOT:PSS solution was diluted with isopropanol and stirred for 1 day. The spin-coating method was performed on a spin coater as shown in **Figure 2.5**. The diluted PEDOT:PSS solution was filtered through a 0.45 µm pore size nylon filter (Orange scientific) and spin-coated onto a fresh patterned ITO glass surface at 3000 rpm for 20 sec. Finally, the patterned ITO glass coated with the PEDOT:PSS film was baked at 120 °C for 15 min for curing.
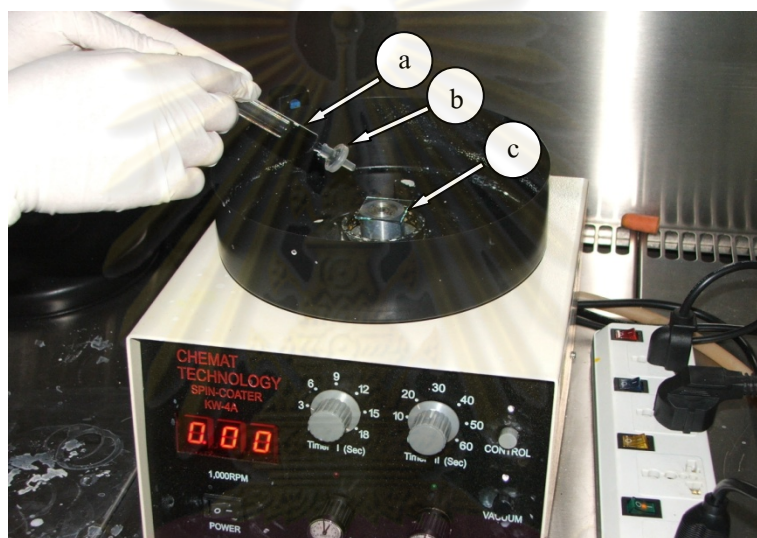
Figure 2.5 Spin-coating method by using a spin coater. (a) PEDOT:PSS solution in the syringe, (b) nylon filter, and (c) fresh patterned ITO glass.

2.2.10 Organic thin film deposition

The deposition of other organic layers was the next step in the fabrication of OLEDs. The organic layers were deposited using thermal evaporation (**Figure 2.2**) with the same procedure described in section 2.2.5. Prior to the deposition, the patterned ITO glass coated with PEDOT:PSS film or/and the fresh patterned ITO glass were placed on a substrate holder. The organic materials, such as Alq_3, were loaded in co-evaporation sources, alumina filament boat 1 and 2, respectively, into a vacuum chamber of the thermal evaporator. These organic materials were deposited on top of glass substrates by co-evaporation of the two

source materials at a background pressure of approximately 1×10^{-5} mbar with 0.2 –
0.4 Å/sec evaporation rate.

2.2.11 Cathode deposition

Finally, an ultra thin LiF layer and Al cathode contact were
sequentially co-evaporated from two tungsten boats through a shadow mask (**Figure
2.6**) with 2 mm wide slits arranged perpendicularly to the ITO fingers, to obtain the
OLED with an active area of 2×2 mm^2 (**Figure 2.7**). The operating vacuum for
evaporation of this cathode was under 1×10^{-5} mbar at high evaporation rates of 5 –
10 Å/sec. The thickness of LiF and Al of all devices were 0.5 and 150 nm,
respectively.
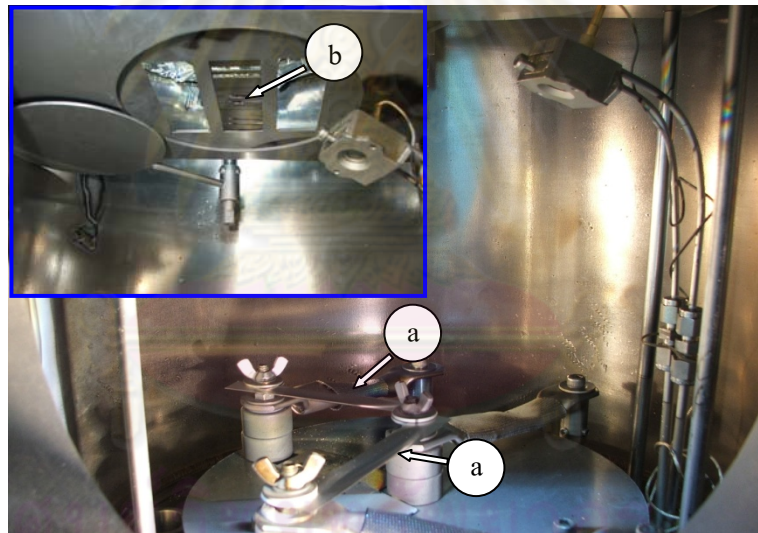
Figure 2.6 Instrument for cathode deposition. (a) tungsten boats and (b) 2 mm wide
fingers of a shadow mask.

Figure 2.7 shows the OLED device fabricated by thermal evaporation with 4 pixels. A pixel active area of a device is 2×2 mm^2.

Al cathode

ITO anode

Organic film
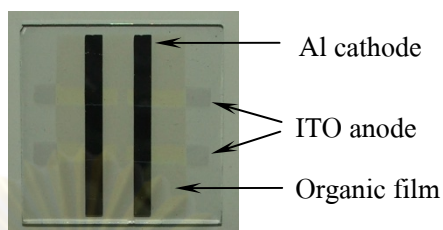
Figure 2.7 OLED device fabricated by thermal evaporation.

2.2.12 Device measurement

The instruments for OLED device measurements are shown in **Figure 2.8**. The computer was used for controlling of the digital source meter, the multifunction optical meter, and the USB spectrofluorometer as well as recording the data. The digital source meter applied the voltages to the device and measured the resulting currents. The multifunction optical meter connected with the calibrated photodiode served in the measurement of the luminance (brightness). The USB spectrofluorometer was used for the EL spectra acquisition.
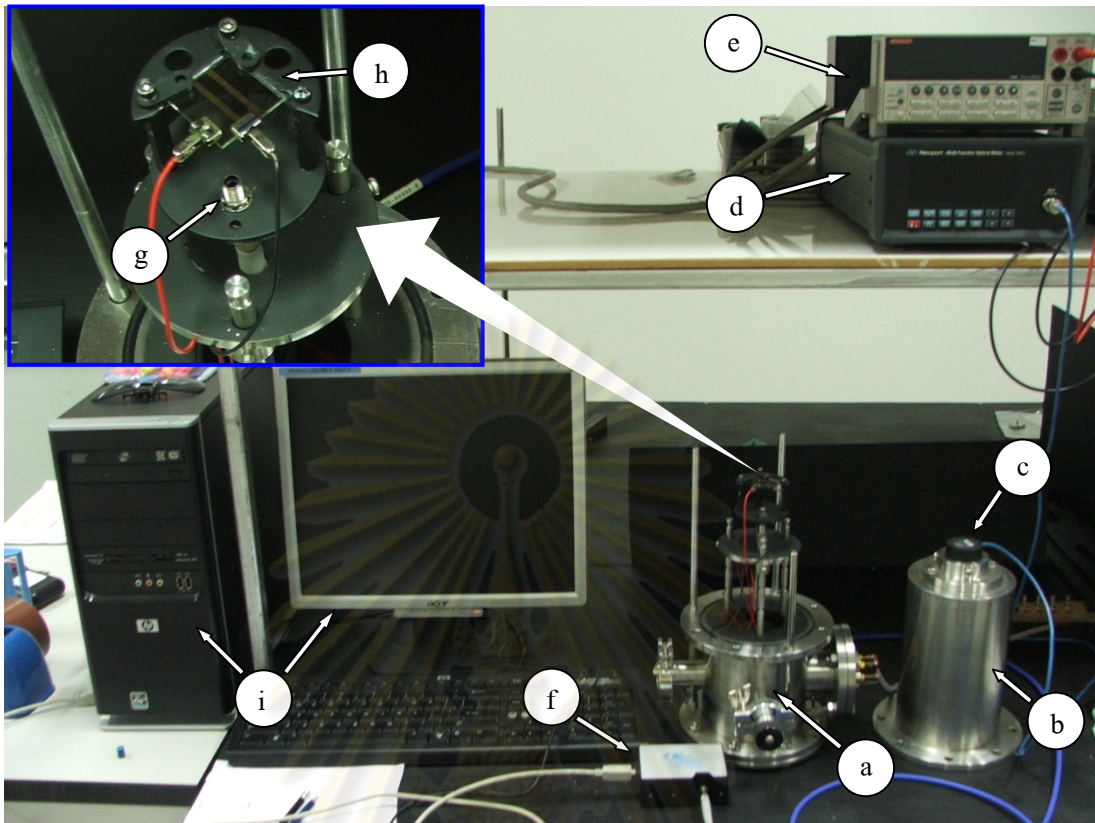
Figure 2.8 Instruments for determination of OLED device performance: (a) OLED test box, (b) lid of OLED test box, (c) calibrated photodiode, (d) multifunction optical meter, (e) digital source meter, (f) USB spectrofluorometer, (g) probe of USB spectrofluorometer, (h) OLED device holder, (i) computer controller and recorder for digital source meter, multifunction optical meter, and USB spectrofluorometer.

All device measurements were performed in an OLED test box by blocking the incident light at room temperature under ambient atmosphere. When voltages were applied, the currents, brightness, and EL spectra were recorded at the same time to give the current density–voltage–luminance (*J-V-L*) characteristics and EL spectra. The turn-on voltage was defined at the brightness of 1 cd/m^2. The current density was calculated as the following formula (1):

$$J = \frac{I}{A} \tag{1}$$

Here, I (mA) is the current and A (cm^2) is the pixel active area of the device. The efficiency of the device was calculated as the following formula (2):

$$\text{Efficiency} = \frac{L}{J} \tag{2}$$

Here, L (cd/m^2) is the luminance and J (mA/cm^2) is the current density.

2.2.13 The coordinate value calculation of Commission Internationale de l'Eclairage 1931 (CIE 1931)

The coordinate value of CIE 1931 was calculated from the EL spectrum. In the study of the perception of color, one of the first mathematically defined color spaces was the CIE 1931 XYZ color space, created by the International Commission on Illumination (CIE) in 1931 [99,100]. The CIE XYZ color space was derived from a series of experiments done in the late 1920s by Wright [70] and Guild [71]. Their experimental results were combined into the specification of the CIE RGB color space, from which the CIE XYZ color space was derived. Firstly, the tristimulus value was calculated as the following formula (3):

$$X = 683 \int_{360}^{830} S(\lambda)\bar{x}(\lambda)\Delta(\lambda), \; Y = 683 \int_{360}^{830} S(\lambda)\bar{y}(\lambda)\Delta(\lambda), \; Z = 683 \int_{360}^{830} S(\lambda)\bar{z}(\lambda)\Delta(\lambda) \tag{3}$$

Here, $S(\lambda)$ is the spectral data; X, Y, and Z are the tristimulus values; and $\bar{x}$, $\bar{y}$, and $\bar{z}$ are the tristimulus functions.

The coordinate value of CIE 1931 was calculated from formula (4):

$$\text{CIE 1931 } x = \frac{X}{X+Y+Z} \; , \text{CIE 1931 } y = \frac{Y}{X+Y+Z} \tag{4}$$

The CIE 1931 chromaticity is shown in **Figure 2.9**.
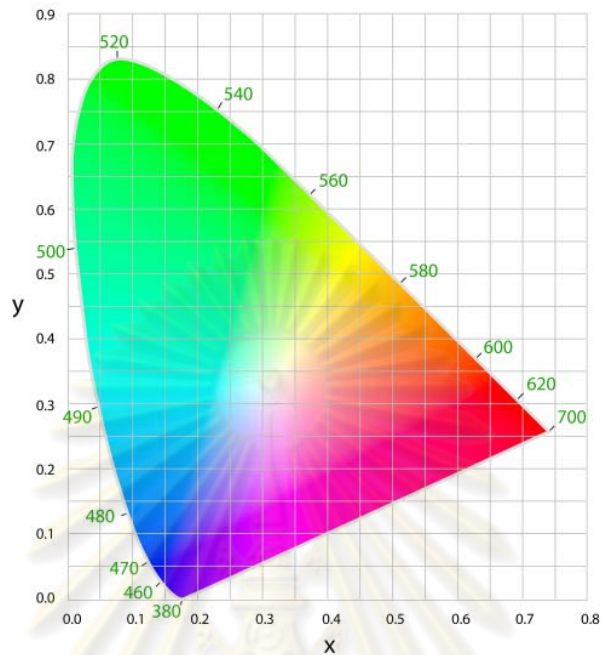
Figure 2.9 CIE 1931 chromaticity.

      Note; the parameters used to evaporate all materials are the parameters of Al only, such as density of Al = 2.7. Thus, to evaluate the real thickness of the organic layers deposited by thermal evaporator and the thickness of PEDOT:PSS layer deposited by spin coating method, in the future, the glass substrate will be measured by scanning electron microscope (SEM) or/and the atomic force microscope (AFM). The real calculation of the CIE coordinate was obtained by the Microsoft office excel 2007 with the calculated formula of CIE 1931.

CHAPTER III

RESULTS AND DISCUSSION

3.1 Synthesis

Three derivatives of 3,6-dipyrenylcarbazole (**2PCT**, **4P2C**, **2PCP**) were synthesized with a 3,6-di(pyren-1-yl)-9*H*-carbazole unit (**8**) as a common building block. Initially, compound **8** was synthesized by a two-steped procedure (**Figure 3.1**). The carbazole was iodinated regioselectively at the 3- and 6-position using KI/KIO$_3$ in refluxing acetic acid for 20 minutes to afford 3,6-diiodo-9*H*-carbazole (**7**) as a brown solid in 98% yield after recrystallization. The structure of **7** was confirmed by ^{1}H and ^{13}C NMR which were in good agreement with the literature report [72]. The ^{1}H NMR of **7** in DMSO-*d*6 (**Figure 3.2**) showed a singlet peak at 11.56 ppm for H(a), two doublet peaks at 7.67 and 7.36 ppm for H(b) and H(c), respectively, and a singlet peak at 8.57 ppm for H(d).
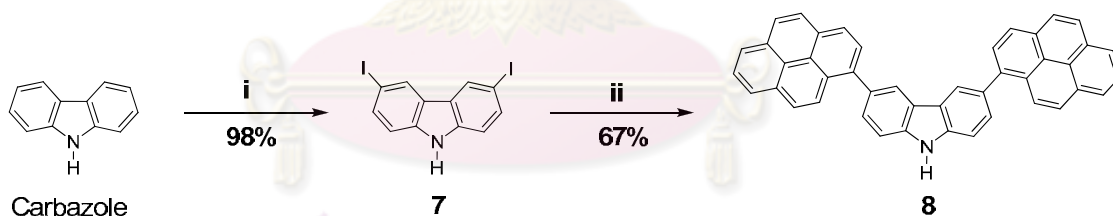
Figure 3.1 The synthesis of **8**. Reagents and conditions: (i) KI, KIO$_3$, acetic acid, reflux, 20 min; (ii) pyrene-1-boronic acid, Pd(PPh$_3$)$_4$, 2M K$_2$CO$_3$, THF, reflux, 24 h.
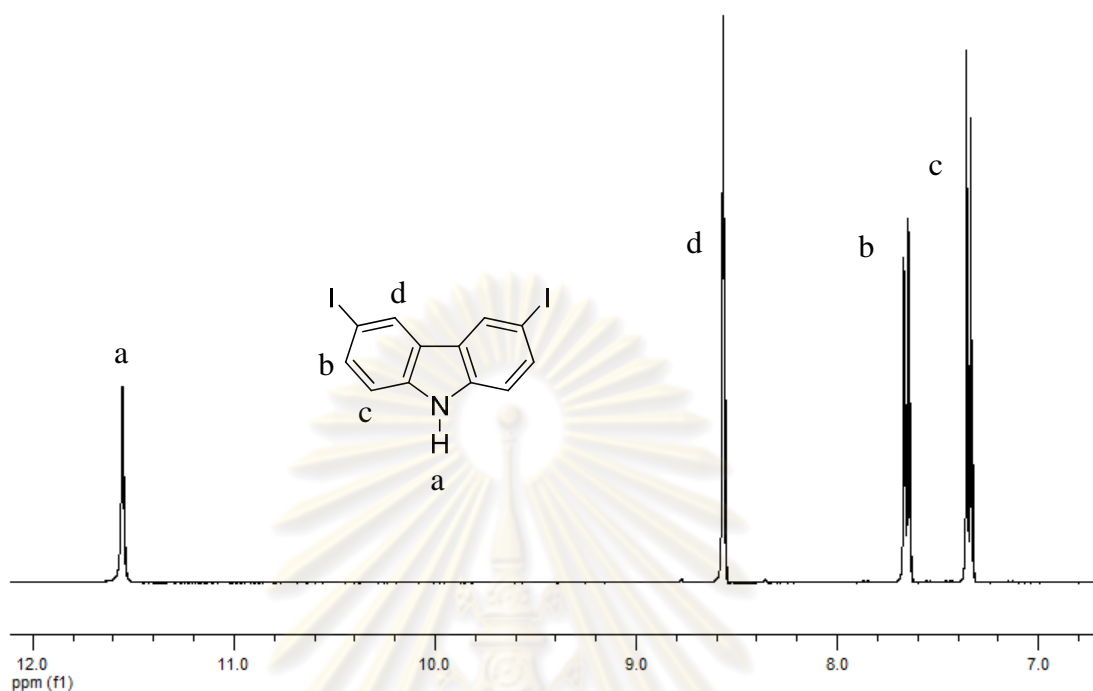
Figure 3.2 Expanded ^{1}H NMR of **7** in DMSO-*d*6.

      The second step involved a coupling of **7** with the commercially available pyrene-1-boronic acid using Suzuki coupling reaction [73-75]. In our early attempts, Pd(OAc)$_2$ was used as a catalyst and the K$_2$CO$_3$ was functioned as a base in a 9:1 mixture of dioxane and H$_2$O (**Table 3.1**). Unfortunately, this condition was not effective for the synthesis as there was no evidence for product observed by TLC analysis. In addition, not much improvement was achieved when a 2M aqueous solution of K$_2$CO$_3$ was used as a base and toluene was utilized as the solvent under a catalysis by either Pd(OAc)$_2$ or Pd(OAc)$_2$-CuI. By changing the Pd catalyst to Pd(PPh$_3$)$_4$ under the conditions outlined in entry 4 (**Table 3.1**), the desired dipyrenylcarbazole (**8**) was successfully obtained as a pale green solid in 67% yield after a column chromatography on silica gel.

Table 3.1 Suzuki cross coupling conditions.

Entry	Catalyst	Base	Solvent	Temp.	Yield (%)
1	Pd(OAc)$_2$	K$_2$CO$_3$	Dioxane : H$_2$O	Reflux	0[a]
2	Pd(OAc)$_2$	2M K$_2$CO$_3$	Toluene	Reflux	0[a]
3	Pd(OAc)$_2$ + CuI	2M K$_2$CO$_3$	Toluene	Reflux	0[a]
4	Pd(PPh$_3$)$_4$	2M K$_2$CO$_3$	Toluene	Reflux	67

[a] No product was detected by TLC.

The mechanism of Suzuki-cross coupling reaction (**Figure 3.3**) involves a three-steped cycle: oxidative addition, transmetallation and reductive elimination. Starting with the oxidative coupling of aryl halide (**7**) with Pd(0) to give a Pd(II) complex, transmetallation with boronic acid in basic condition gives rise to the intermediate (**12**) which undergoes a reductive elimination to eventually afford the coupling product and regenerate the active palladium species.
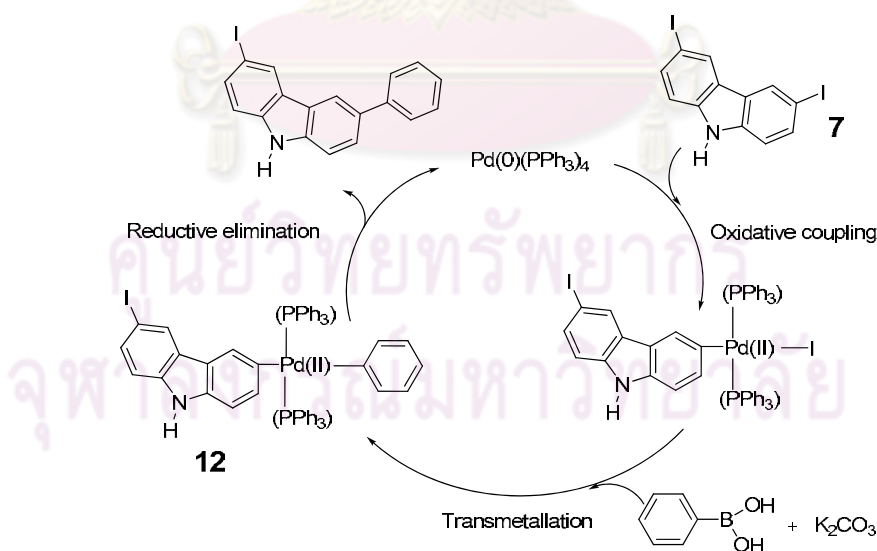
Figure 3.3 The mechanism of Suzuki-cross coupling reaction.

The chemical structure of **8** was confirmed by ^{1}H and ^{13}C NMR as well as mass spectrometry. The ^{1}H NMR of **8** (**Figure 3.4**) in DMSO-*d*6 showed a singlet peak at 11.72 ppm for H(a), two doublet peaks at 7.80 ppm (J = 8.3 Hz) and 7.70 ppm (J = 8.3 Hz) for H(b) and H(c), a singlet peak at 8.50 ppm for H(d), a doublet peak at 8.36 ppm (J = 7.8 Hz) for H(e) and a triplet peak at 8.06 ppm (J = 7.6 Hz) for H(f).

Figure 3.4 ^{1}H NMR of **8** in DMSO-*d*6 (inset is the expansion of the aromatic region).

The synthesis of target molecule **2PCT** is shown in **Figure 3.5**. 1-Iodo-4-methylbenzene (**9**) was prepared in house by a sequential diazotization-iodination reaction of *p*-toluidine. The target molecule was synthesized by the reaction of **8** with an excess amount of **9** under a Cu-catalyzed C-N coupling conditions in the presence of Cu-bronze and K_2CO_3 in refluxing nitrobenzene. **2PCT** was obtained as a pale green solid in 56% yield.
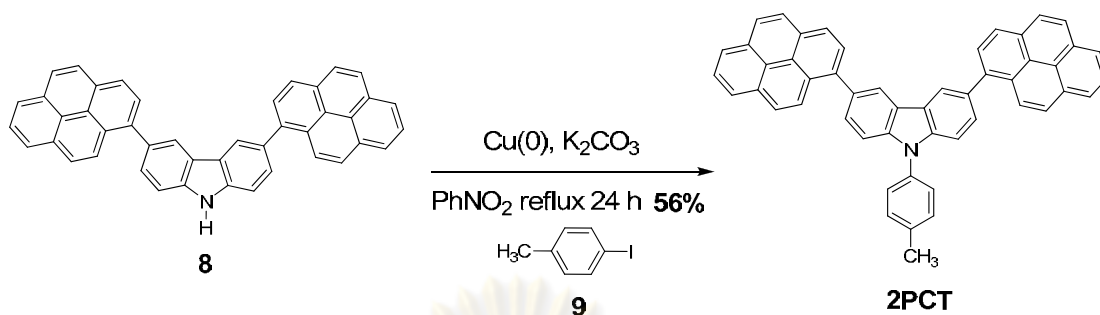
Figure 3.5 The synthesis of **2PCT**.

The mechanism of Cu-catalyzed C-N coupling reaction is illustrated in **Figure 3.6**. Initially, the N-H carbazole is deprotonated catalytically by K_2CO_3, presumably accelerated by the formation of a Cu-carbazole complex (**13**) as the first intermediate. An oxidative addition between the complex **13** and the aryl halide then takes place to yield the intermediate **14**. The last step involves a reductive elimination to give the final *N*-arylated product and regenerate the Cu(0) catalyst.
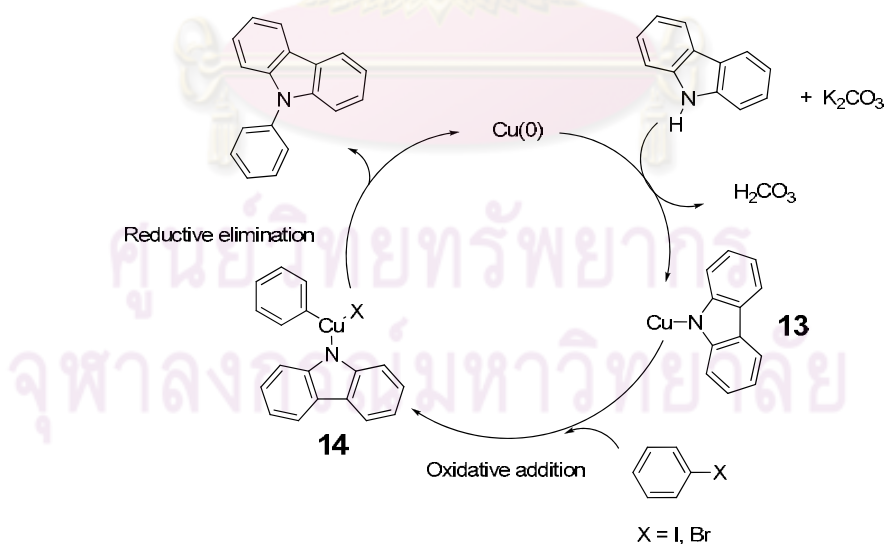
Figure 3.6 The mechanism of Cu-catalyzed C-N coupling reaction.

The chemical structure of **2PCT** was verified by ^{1}H NMR, ^{13}C NMR, mass spectroscopy and elemental analysis. The ^{1}H NMR of **2PCT** (**Figure 3.7**) in CDCl$_3$ showed a singlet peak at 2.56 ppm for H(a), a doublet peak at 7.52 ppm (J = 8.0 Hz) for H(b), a doublet peak at 7.66 ppm (J = 7.5 Hz) for H(c), a doublet peak at 7.64 ppm (J = 8.3 Hz) for H(d), a doublet peak at 7.73 ppm (J = 8.4 Hz) for H(e) and a singlet peak at 8.44 ppm for H(f).
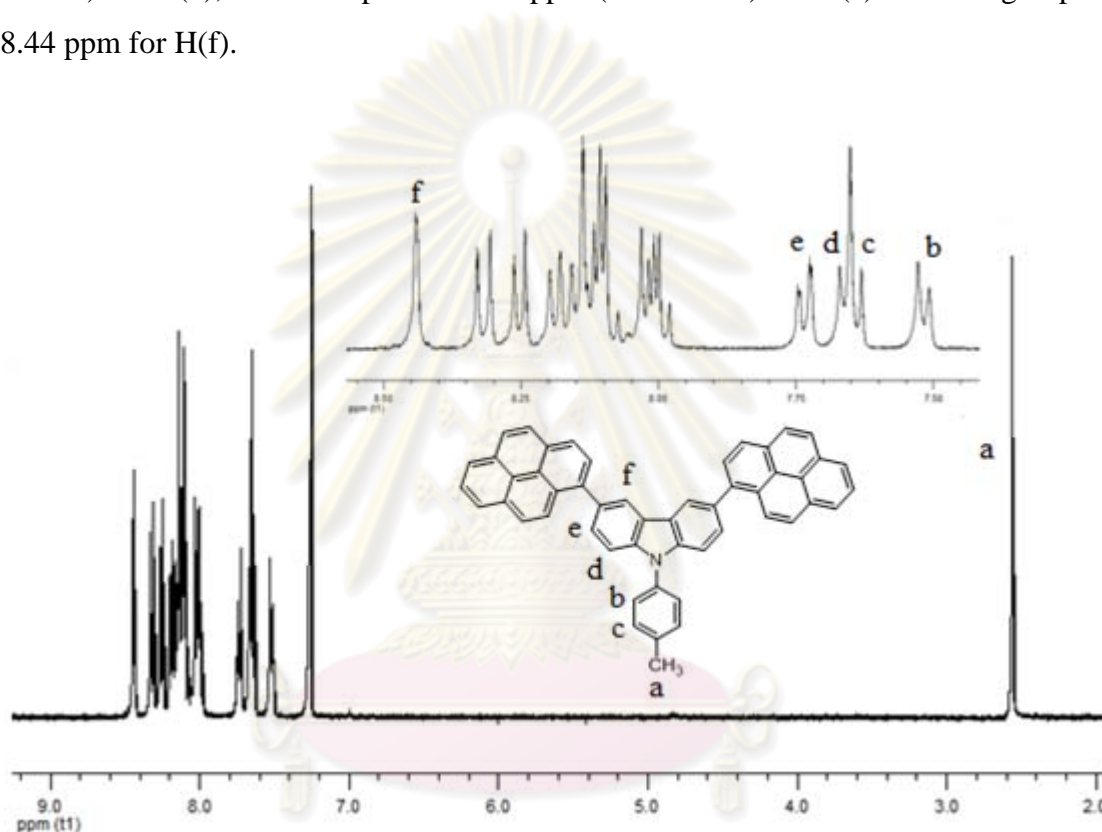
Figure 3.7 ^{1}H NMR of **2PCT** in CDCl$_3$ (inset is the expanded of aromatic region).

The synthesis of another target molecule, **4P2C,** is shown in **Figure 3.8**. First, ethane-1,2-diyl bis(2-chloroacetate) (**10**) was prepared by double chloroacylation of ethylene glycol with chloroacetyl chloride [76]. The target molecule was synthesized by *N*-alkylation of **8** with an excess amount of **10** in the presence of K$_2$CO$_3$ in DMSO at room temperature. **4P2C** was obtained as a slightly yellow solid in 42% yield.
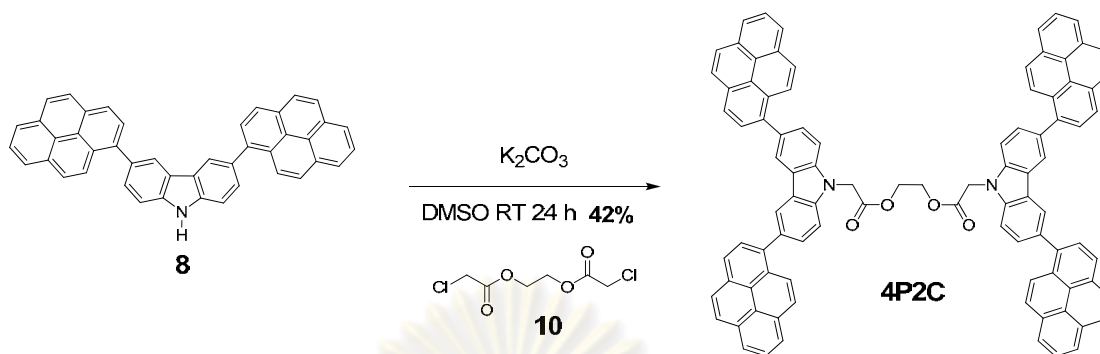
Figure 3.8 The synthesis of **4P2C**.

The structure of **4P2C** was characterized by ^{1}H NMR, ^{13}C NMR, mass spectrometry and elemental analysis. The ^{1}H NMR of **4P2C** (**Figure 3.9**) in CDCl$_3$ showed a singlet peak at 4.55 ppm for H(a), a singlet peak at 5.11 ppm for H(b), a doublet peak at 7.44 ppm (J = 8.4 Hz) for H(c), a doublet peak at 7.67 ppm (J = 8.3 Hz) for H(d) and a singlet peak at 8.37 ppm for H(e).
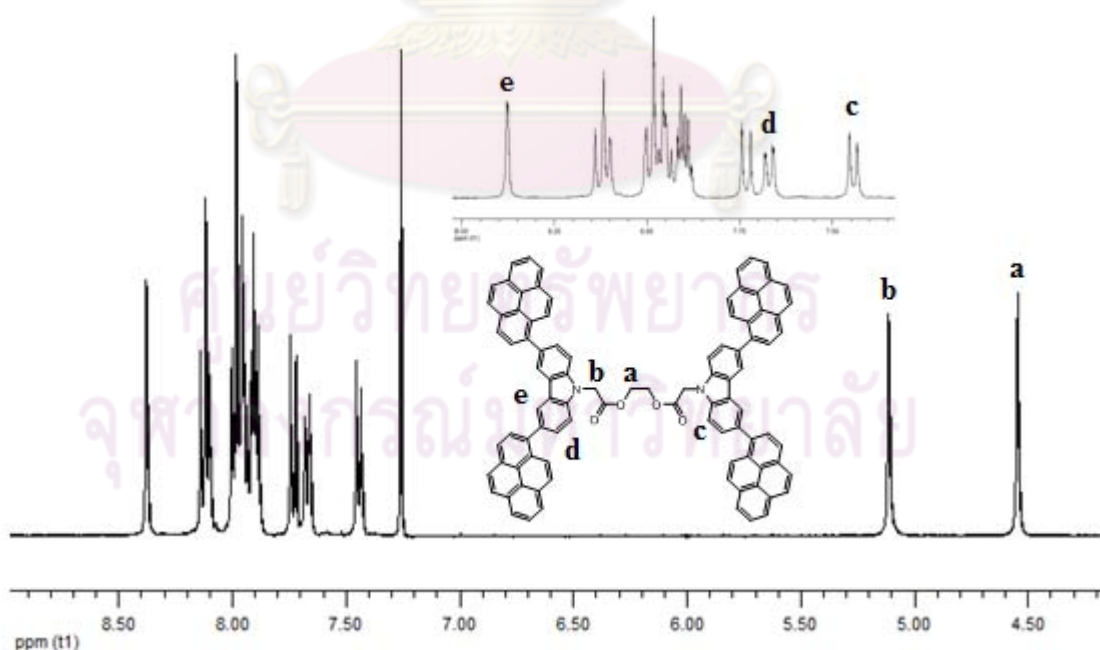
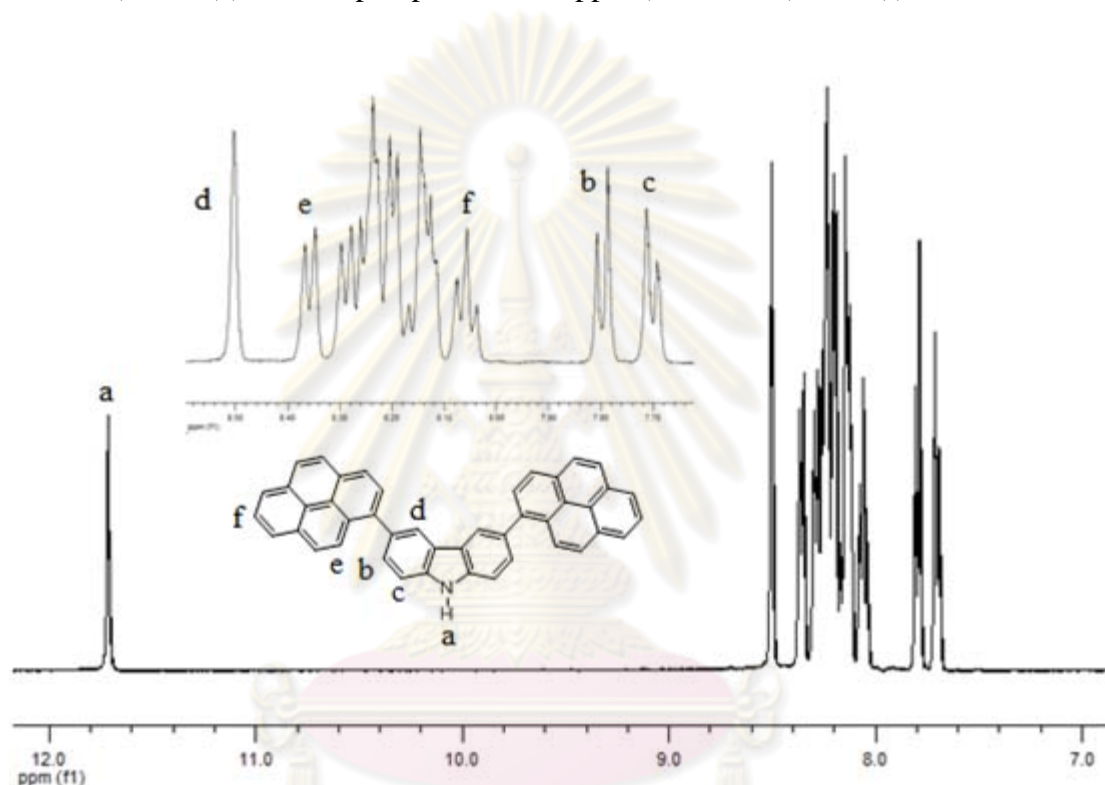**Figure 3.9** ^{1}H NMR of **4P2C** in CDCl$_3$ (inset is the expansion of the aromatic region).

The synthesis of target molecule **2PCP** is shown in **Figure 3.10**. 4-bromo-*N,N*-diphenylaniline (**11**) was prepared by bromination of triphenylamine using *N*-bromosuccinimide [77]. The target molecule was synthesized by reaction of the building block **8** with aryl bromide **11** under Cu-catalyzed C-N coupling conditions in which the Cu-bronze was used as a catalyst and K_2CO_3 as base in refluxing nitrobenzene. The expected compound **2PCP** was obtained after chromatographic purification as a pale yellow solid in 70% yield.
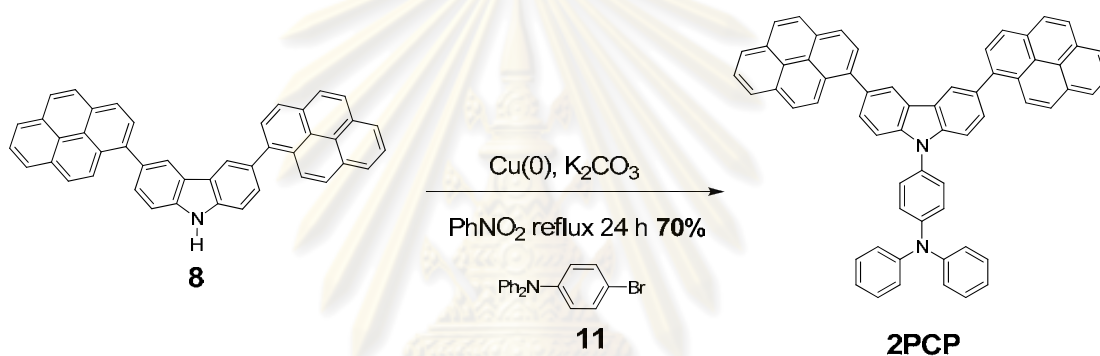
Figure 3.10 The synthesis of **2PCP**.

The structure of **2PCP** was confirmed by ^{1}H NMR, ^{13}C NMR, mass spectrometry and elemental analysis. The ^{1}H NMR of **2PCP** (**Figure 3.11**) in CDCl$_3$ shows a quartet peak at 7.13 ppm for H(a), a doublet peak at 7.37 ppm (J = 7.5 Hz) for H(b), a doublet peak at 7.61 ppm (J = 7.8 Hz) for H(c), a doublet peak at 7.70 ppm (J = 8.3 Hz) for H(d), a doublet peak at 7.76 ppm (J = 8.3 Hz) for H(e) and a singlet peak at 8.44 ppm for H(f).
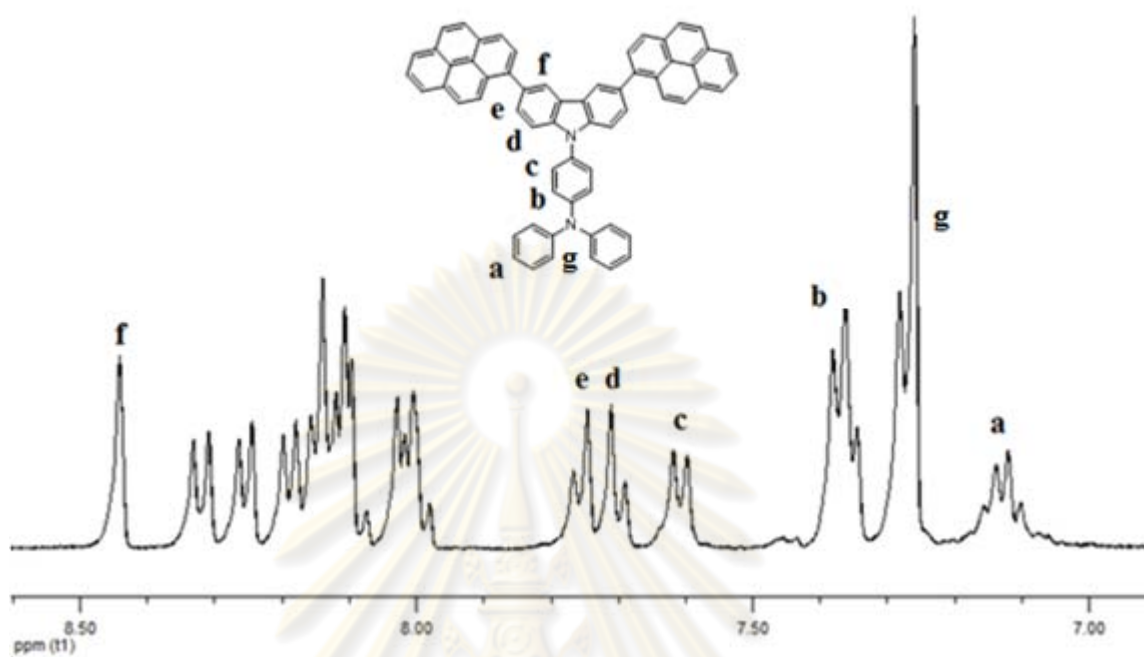
Figure 3.11 Expanded ^{1}H NMR of **2PCP** in CDCl$_3$.

3.2 Optical properties

The UV-Vis absorption and emission spectra of **2PCT**, **4P2C**, and **2PCP** were obtained both in CH$_2$Cl$_2$ solution phase and thin film. The results are summarized in **Table 3.2**. In solution phase, the absorption spectra of all three compounds appeared very similar in which there were three bands at 250, 280, and 350 nm. Although these absorption bands were in the same region as free carbazole and pyrene, their relatively broader shapes indicated a strong electronic coupling between these two π-conjugated units. This electronic communication was also evident by the fact that the emission wavelengths of **2PCT**, **4P2C**, and **2PCP** were significantly longer than that of pyrene [78]. Compound **2PCT**, **4P2C**, and **2PCP** exhibited the maximum wavelength of absorption at 347, 347 and 345 nm, respectively (**Figure 3.12**). The optical band gap energies of **2PCT**, **4P2C**, and **2PCP** were then calculated from the onset wavelength of absorption spectra to be 3.06, 3.06 and 2.73 eV, respectively. For the thin films obtained by spin casting technique, the solid phase absorption spectra of all three compounds exhibited a significant bathochromic shift indicating a better π-electron delocalization in

the conjugated systems which is probably a result of a greater planarity between the carbazole and pyrene units forced by the solid-state packing [79].
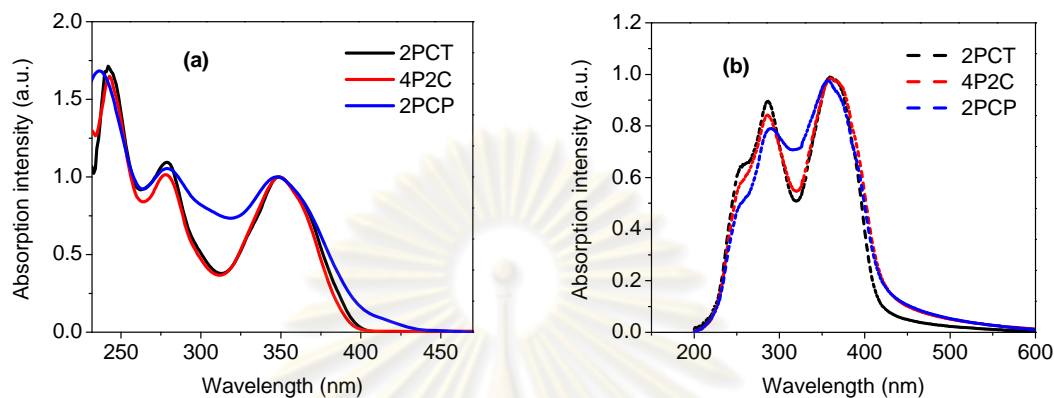
Figure 3.12 Absorption spectra of **2PCT**, **4P2C**, **2PCP** in CH_2Cl_2 (a) and thin film (b).

The fluorescence spectra obtained from CH_2Cl_2 solutions of **2PCT** and **4P2C** exhibited maximum emission wavelengths at 427 and 425 nm, respectively (**Figure 3.13**). The fact that the two spectra were very similar suggested that the luminescent moiety of these molecules should be the dipyrenylcarbazole unit. With two dipyrenylcarbazole units connected with a flexible glycolic chain, **4P2C** showed an emission shoulder at 470 nm corresponding to the pyrene excimer [80]. For compound **2PCP** containing a triphenylamine group, the maximum emission peak appeared at a longer wavelength (465 nm), while its absorption band appeared at the same location as **2PCT** and **4P2C**. These suggest that the incorporation of triphenylamine moiety promotes the electron-vibration coupling in the electronic excited state of **2PCP** resulting in the geometrically relaxed exciton with lower energy. The quantum yield of **2PCT**, **4P2C**, and **2PCP** were 0.79, 0.79 and 0.73 respectively, measured from CH_2Cl_2 solutions (A<0.1) at room temperature using quinine sulfate solution in 0.01 M H_2SO_4 ($\Phi_F = 0.54$) as the standard. In solid states (thin films) which were prepared by spin casting technique, the emission spectra of **2PCT** and **4P2C** showed substantial bathochromic shifts (~ 30 and 35 nm, respectively). These results can describe with the same reason in the absorption spectra. Since both the absorption and emission spectra of the three compounds in solid state were very similar in shape and wavelength, it may be assumed

that the dipyrenylcarbazole is the photoactive module in these compounds, regardless of the substituent on the nitrogen atom. In addition, the solid state emission spectra of **2PCP** exhibited a hypsochromic shift compared to the solution phase spectrum. This result may also be attributed to the aforementioned solid-state packing force which geometically precludes the electron-vibration coupling between the triphenylamine substituent and the photoactive unit.
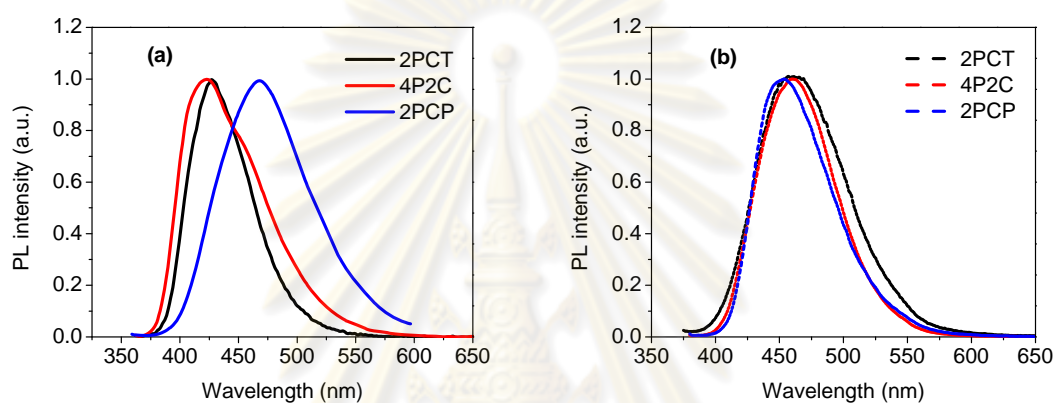
Figure 3.13 Fluorescence spectra of **2PCT**, **4P2C** and **2PCP** in CH_2Cl_2 (a) and thin film (b).

Table 3.2 Optical properties of dipyrenylcarbazole derivatives **2PCT**, **4P2C** and **2PCP** measured in CH_2Cl_2 solutions and in thin films.

Compound	λ_{max}^{Abs}/nm ($\log\varepsilon$/dm^{3}mol^{-1}cm^{-1})		λ_{max}^{Emit}/nm		Φ_F^e	E_g^f/eV
	Solution[a]	Thin film[b]	Solution[c]	Thin film[d]		
2PCT	347(4.87)	359	427	456	0.79	3.06
4P2C	347(5.15)	360	425	460	0.79	3.06
2PCP	345(4.94)	356	465	453	0.73	2.73

[a] The absorption spectra from the UV-Vis spectra measured in dilute CH_2Cl_2 solution.
[b] The absorption spectra from the UV-Vis spectra measured in thin film. [c] The PL emission excited at the absorption maxima in dilute CH_2Cl_2 solution. [d] The PL emission excited at the absorption maxima in thin film.
[e] PL quantum yield determined in CH_2Cl_2 solution (A<0.1) at room temperature using quinine sulfate solution in 0.01 M H_2SO_4 ($\Phi_F = 0.54$) as a standard.
[f] The optical energy gap estimated from the onset of the absorption spectra ($E_g = 1240/\lambda_{onset}$).

3.3 Electrochemical property

Cyclic voltammetry (CV) is an electroanalytical technique measuring the electrical current versus potential of a solution of a compound (analyte). A typical electrochemical cell consists of three electrodes which are called the working, the counter (auxiliary) and the reference electrodes, all of which are controlled by a potentiostat. The potential difference is applied between the working and the reference electrodes. For the reference electrode, there is no current flow and it functions as the electrode from which the potentials of the other electrodes are measured. The electrical circuit is completed by the use of the counter electrode. Apart from the analyte, the solutions should also contain an electrolyte which can decrease the effect of electrical migration due to charge attraction and repulsion.

In a CV experiment the potential is varied with time, either in a positive or negative direction, in a linear sweep to a potential E_λ, called the switching potential, and then back to the starting potential (**Figure 3.14a**). During the linear sweep potential, the

current is measured and the presence of a peak during a sweep indicates that a redox process has occurred (**Figure 3.14b**).
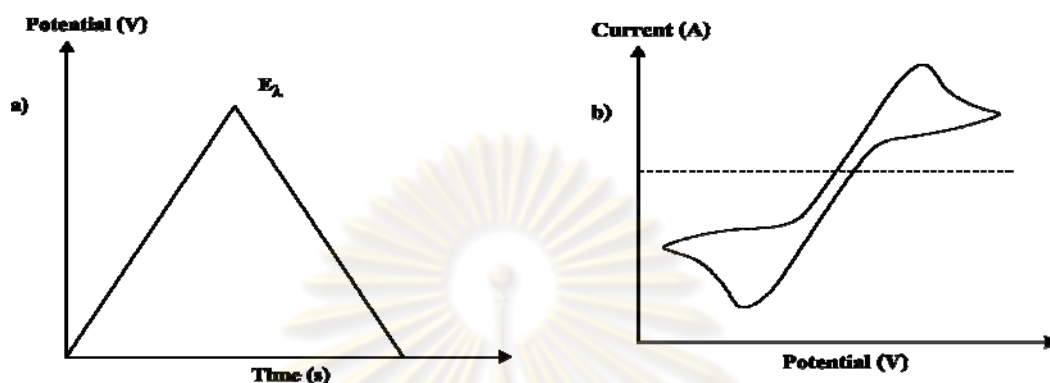
Figure 3.14 a) the triangular potential sweep used for CV b) a quasi-reversible CV traces for a redox process.

A negative sweep of potential can cause reduction and a positive sweep can cause oxidation. If there is a reverse of the peak observed in the forward potential sweep, then the redox process is chemically reversible. This means the reduced or oxidized species is stable or the kinetics of the electron transfer process between the electrodes and the solution are fast on the timescale of the experiment. If there is no reverse peak, the redox process may be chemically irreversible. The irreversibility may result from either the chemical process occurs faster than the experiment time scale, or the heterogeneous electron transfer is slower than the experiment time scale. In CV, with a reversible oxidation and reduction process, the difference in potential (ΔE_p) between the cathodic and anodic peaks for a one-electron process at 25 $^{\circ}$C is 57 mV. This value for a two-electron process is 28.5 mV. When ΔE_p is significantly greater than 57 mV at 25 $^{\circ}$C but the oxidation and reduction are chemically reversible, the process is considered as quasi-reversible which can occur when reduced or oxidized species is stable, but the rate of heterogeneous electron transfer between the compound and the electrode is slow in comparison to the experiment timescale.

In this work all CV experiments were performed in dry dichloromethane using a platinum wire counter electrode, a Ag/AgCl/NaCl reference electrode, and glassy carbon working electrode. The electrolyte was *tetra*-n-butylammonium hexafluorophosphate which was chosen for its good solubility in organic solvents. The electrolyte concentration was 0.1 M, and the concentration of the analytes (dipyrenylcarbazole derivatives) was 1.0 mM. It is important to use anhydrous solvents degassed with an inert gas because O_2 is a good radical scavenger and can react with many oxidized and reduced species. The internal standard was the ferrocenium/ferrocene (Fc^+/Fc) couple, and the data is relative to this standard. The values of $E_{1/2}$ of redox couples are the average values of the cathodic and anodic potentials.

The redox potentials of **2PCT**, **4P2C** and **2PCP** in CH_2Cl_2 solution at a scan rate of 0.05 V/s are compiled in **Table 3.3** and the cyclic voltammograms of all compounds are shown in **Figure 3.15**.
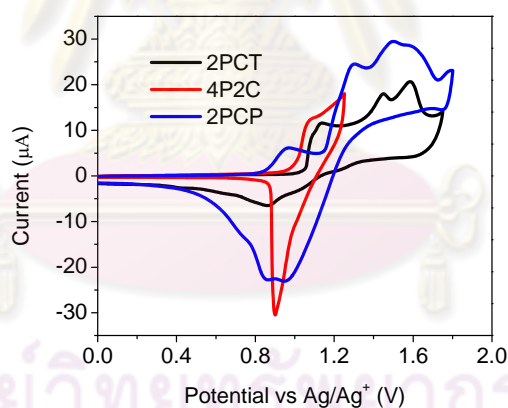
Figure 3.15 Cyclic voltammograms of **2PCT**, **4P2C** and **2PCP** in dry CH_2Cl_2.

The electrochemical stability of all compounds was tested by seven subsequent redox cycles. Compounds **2PCT** and **2PCP** which have aromatic substituents on their carbazole nitrogens were electrochemically unstable (**Figure 3.16**).
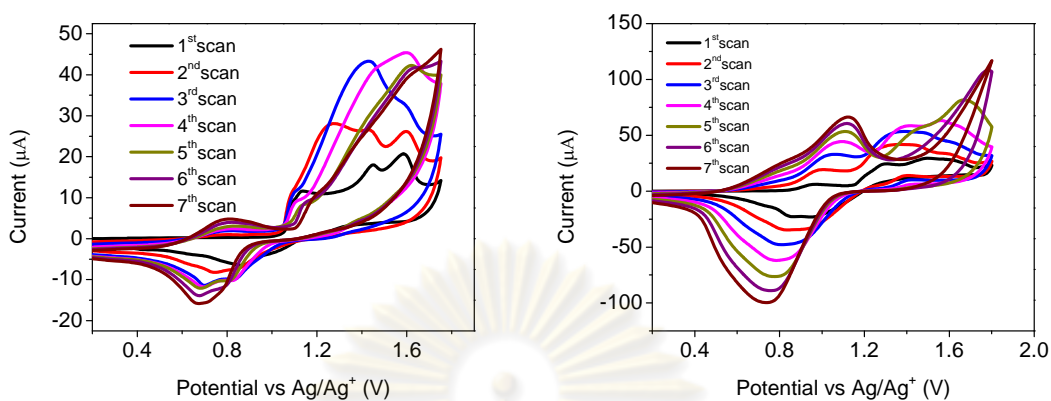
Figure 3.16 Multi scan of **2PCT** (left) and **2PCP** (right) in dry CH_2Cl_2 with 0.1 M *n*-Bu_4NPF_6 electrolyte at a scan rate of 0.05 V/s.

For **2PCT**, the oxidation may first take place at the nitrogen atom. Subsequent delocalization of the unpaired electron and a loss of hydrogen radical could lead to a benzylic radical-cation that could undergo a dimerization (**Figure 3.17**).
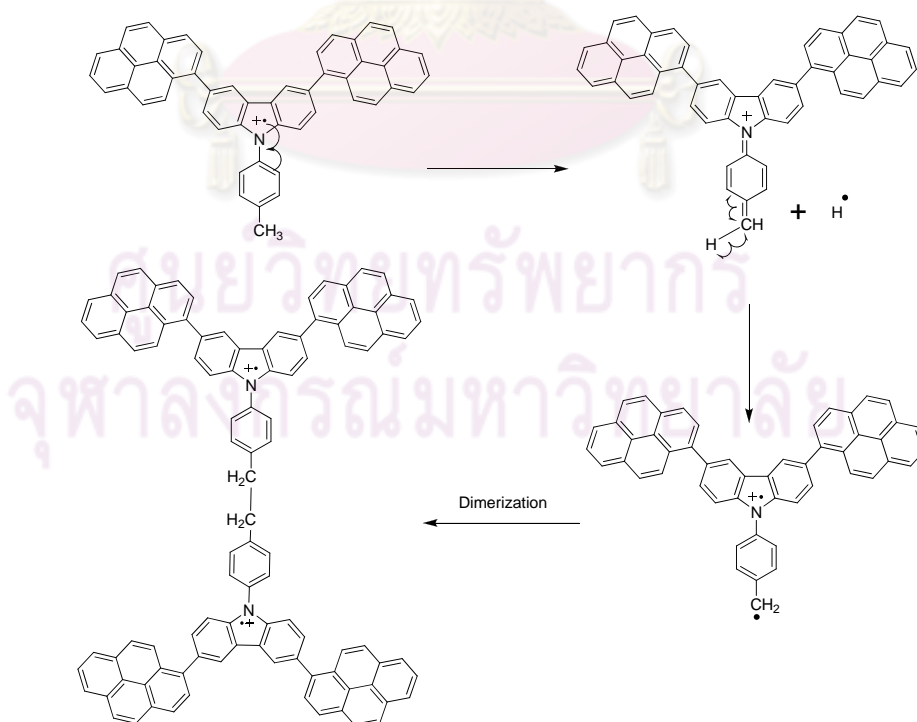
Figure 3.17 Dimerization process of **2PCT**.

In the case of **2PCP**, the dimerization could occur at the *p*-position of one of the phenyl rings in the triphenylamine moiety (**Figure 3.18**). The observation of these oxidative couplings is in good agreement with results previously reported for other systems containing triphenylamine [81,82].
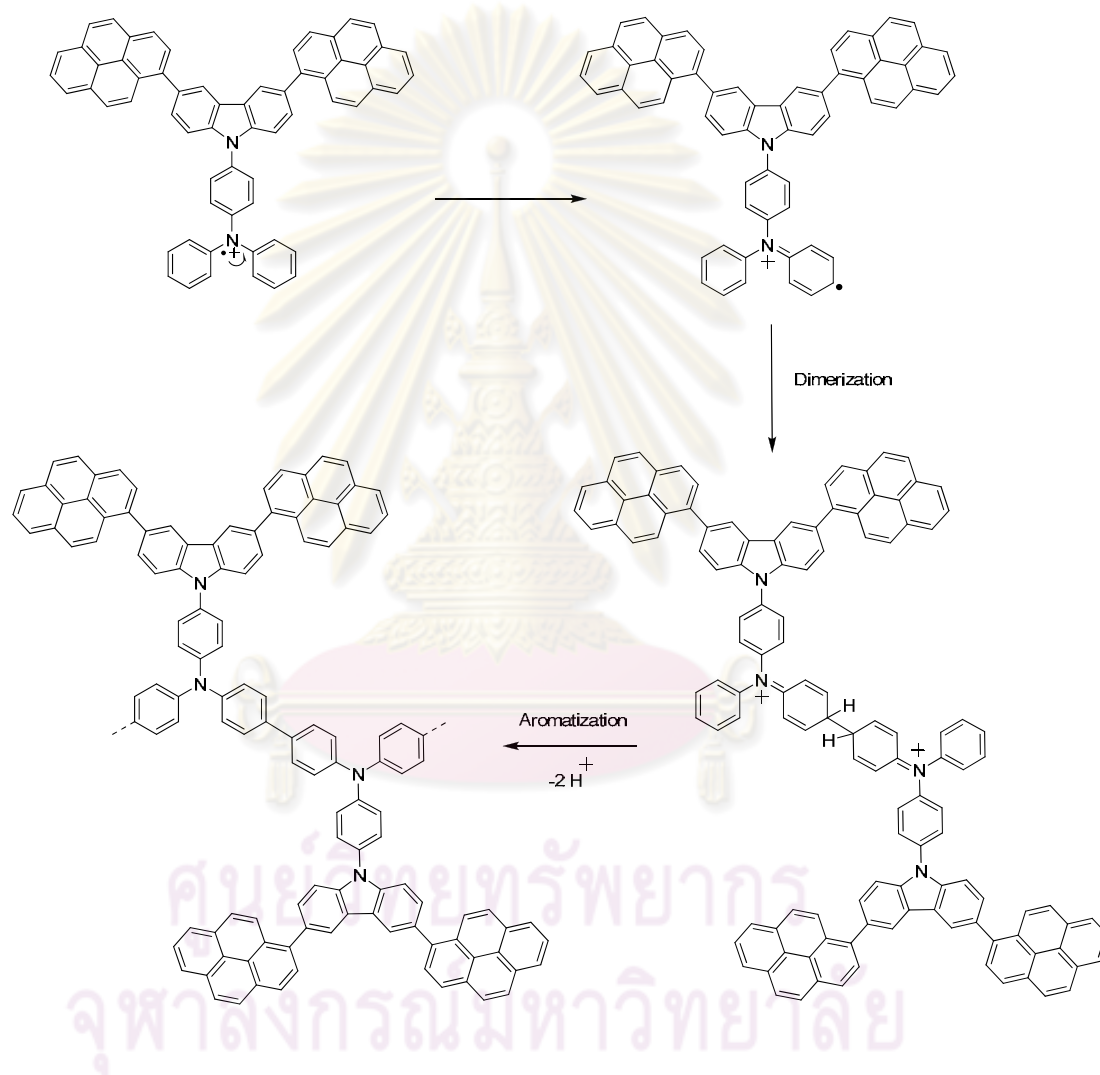
Figure 3.18 Dimerization process of **2PCP**.

Repetitive scanning by cyclic voltammeter revealed that **4P2C** had a good electrochemical stability as it did not show any change on cyclic voltammogram during a duplicated scanning process (**Figure 3.19**).
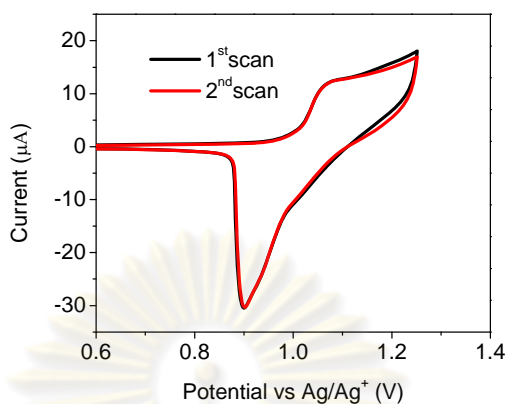
Figure 3.19 Two potential scanning of **4P2C** in dry CH_2Cl_2 with 0.1 M n-Bu_4NPF_6 electrolyte at a scan rate of 0.05 V/s.

The HOMO energy levels were calculated from the onset of oxidation potential (E_{onset}) according to an empirical formula, HOMO = -(4.44+E_{onset}) (eV) [83,84]. The LUMO energy levels were calculated by subtracting the HOMO energy levels with the energy band gaps estimated from the onset of UV–Vis absorption. The results are shown in **Figure 3.20** and tabulated in **Table 3.3**. The HOMO energy levels of all compounds were in the range of 5.29-5.50 eV, which were lower than ITO (4.80 eV). It is therefore possible that these compounds could reduce the energy barrier for the hole injection from ITO to the emissive material such as Alq_3 (5.70 eV).
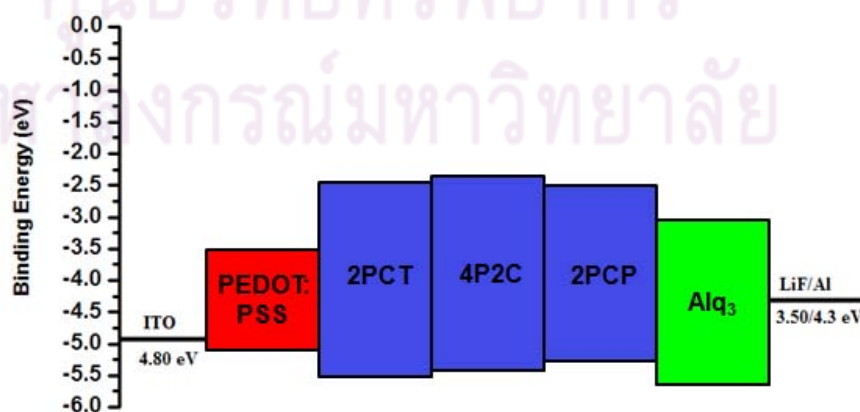
Figure 3.20 Band diagram of ITO, PEDOT:PSS, **2PCT, 4P2C, 2PCP**, Alq3 and LiF:Al.

Table 3.3 The electrochemical properties of **2PCT**, **4P2C** and **2PCP**.

Compound	$E_{1/2}/V$ ($\Delta E^a/mV$)	HOMO[b] (eV)	LUMO[c] (eV)
2PCT	1.09(129)	5.50	2.44
4P2C	1.03(170)	5.44	2.38
2PCP	0.91(85)	5.29	2.56

[a] Measured using a platinum disk as a working electrode, a platinum rod as a counter electrode, and SCE as a reference electrode in CH_2Cl_2 containing 0.1M n-Bu$_4$NPF$_6$ as a supporting electrolyte at a scan rate of 50 mV/s under an argon atmosphere. [b] Calculated by the empirical equation: HOMO = $(4.44 + E_{onset})$. [c] Calculated from LUMO = HOMO - E_g.

3.4 Thermal property

For optoelectronic applications, the thermal stability of organic materials is crucial for device stability and lifetime. The degradation of organic optoelectronic devices depends on morphological changes resulting from the thermal stability of the amorphous organic layer. Morphological change might be promoted by rapid molecular motion near the glass transition temperature (T_g). The thermal properties of all compounds were determined by differential scanning calorimetry (DSC) and thermogravimetric analysis (TGA) under nitrogen atmosphere.

The thermal properties of **2PCT**, **4P2C** and **2PCP** are shown in **Figure 3.21** and summarized in **Table 3.4**. The TGA curves suggested that all three compounds were thermally stable with 5% weight loss temperatures ($T_d^{5\%}$) at 459, 414 and 398 °C, respectively. During the second heating cycle in the DSC experiments, there were sharp endothermic peaks for **2PCT** at 354 °C due to melting temperature (T_m). Compound **2PCT** also showed an endothermic baseline shift due to glass transition temperature (T_g) at 165 °C and an exothermic peak at 294 °C due to crystallization. For compound **4P2C**, only a T_g at 199 °C was observed and there were no signals for crystallization or melting upon further heating. For compound **2PCP**, there was no endothermic peak on both the first and second heating cycle, but a T_g of 166 °C was observed. These results suggested that the amorphous compounds **4P2C** and **2PCP** are able to form molecular glasses with high T_g.
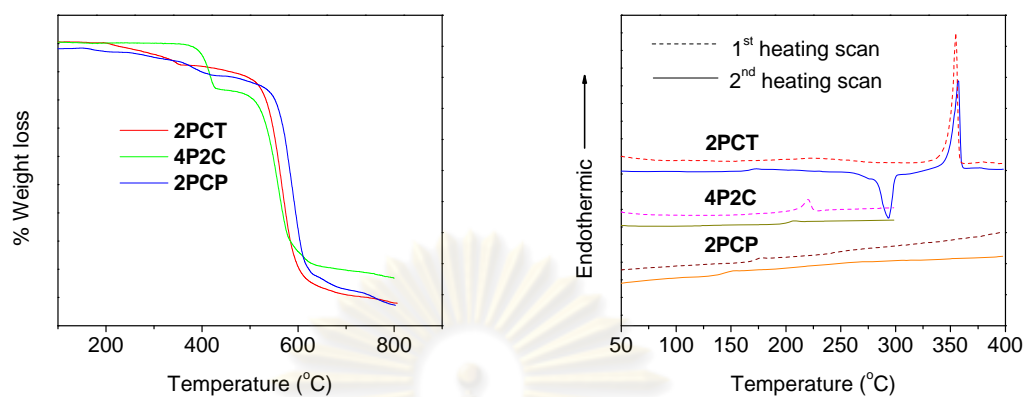
Figure 3.21 DCS (right) and TGA (left) traces of **2PCT**, **4P2C** and **2PCP** measured under nitrogen atmosphere at heating rate of 10 $^{\circ}$C/min.

Table 3.4 The thermal properties of **2PCT**, **4P2C** and **2PCP**.

Compound	T_g^a ($^{\circ}$C)	T_d^a ($^{\circ}$C)	T_m^b ($^{\circ}$C)	T_c^b ($^{\circ}$C)
2PCT	165	459	356	293
4P2C	199	414	-	-
2PCP	166	398	-	-

[a] Obtained from DSC measurements on the second heating cycle with a heating rate of 10 $^{\circ}$C/min under N_2. [b] Obtained from TGA measurements with a heating rate of 10 $^{\circ}$C/min under N_2.

3.5 Electroluminescent (EL) properties

      3.5.1 Investigation of the hole-transporting property

          The HOMO energies of **2PCT**, **4P2C** and **2PCP** were at 5.50, 5.44 and 5.29 eV, respectively. These energy levels lie between the work function of ITO (4.80 eV) and HOMO energy of Alq_3 (5.70 eV) which indicated that all compounds could potentially be used as a HTL in OLED. Since the barrier energies between ITO and **2PCT**, **4P2C** and **2PCP** were 0.7, 0.64 and 0.49 eV, respectively, it could be estimated that hole injection from ITO to **2PCP** could be most easily occurred. To investigate their hole-transporting properties, double-layer OLED devices with the structure of ITO / HTL[30nm] / Alq_3[30nm] / LiF[0.5nm] / Al[120nm] were fabricated using **2PCT** (device 1), **4P2C** (device 2) and **2PCP** (device 3) as the HTL, ITO as the anode and LiF:Al as the cathode and Alq_3 as the light-emitting and electron-transporting layers. All devices emit the green color of Alq_3 (530 nm), suggesting that **2PCT**, **4P2C** and **2PCP** functioned only as a HTL in these devices.
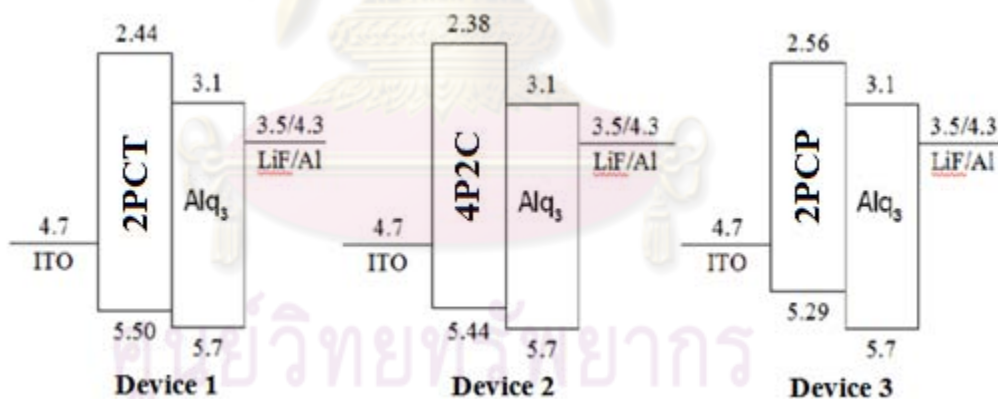
Figure 3.22 Energy level diagrams of device 1-3.

          The voltage-luminance and voltage-current density characteristics of the devices are shown in **Figure 3.23** and summarized in **Table 3.5**. Device 3 exhibited the best performance with a maximum luminance of 9,300 cd/m^2 at 8.8 V, a turn-on voltage of 4.2 V and an external efficiency of 0.1%. This is possibly attributed to the fact that device 3 has charge balance better than the other two devices due to a small energy barrier between **2PCP** and ITO (**Figure 3.22**).

Figure 3.23 Current density and luminance VS voltage characteristics of device 1-3.

Table 3.5 Electroluminescent properties of device 1-3.

Device	HTM	V_{on}[a]	L_{max}[b]	η_{lum}[c]	η_{ex}[d]	J[e]
1	**2PCT**	4.7	1600 (8.8)	0.65	0.03	1950
2	**4P2C**	4.8	6900 (9.6)	2.50	0.10	1342
3	**2PCP**	4.2	9300 (8.8)	2.00	0.10	1555

[a] Turn-on voltage (V). [b] Maximum luminance (cd/m^2) (at applied potential, V).
[c] Luminance efficiency (cd/A). [d] External efficiency (%). [e] Current density (mA/m^2).

3.5.2 Investigation of the electroluminescent property

The high photoluminescence (PL) quantum yields of **2PCT**, **4P2C** and **2PCP** motivated us to use these compounds as light-emitting layers for OLED. To investigate their light-emitting properties, single-layer OLED device was fabricated using **2PCT**, **4P2C** and **2PCP** as emissive material layer (EML) in devices of structure ITO / EML[30nm] / LiF[0.5nm] / Al[120nm] (device 4-6). The voltage-luminance and voltage-current density characteristics of the devices are shown in **Figure 3.25** and summarized in **Table 3.6**. The results showed that device 6 exhibited the highest device performances

with a maximum luminance of 1,450 cd/m^2 at 9.8 V, a turn-on voltage at 4.8 V and an external efficiency of 0.15%. This was also corresponded to smallest energy barrier between LUMO level of **2PCP** and work function of LiF/Al (**Figure 3.24**).

Since the most promising result was obtained from **2PCP**, it was therefore subjected to a fabrication of a device 7, a double-layer device which used a mixture of conductive polymers PEDOT:PSS as an HTM. We found that the incorporation of this HTM decreased the turn-on voltage and current density, while the maximum luminance, luminance efficiency, and external efficiency were raised.

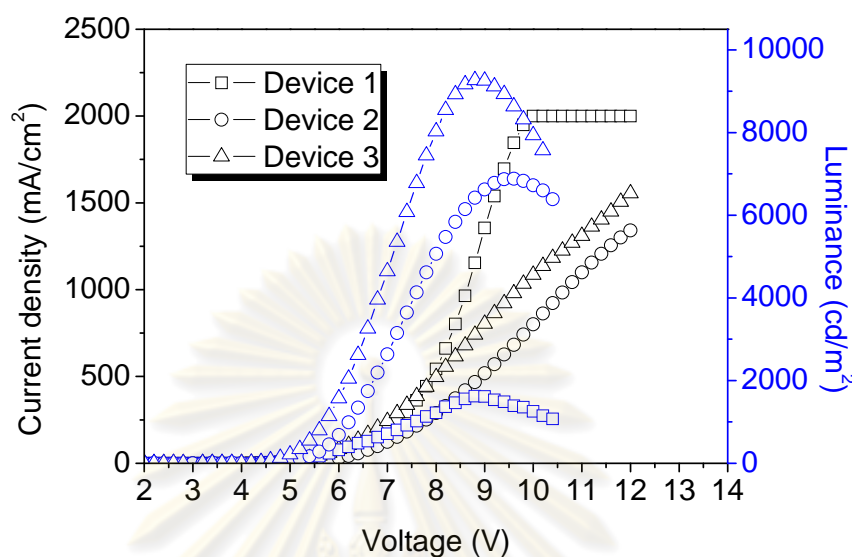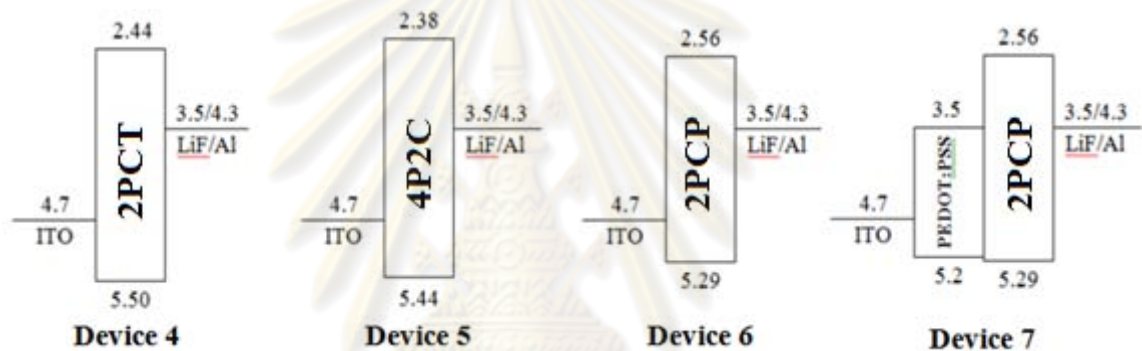**Figure 3.24** Energy level diagrams of device 4-7.
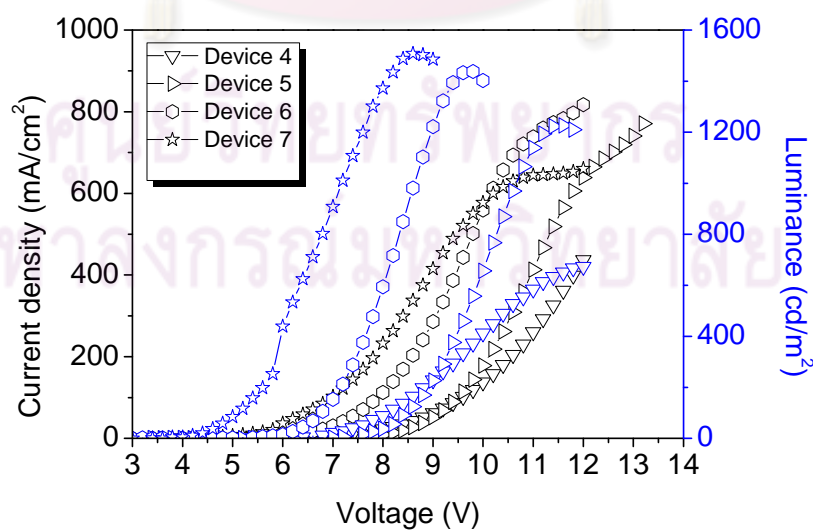
Figure 3.25 Current density and luminance VS voltage characteristics of device 4-7.

Table 3.6 Electroluminescent properties of device 4-7.

Device	EM	V_{on}[a]	L_{max}[b]	η_{lum}[c]	η_{ex}[d]	J[e]	CIE[f]
4	**2PCT**	5.4	670 (12.0)	0.41	0.07	440	(0.18,0.25)
5	**4P2C**	6.9	1200 (11.6)	0.48	0.07	770	(0.21,0.33)
6	**2PCP**	4.8	1450 (9.8)	0.50	0.15	820	(0.18,0.17)
7	**2PCP**	3.8	1600 (8.8)	1.50	0.40	660	(0.17,0.15)

[a] Turn-on voltage (V). [b] Maximum luminance (cd/m^2) (at applied potential V).
[c] Luminance efficiency (cd/A). [d] External efficiency (%). [e] Current density (mA/m^2).
[f] Commission International d'Eclairage coordinates (x, y).
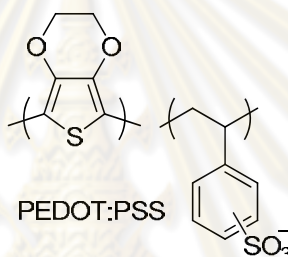
Figure 3.26 Chemical structure of PEDOT:PSS.

The electroluminescent (EL) spectra of the double-layered devices are shown in **Figure 3.27**. The EL peaks of device 4-7 were at 473, 488, 437 and 436 nm, respectively. For device 4, the EL spectrum matched with the corresponding PL (thin film) emission. This indicated that the same radiative excited states involved in both EL and PL processes [85]. Interestingly, for device 6 and 7, the EL spectra showed hypsochromic shift compared to PL spectra. We, therefore, propose that the exciton formation in device 6 and 7 may occur closer to the cathode, where the injected electron has less chance to relax, due to the greater hole-transporting ability of **2PCP**. The EL spectrum of device 5 appeared at a longer wavelength in comparison with the PL spectrum of **4P2C** thin film. This could cause by a difference in fabrication methods or the weak hole-transporting ability of this compound.

Figure 3.27 EL spectra of device 4-7, solid line (PL thin film) and dash line (EL).

The Commission International d'Eclairage (CIE) coordinates for device 4-7 were in the pure blue region as shown in **Figure 3.28** and summarized in **Table 3.6**.

Figure 3.28 CIE coordination (x,y) of device 4-7.

CHAPTER IV

CONCLUSION

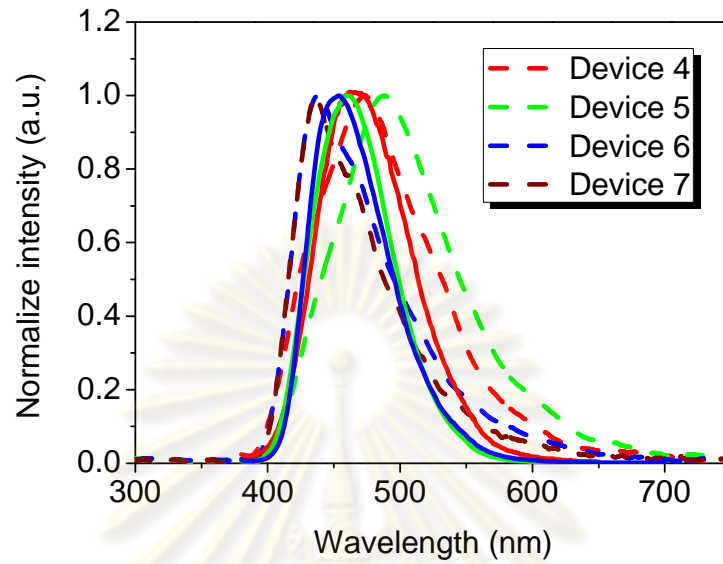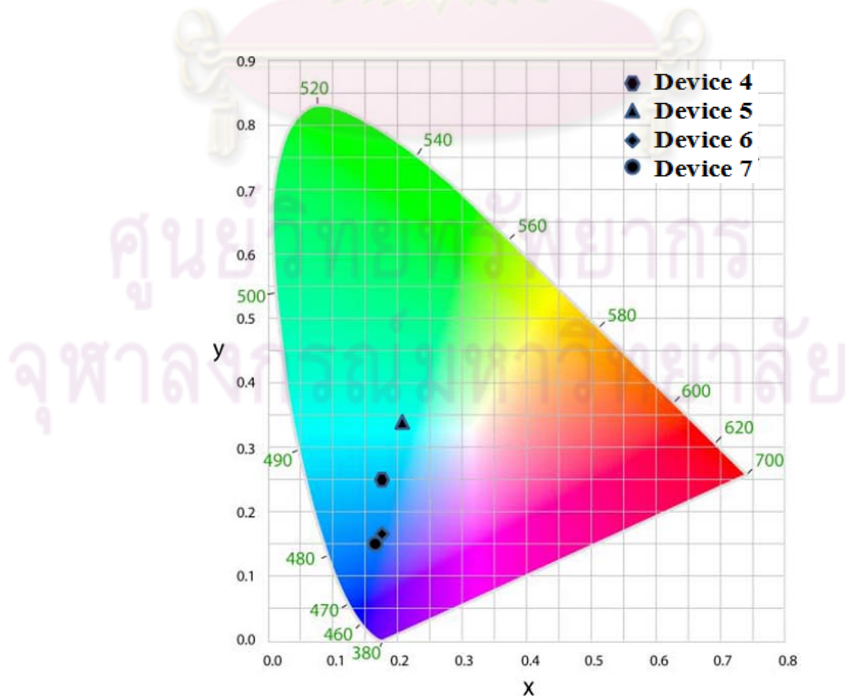Three derivatives of 3,6-dipyrenylcarbazole **2PCT**, **4P2C** and **2PCP** were successfully synthesized. The key transformations involved regioselective iodination of carbazole, Suzuki coupling of the resulting diiodo carbazole with pyrene-1-boronic acid, and the alkylation or arylation of the carbazole N-H position. All compounds were characterized by NMR spectroscopy, UV-Vis and fluorescence spectrophotometry, mass spectrometry and elemental analysis. The UV-Vis absorption spectra of **2PCT**, **4P2C**, and **2PCP** were obtained both in CH_2Cl_2 solution phase and thin film. In solution phase, the compounds exhibited the maximum wavelengths of absorption at 347, 347 and 345 nm, respectively. The onset absorption edge of **2PCT**, **4P2C**, and **2PCP** were at 405, 405 and 425 nm, which could translate into the optical band gap energies of 3.06, 3.06 and 2.73 eV, respectively. In solid state (thin film), compound **2PCT**, **4P2C**, and **2PCP** exhibited the maximum wavelengths of absorption at 359, 360 and 356 nm, respectively. Also, the fluorescence spectra of **2PCT**, **4P2C**, and **2PCP** were obtained both in CH_2Cl_2 solution phase and thin film. In solution phase, **2PCT**, **4P2C**, and **2PCP** exhibited the maximum wavelength of emission at 427, 425 and 465 nm, while those obtained from solid samples (thin film) were at 456, 460 and 453 nm, respectively. The quantum yield of **2PCT**, **4P2C**, and **2PCP** which were measured in CH_2Cl_2 solutions using quinine sulfate solution as a standard were 0.79, 0.79 and 0.73 respectively. The electrochemical properties of the compounds were studied by cyclic and differential pulse voltammetric methods. Compounds **2PCT** and **2PCP** which contained aromatic substituents on their carbazole nitrogens were electrochemically unstable. For compound **2PCT**, the oxidation may first take place at the nitrogen atom. Delocalization of the unpaired electron and a loss of hydrogen radical could lead to a benzylic radical-cation that could undergo a dimerization. In the case of **2PCP**, the oxidative coupling could occur at *p*-position of the phenyl rings in the triphenylamine moiety. Repetitive scanning by cyclic voltammeter revealed that **4P2C** had good electrochemical stability. Thermal properties of all compounds were determined by

differential scanning calorimetry (DSC) and thermogravimetric analysis (TGA) under nitrogen atmosphere. The results suggested that **4P2C**, and **2PCP** were amorphous materials with excellent thermal stability that could form molecular glass, which were an essential property for the preparation of thin films by evaporation and by solution casting. The HOMO energies of **2PCT**, **4P2C** and **2PCP** were at 5.50, 5.44 and 5.29 eV, respectively. For an investigation of the hole-transporting property, the three compounds were used as a HTL in devices of structure ITO / HTL[30nm] / Alq_3[30nm] / LiF[0.5nm]/Al[120nm]. These devices emitted bright green light with maximum brightness of 1,600, 6,900 and 9,300 cd/m^2 at turn-on voltage of 4.7, 4.8 and 4.2 V and current density of 1,950, 1,342 and 1,555 mA/cm^2, respectively. In a study of electroluminescent property **2PCP** was used as an emissive layer in devices of structure ITO / PEDOT:PSS / **2PCP**[30nm] / LiF[0.5nm]/Al[120nm]. This device emitted bright blue light with maximum brightness of 1,600 cd/m^2 at 8.8 V with turn-on voltage of 3.8 V and current density of 660 mA/cm^2 respectively.

ศูนย์วิทยทรัพยากร
จุฬาลงกรณ์มหาวิทยาลัย

REFERENCES

[1]   John, B. HP. LCD vs. CRT. <u>HP monitor buying guides</u> [Online]. 2008. Available
        from : http://www.hp.com.html [2008, April]

[2]   Pope, M.; Kallmann, H. P. and Magnante, P. Electroluminescence in organic crystal.
        <u>Journal of Chemical Physics</u> 38 (1963) : 2042-2043.

[3]   Tang, C. W. and VanSlyke, S. A. Organic electroluminescent diodes. <u>Applied Physics
        Letters</u> 51 (1987) : 913-915.

[4]   Burroughes, J. H.; Bradley, D. D. C.; Brown, A. R.; Marks, R. N.; Mackay, K.;
        Friend, R. H.; Burns, P. L. and Holmes, A. B. Light-emitting diodes based on
        conjugated polymers. <u>Nature</u> 347 (1990) : 539 – 541.

[5]   Zhu, F. <u>OLED activity and technology development.</u> Singapore: Institute of materials
        research and engineering, 2009.

[6]   Hung, L. S. and Chen, C.H. Recent progress of molecular organic electroluminescent
        materials and devices. <u>Materials Science and Engineering Reports : A Review
        Journals</u> 39 (2002) : 143-206.

[7]   Stark, P. and Westling, D. <u>OLED-Evaluation and clarification of the new Organic
        Light Emitting Display technology.</u> Sweden: Department of Science and
        Technology, Linköping University, 2002.

[8]   Veinot, J. G. C. and Marks, T. J. Toward the Ideal Organic Light-Emitting Diode: The
        Versatility and Utility of Interfacial Tailoring by Cross-Linked Siloxane
        Interlayers. <u>Accounts of Chemical Research</u> 38 (2005) : 632-643.

[9]   Kulkarni, A. P.; Tonzola, C. J.; Babel, A. and Jenekhe, S. A. Electron Transport
        Materials for Organic Light-Emitting Diodes. <u>Chemistry of Materials</u> 16
        (2004) : 4556-4573.

[10]   Kitai, A. <u>Luminescent Materials and Applications.</u> The Atrium, Southern Gate,
        Chichester, West Sussex PO19 8SQ, England : Wiley & Sons Ltd, 2008.

[11]   Helfrich, W. and Schneider, W.G. Recombination Radiation in Anthracene Crystals.
        <u>Physical Review Letters</u> 14 (1965) : 229-231.

[12]   Braun, D. and Heeger, A.J. Visible light emission from semiconducting polymer
        diodes. <u>Applied Physics Letters</u> 58 (1991) : 1982-1984.

[13]   Braun, D. and Heeger, A.J. Electroluminescence from light-emitting diodes fabricated from conducting polymers. Thin Solid Films 216 (1992) : 96-98.

[14]   Halls, J. J. M.; Walsh, C.A.; Greenham, N.C.; Marseglia, E.A.; Friend, R.H.; Moratti, S.C. and Holmes, A.B. Efficient photodiodes from interpenetrating polymer networks. Nature 376 (1995) : 498-500.

[15]   Drury, C. J.; Mutsaers, C. M. J.; Hart, C. M.; Matters, M. and De Leeuw, D. M. Low cost all polymer integrated circuits. Applied Physics Letter 73 (1998) : 108-110.

[16]   Horowitz, G.; Fichou, D.; Peng, X.; Xu, Z. and Garnier, F. A field-effect transistor based on conjugated alphasexithienyl. Solid State Communications 72 (1989) : 381-384.

[17]   Sirringhaus, H.; Tessler, N. and Friend, R. H. Recent Progress in Materials for Organic Electronics. Science 280 (1998) : 1741-1744.

[18]   Bao, Z.; Lovinger, A. and Brown, J. New air-stable n-channel organic thin-film transistors. Journal of the American Chemical Society 120 (1998) : 207.

[19]   Ducharme, S.; Scott, J.C.; Twieg, R.J. and Moerner, W.E. Observation of the photorefractive effect in a polymer. Physical Review Letters. 66 (1991) : 1846-1849.

[20]   Hofmann, U. Optimization of Multilayer Organic Light-Emitting Devices. SPIE International Society for Optical Engineering. 124 (1998) : 3417.

[21]   Meerholtz, K.; Volodin, B.; Sandalphon.; Kippelen, B. and Peyghambarian, N. Advanced Photorefractive and Light-Emitting Organic Materials. Nature 371 (1994) : 497-500.

[22]   Salzner, U. and Kızıltepe, T. Theoretical Analysis of Substituent Effects on Building Blocks of Conducting Polymers: 3,4'-Substituted Bithiophenes. The Journal of Organic Chemistry 64 (1999) : 764–769.

[23]   Brabec, C. J.; Sariciftci, N. S. and Hummelen, J.C. Origin of the Open Circuit Voltage of Plastic Solar Cells. Advanced Functional Materials. 11(2001) : 15-26.

[24]   Zhao, T.; Liu, Z.; Song, Y.; Xu, W.; Zhang, D. and Zhu, D. Novel Diethynylcarbazole Macrocycles: Synthesis and Optoelectronic Properties. Journal of Organic Chemistry. 71 (2006) : 7422-7432.

[25] Giro, G.; Cocchi, M.; Di Marco, P.; Di Nicolò, E.; Fattori, V.; Kalinowski, J. and Ghedini, M. The role played by cell configuration and layer preparation in LEDs based on hydroxyquinoline metal complexes and a triphenyl-diamine derivative (TPD). Synthetic Metals 102 (1999) : 1018-1019.

[26] Fang, Q.; Xu, B.; Jiang, B.; Fu, H.; Zhu, W.; Jiang, X. and Zhang, Z. A novel fluorine derivative containing four triphenylamine groups: Highly thermostable blue emitter with hole-transporting ability for organic light-emitting diode (OLED). Synthetic Metals. 155 (2005) : 206-210.

[27] Sharma, A.; Singh, D.; Makrandi, J.K.; Kamalasanan, M.N.; Shrivastva, R. and Singh, I. Fabrication and characterization of OLED with Mg complex of 5-chloro-8-hydroxyquinoline as emission layer. Materials Chemistry and Physics. 108 (2008) : 179-183.

[28] Son, S.-H.; Yun, J.-J.; Oh, G.-C.; Jung, S.-Y.; Kim, Y.-K.; Kuhta, A.V.; Olkhovik, V. K.; Sasnouski, G. and Han, E.-M. Electroluminescence characteristics of a novel biphenyl derivative with benzoxazole for organic light-emitting diodes Current Applied Physics 5 (2005) : 75-78.

[29] Ko, C.W.; Tao, Y.T.; Danel, A.; Krzemińska, L. and Tomasik, P. Organic Light Emitting Diodes Based on 2-(Stilben-4-yl)-benzo-xazole Derivatives: An Implication on the Emission Mechanism. Chemistry of Materials 13 (2001) : 2441-2446.

[30] Ko, C.W.; Tao, Y.T. 9,9-Bis{4-[di-(*p*-biphenyl)aminophenyl]}fluorene: a high T_g and efficient hole-transporting material for electroluminescent devices. Synthetic Metals 126 (2002) : 37.

[31] Ren, X.; Alleyne, B.D.; Djurovich, P.I.; Adachi, C.; Tsyba, I.; Bau, R. and Thompson, M.E. Organometallic Complexes as Hole-Transporting Materials in Organic Light-Emitting Diodes Inorganic Chemistry 43 (2004) : 1697-1707.

[32] Chen, C.-H.; Shen, W.-J.; Jakka, K. and Shu, C.-F. Synthesis and characterization of spiro(adamantane-2,9′-fluorene)-based triaryldiamines: thermally stable hole-transporting materials Synthetic Metals 143 (2004) : 215-220).

[33] Zhi-feng, Z.; Zhen-bo, D.; Dong, G.; Chun-jun, L. and Peng, L. Improved performance of organic light-emitting devices with 2-(4-biphenyl)-5-(4-butylphenyl)-1,3,4-oxadiazole. Displays. 26 (2005) : 133-136.

[34] Kao, P.-C.; Chu, S.-Y.; You, Z.-X.; Liou, S.J. and Chuang C-A. Improved efficiency of organic light-emitting diodes using CoPc buffer layer. <u>Thin Solid Films</u>. 498 (2006) : 249-253.

[35] Tong, Q.-X.; Lai, S.-L.; Chan, M.-Y.; Lai, K.-H.; Tang, J.-X.; Kwong, H.-L.; Lee, C.-S. and Lee, S.-T. High T_g Triphenylamine-Based Starburst Hole-Transporting Material for Organic Light-Emitting Devices. <u>Chemistry of Materials</u>. 19 (2007) : 5851-5855.

[36] Chen, C.-T. Evolution of Red Organic Light-Emitting Diodes: Materials and Devices. <u>Chemistry of Materials</u>. 16 (2004) : 4389-4400.

[37] Lu, H.-T.; Tsou, C.-C. and Yokoyama, M. Organic light-emitting devices with energy-level aligned double-buffer layers. <u>Journal of Crystal Growth</u>. 289 (2006) : 161-163.

[38] Mu, H.; Li, W.; Jones, R.; Steckl, A. and Klotzkin, D. A comparative study of electrode effects on the electrical and luminescent characteristics of Alq$_3$/TPD OLED: Improvements due to conductive polymer (PEDOT) anode. <u>Journal of Luminescence</u>. 126 (2007) : 225-229.

[39] Fang, Q.; Xu, B.; Jiang, B.; Fu, H.; Zhu, W.; Jiang, X. and Zhang, Z. A novel fluorene derivative containing four triphenylamine groups: Highly thermostable blue emitter with hole-transporting ability for organic light-emitting diode (OLED). <u>Synthetic Metals</u>. 155 (2005) : 206-210.

[40] Pei, Q. and Yang, Y. Efficient Photoluminescence and Electroluminescence from a Soluble Polyfluorene. <u>Journal of the American Chemical Society</u>. 118 (1996) : 7416-7417.

[41] Grice, A. W.; Bradley, D. D. C.; Bernius, M. T.; Inbasekaran, M.; Wu, W. W. and Woo, E. P. High brightness and efficiency blue light-emitting polymer diodes. <u>Applied Physics Letters</u>. 73 (1998) : 629.

[42] Higginson, K. A.; Zhang, X.-M. and Papadimitrakopoulos, F. Thermal and Morphological Effects on the Hydrolytic Stability of Aluminum Tris(8-hydroxyquinoline) (Alq$_3$). <u>Chemistry of Materials</u>.10 (1998) : 1017-1020.

[43] Papadimitrakopoulos, F. A Chemical Failure Mechanism for Aluminum(III) 8 Hydroxy-quinoline Light-Emitting Devices. <u>Chemistry of Materials</u>. 8 (1996) : 1363-1365.

[44] Zhao, Z.; Xu, B.; Yang, Z.; Wang, H.; Wang, X.; Lu, P. and Tian,W. White Light from Excimer and Electromer in Single-Emitting-Component Electroluminescent Diodes. Journal of Physical Chemistry C 112 (2008) : 8511-8515.

[45] Cao, H.; Chen, Z.; Liu, Y.; Qu, B.; Xu, S.; Cao, S.; Lan, Z. and Gong, Q. Undoped yellow-emitting organic light-emitting diodes from a phenol-thiazine-based derivative. Synthetic Metals 157 (2007) : 427-431.

[46] Si, Z.; Li, J.; Li, B.; Hong, Z.; Liu, S. and Li, W. Electroluminescence from Singlet Excited-State of the Exciplex between (2,3-Dicarbonitrilopyrazino [2,3-f][1,10]phenanthroline)Re(CO)$_3$Cl and CBP. Journal of physical chemistry C. 112 (2008) : 3920-3925.

[47] Park, J.-W.; Kang, P.; Park, H.; Oh, H.-J.; Yang, J.-H.; Kim, Y.-H. and Kwon, S.-K. Synthesis and properties of blue-light-emitting anthracene derivative with diphenylamino-fluorene Dyes and Pigments 85 (2010) : 93-98.

[48] Chiechi, R. C.; Tseng, R. J.; Marchioni, F.; Yang, Y.; Wudl, F. Efficient Blue-Light Emitting Electroluminescent Devices with a Robust Fluorophore: 7,8,10-Triphenylfluoranthene Advanced Functional Materials. 18 (2006) : 325-328.

[49] Tonzola, C. J.; Kukarni, A. P.; Gifford, A. P.; Kaminsky, W.; Jenekhe, S. A. Oligoquinolines: Synthesis, Properties, and High-Efficiency Blue-Light-Emitting Diodes Advanced Functional Materials 17 (2007) : 863-874.

[50] Liu, Q. D.; Lu, J.; Ding, J.; Day, M.; Tao, Y.; Barrios, P.; Stupak, J.; Chan, K.; Li, J.; Chi, Y. Monodisperse Starburst Oligofluorene-Functionalized 4,4',4''-Tris(carbazol-9-yl)-triphenylamines: Their Synthesis and Deep-Blue Fluorescent Properties for Organic Light-Emitting Diode Applications. Advanced Functional Materials 17 (2007) : 1028-1036.

[51] Wong, K. T.; Chen, R. T.; Fang, F. C.; Wu. C. C.; Lin, Y. T. 4,5-Diazafluorene Incorporated Ter(9,9-diarylfluorene) : A Novel Molecular Doping Strategy for Improving the Electron Injection Property of a Highly Efficient OLED Blue Emitter. Organic Letters 7 (2005) : 1979-1982.

[52] Yanga, C.-H.; Guob, T.-F. and Sun, I.-W. Highly efficient greenish blue-emitting organic diodes based on pyrene derivatives. Journal of Luminescence 124 (2007) : 93–98.

[53]   Fu, Y.; Li, Y.; Li, J.; Yan, S. and Bo, Z. High Molecular Weight Dendronized
        Poly(fluorene)s with Peripheral Carbazole Groups: Synthesis,
        Characterization, and Properties Macromolecules 37 (2004) : 6395-6400.

[54]   Loiseau, F.; Campagna, S.; Hameurlaine, A. and Dehaen, W. Dendrimers Made of
        Porphyrin Cores and Carbazole Chromophores as Peripheral Units.
        Absorption Spectra, Luminescence Properties, and Oxidation Behavior.
        Journal of the American Chemical Society 127 (2005) : 11352–11363.

[55]   Promarak, V.; Ichikawa, M.; Meunmart, D.; Sudyoadsuk, T.; Saengsuwan, S. and
        Keawin, T. Synthesis and properties of stable amorphous hole-transporting
        molecules for electroluminescent devices. Tetrahedron Letters 47 (2006) :
        8949-8952.

[56]   Promarak, V.; Ichikawa, M.; Sudyoadsuk, T.; Saengsuwan, S.; Jungsuttiwong, S. and
        Keawin, T. Synthesis of electrochemically and thermally stable amorphous
        hole-transporting carbazole dendronized fluorene. Synthetic Metals 157
        (2007) : 17-22.

[57]   Shih, P.-I.; Chiang, C.-L.; Dixit, A.K.; Chen, C.-K.; Yuan, M.-C.; Lee, R.-Y.; Chen,
        C.-T.; Diau, E.W.-G. and Shu, C.-F. Novel Carbazole/Fluorene Hybrids
        : Host Materials for Blue Phos-phorescent OLEDs. Organic Letters 8(2006) :
        2799-2802.

[58]   Lu, J.; Xia, P.F.; Lo, P.K.; Tao, Y. and Wong, M.S. Synthesis and Properties of Multi
        Triarylamine-Substituted Carbazole-Based Dendrimers with an
        Oligothiophene Core for Potential Applications in Organic Solar Cells and
        Light-Emitting Diodes. Chemistry of Materials 18 (2006) : 6194-6203.

[59]   Wagner, J.; Pielichowski, J.; Hinsch, A.; Pielichowski, K.; Bogdal, D.; Pajda, M.;
        Kurek S.S. and Burczyk, A. New carbazole-based polymers for dye solar cells
        with hole-conducting polymer. Synthetic Metals 146 (2004) : 159-165.

[60]   Promarak, V.; Punkvuang, A.; Sudyoadsuk, T.; Saengsuwan, S.; Jungsuttiwong, S.
        and Keawin, T. Synthesis, optical, electrochemical, and thermal properties of
        $\propto,\propto'$-bis(9,9-bis-n-hexylfluorenyl)-substituted oligothiophenes. Tetrahedron
        Letters 48 (2007) : 3661-3665.

[61]   Smalley, M.K. and Silverman, S.K. Fluorescence of covalently attached pyrene as a
        general RNA folding probe. Nucleic Acids Research 34 (2006) : 152-166.

[62]   Fujimoto, J.; Bando, T.; Minoshima, M.; Uchida, S.; Iwasaki, M.; Shinohara, K.-I. and Sugiyama, H. Detection of triplet repeat sequences in the double-stranded DNA using pyrene-functionalized pyrrole–imidazole polyamides with rigid linkers. Bioorganic & Medicinal Chemistry 16 (2008) : 5899–5907.

[63]   Kumar, R.; Bhalla, V. and Kumar M. Cu^{2+} and CN^--selective fluorogenic sensors based on pyrene-appended thiacalix[4]arenes. Tetrahedron 64 (2008) : 8095-8101.

[64]   Zhao, Z.; Xu, X.; Chen, X.; Wang, X.; Lu, P.; Yu, G. and Liu, Y. Synthesis and characterization of deep blue emitters from starburst carbazole/fluorene compounds. Tetrahedron 64 (2008) : 2658-2668.

[65]   Lengvinaite, S.; Grazulevicius, J.V.; Grigalevicius, S.; Gub, R.; Dehaen, W.; Jankauskas, V.; Zhang, B. and Xie, Z. Indolo[3,2-b]carbazole-based functional derivatives as materials for light emitting diodes. Dyes and Pigments 85 (2010) : 183-188.

[66]   Promarak, V.; Ichikawa, M.; Sudyoadsuk, T.; Saengsuwan, S.; Jungsuttiwong, S. and Keawin, T. Thermally and electrochemically stable amorphous hole-transporting materials based on carbazole dendrimers for electroluminescent devices. Thin Solid Films 516 (2008) : 2881–2888.

[67]   Yang, C.-H.; Guo, T.-F. and Sun, I.-W. Highly efficient greenish blue-emitting organic diodes based on pyrene derivatives. Journal of Luminescence 124 (2007) : 93–98.

[68]   Williams, A. T. R.; Winfield, S. A. and Miller, J. N. Relative fluorescence quantum yields using a computer controlled luminescence spectrometer. Analyst 108 (1983) : 1067.

[69]   Warf, A. Negative Dryfilm Photo resist manual. Negative Dryfilm [Online]. 2004. Available from : http://www.warf.com.html [2004, May]

[70]   Wright, W. D. A re-determination of the trichromatic coefficients of the spectral colours. Transactions of the Optical Society 30 (1928) : 141.

[71]   Guild, J. The colorimetric properties of the spectrum. Philosophical Transactions of the Royal Society of London A 230 (1931) : 149.

[72] Zhang, Y.; Wada, T.; Wang, L. and Sasabe, H. Amorphous Conjugated Carbazole
      Trimers for Photorefractive Materials. Chemistry of Materials 9 (1997) :
      2798–2804.

[73] Hosoya, T.; Inoue, A.; Hiramatsu, T.; Aoyama, H.; Ikemoto, T.; Suzuki, M. Facile
      synthesis of diazido-functionalized biaryl compounds as radioisotope-free
      photoaffinity probes by Suzuki–Miyaura coupling. Bioorganic & Medicinal
      Chemistry 17 (2009) : 2490–2496.

[74] Mohanty, S.; Suresh, D.; Balakrishna, M.S. and Mague, J.T. An inexpensive and
      highly stable ligand 1,4-bis(2-hydroxy-3,5-ditert-butylbenzyl)piperazine for
      Mizoroki-Heck and room temperature Suzuki-Miyaura cross-coupling
      reactions. Tetrahedron 64 (2008) : 240-247.

[75] Li, Z.H. and Wong, M.S. Synthesis and Functional Properties of End-Dendronized
      Oligo(9,9-diphenyl)fluorenes. Organic Letters 8 (2006) : 1499-1502.

[76] Lin, W.O.; Figueira, J.A.A. and Alt, H.G. New Multidentate Potential Ionophors of
      Ether-Amide Type. Monatshefte fur Chemie 116 (1985) : 217-221.

[77] Bacher, E.; Bayerl, M.; Rudati, P.; Reckefuss, N.; Muller, C.D.; Meerholz, K. and
      Nuyken, O. Synthesis and Characterization of Photo-Cross-Linkable Hole-
      Conducting Polymers. Macromolecules 38 (2005) : 1640-1647.

[78] Du, H.; Fuh, R. A.; Li, J.; Corkan, A. and Lindsey, J. S. A computer-aided design and
      research tool in photochemistry. Photochemistry and Photobiology 68 (1998) :
      141-142.

[79] Pan, J.-F.; Chua, S.-J. and Huang, W. Conformational analysis (ab initio HF/3-21G*)
      and optical properties of poly(thiophene-phenylene-thiophene) (PTPT).
      Chemical Physics Letters 363 (2002) : 18-24.

[80] Khakhel, O. A.; Nekrasov, V. V.; Sakhno, T. V.; Barashkov, N. N. and
      Nurmukhametov, R. N. Nature of longwave fluorescence of pyrene. Journal
      of Applied Spectroscopy 60 (1994) : 66-70.

[81] Wu, T.-Y.; Chen, Y. and Polym, J. Electron Transfer Studied at the Molecular Level.
      Journal of Polymer Science 41 (2003) : 1444.

[82] Zhang, X.H.; Wu, S.K.; Gao, Z.;Q.; Lee, C.S.; Lee, S.T. and Kwong, H.-L. Pyrazoline
      derivatives for blue color emitter in organic electroluminescent devices. Thin
      Solid Films 371 (2000) : 40-46.

[83] Yang, F.; Zhang, X.L.; Sun, K.; Xiong, M.J.; Xia, P.F.; Cao, Z.J.; Li, Z.H. Enhanced electroluminescent properties of triarylamine-endcapped X-branched oligofluorene. <u>Synthetic Metals</u> 158 (2008) : 988–992.

[84] Zhu, W.; Hu, M.; Yao, R. and Tian, H. A novel family of twisted molecular luminescent materials containing carbazole unit for single-layer organic electroluminescent devices. <u>Journal of Photochemistry and Photobiology A: Chemistry</u> 154 (2003) : 169–177.

[85] Liu, Y.; Di, C.-A.; Xin, Y.; Yu, G.; Liu, Y.; He, Q.; Bai, F.; Xu, S. and Cao, S. Organic light-emitting diode based on a carbazole compound. <u>Synthetic Metals</u> 156 (2006) : 824–827.

APPENDIX

APPENDIX
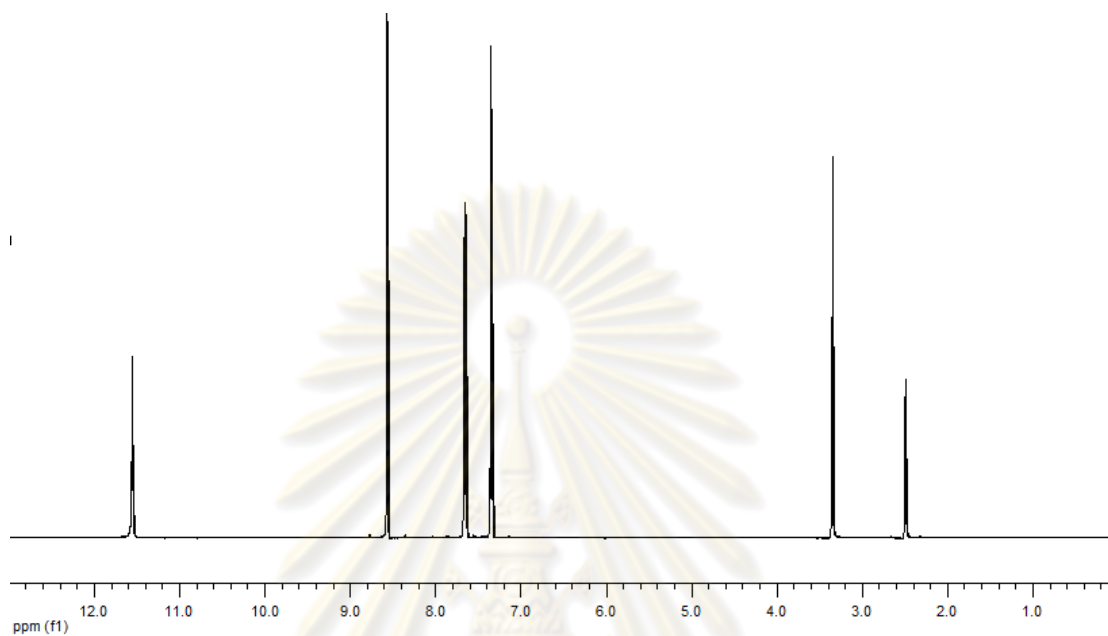
Figure 1 ^{1}H-NMR spectrum of 3,6-diiodo-9*H*-carbazole (**7**)
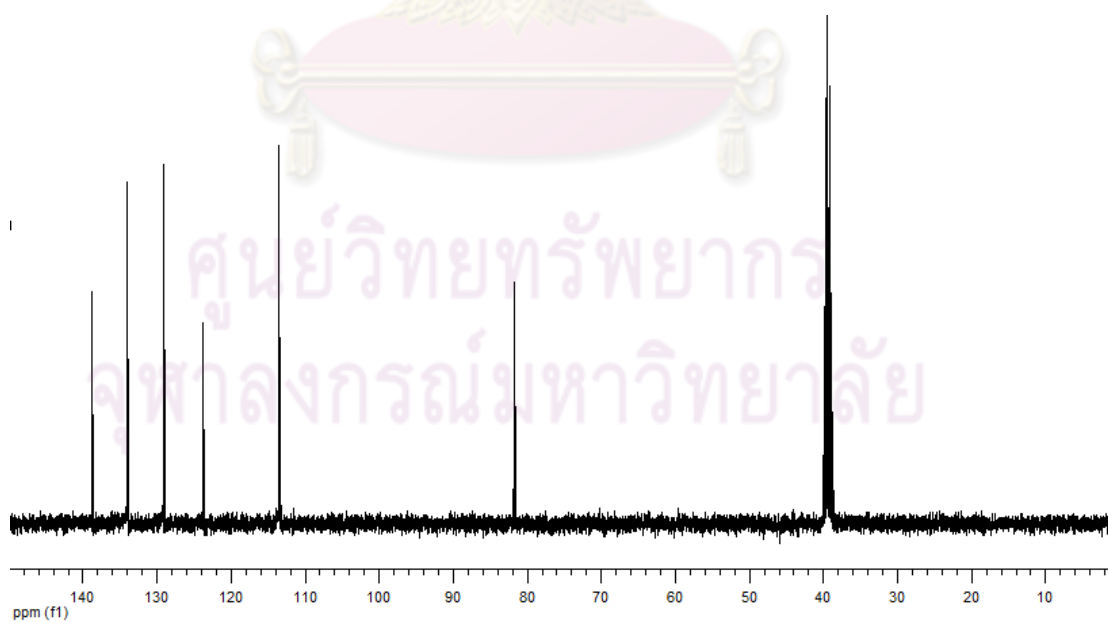
Figure 2 ^{13}C-NMR spectrum of 3,6-diiodo-9*H*-carbazole (**7**)
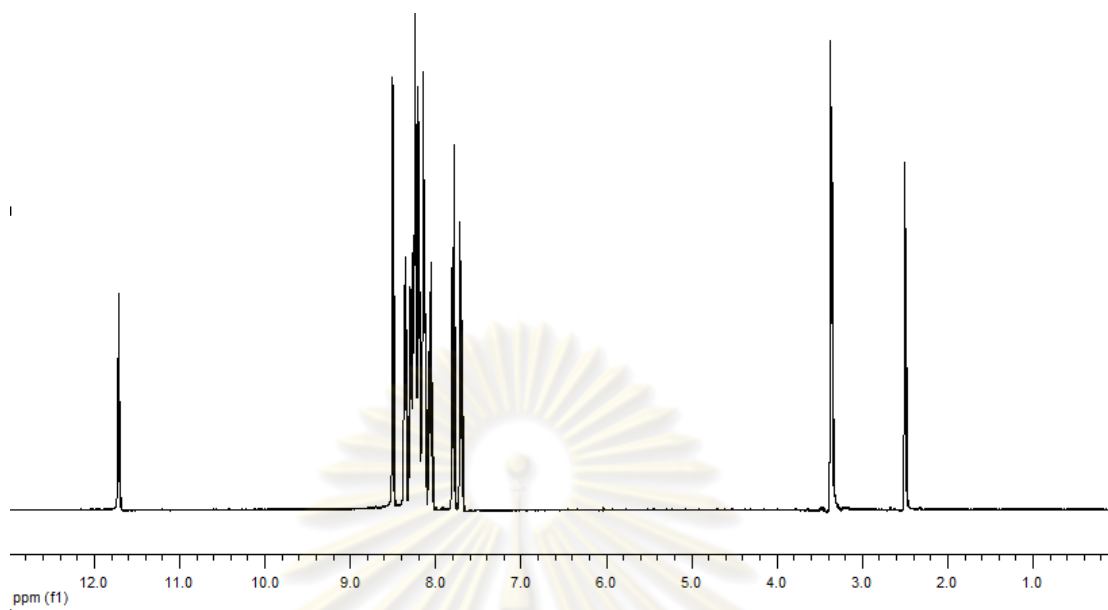
Figure 3 ^{1}H-NMR spectrum of 3,6-di(pyren-1-yl)-9*H*-carbazole **(8)**
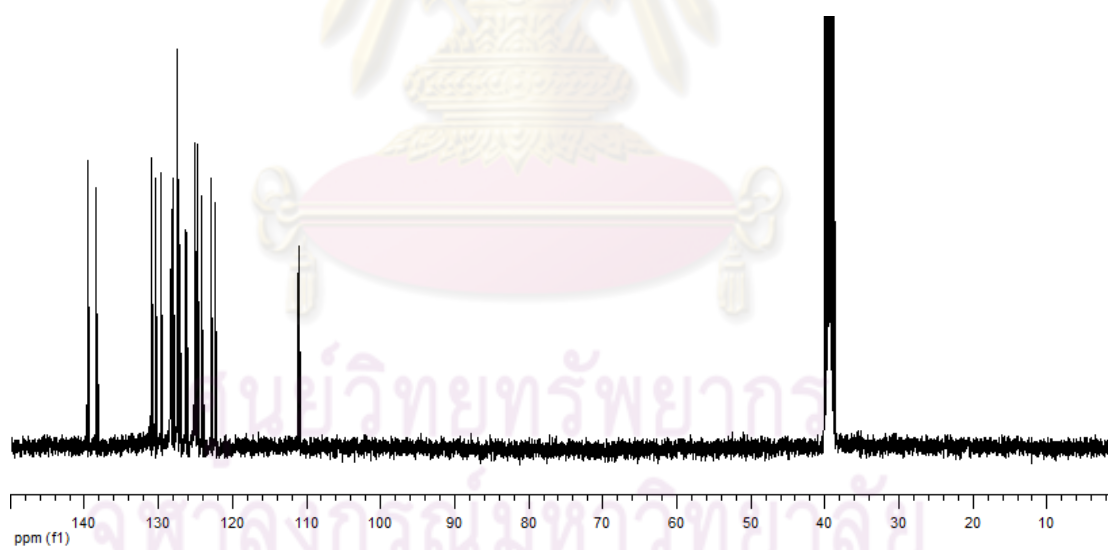
Figure 4 ^{13}C-NMR spectrum of 3,6-di(pyren-1-yl)-9*H*-carbazole **(8)**

Mass Spectrum List Report

Analysis Info

Analysis Name	TK-I-60A1.d	Acquisition Date	10/29/2008 4:49:18 PM
Method	flowinjection_pos.m	Operator	Administrator
Sample Name	TK-I-60A1	Instrument	micrOTOF 72
	TK-I-60A1		

Acquisition Parameter

Source Type	ESI			Set Corrector Fill	47 V
Scan Range	n/a	Ion Polarity	Positive	Set Pulsar Pull	394 V
Scan Begin	50 m/z	Capillary Exit	100.0 V	Set Pulsar Push	394 V
Scan End	3000 m/z	Hexapole RF	500.0 V	Set Reflector	1300 V
		Skimmer 1	30.0 V	Set Flight Tube	9000 V
		Hexapole 1	23.0 V	Set Detector TOF	2150 V
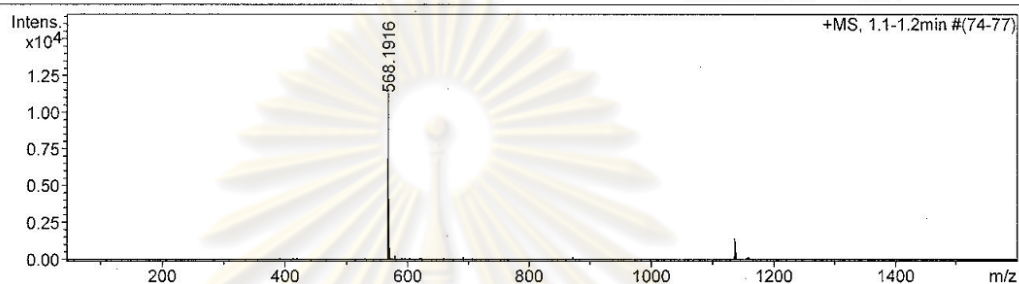
Figure 5 Mass spectrum of 3,6-di(pyren-1-yl)-9*H*-carbazole **(8)**

```
DATE 26 11 09      TIME 14 28 40      OPERATOR ID YUI

     ID DENDRON          WEIGHT 1.152

                                       SIGNALS

                                       ZR 9734
     CARBON 91.52%                     NR 9871
     HYDROGEN 4.60%                    CR 24178
     NITROGEN 2.15%                    HR 26228
```

Figure 6 Elemental analysis data of 3,6-di(pyren-1-yl)-9*H*-carbazole **(8)**
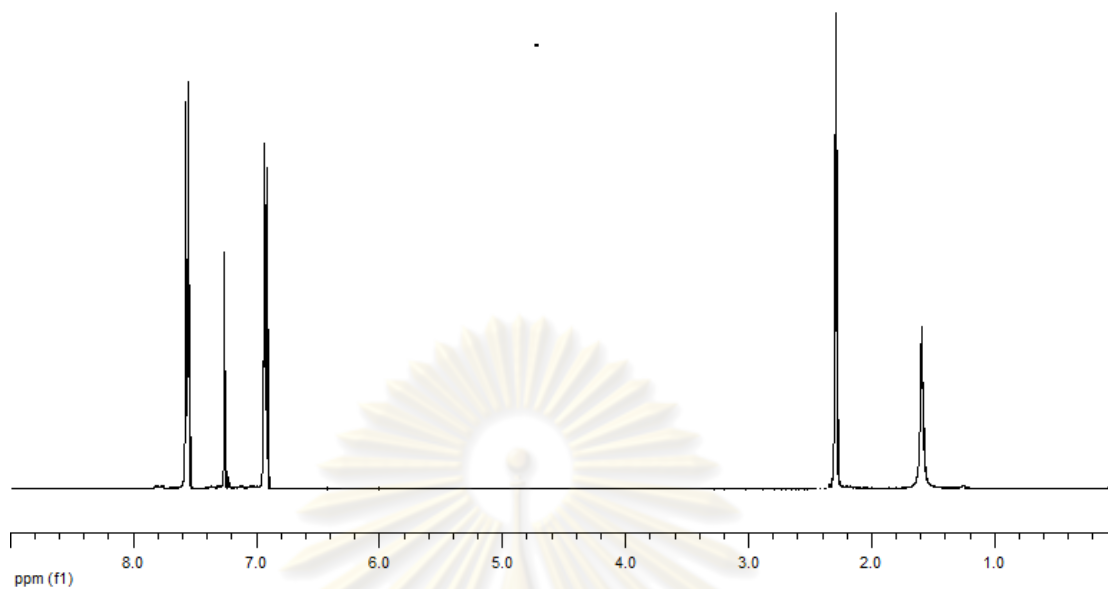
Figure 7 ^{1}H-NMR spectrum of 4-iodotoluene (**9**)
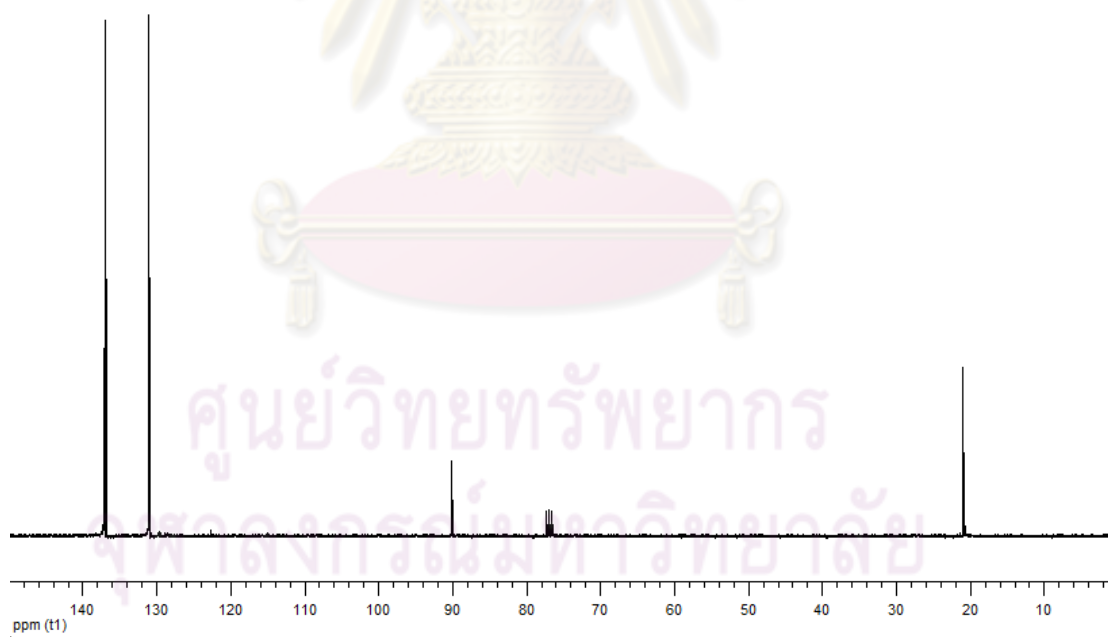
Figure 8 ^{13}C-NMR spectrum of 4-iodotoluene (**9**)
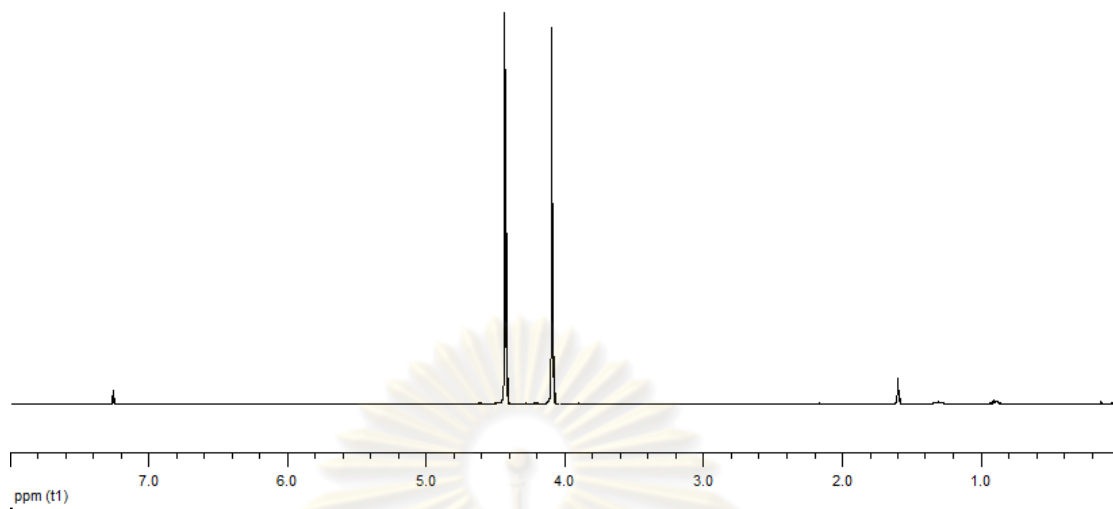
Figure 9 ^{1}H-NMR spectrum of 1,2-bis(chloroacetoxy)ethane **(10)**
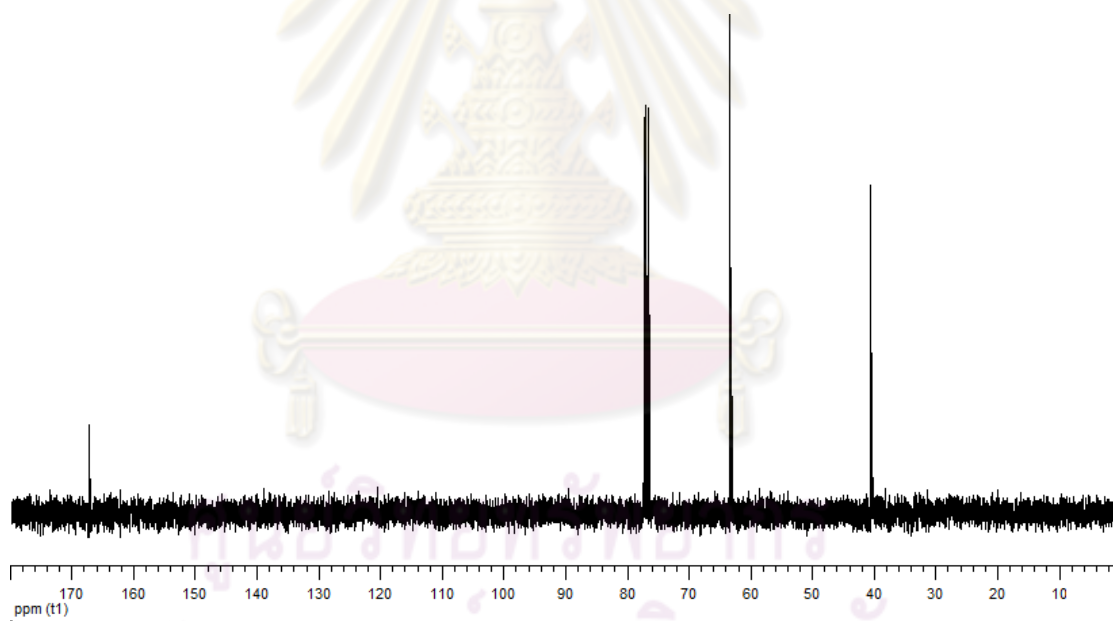
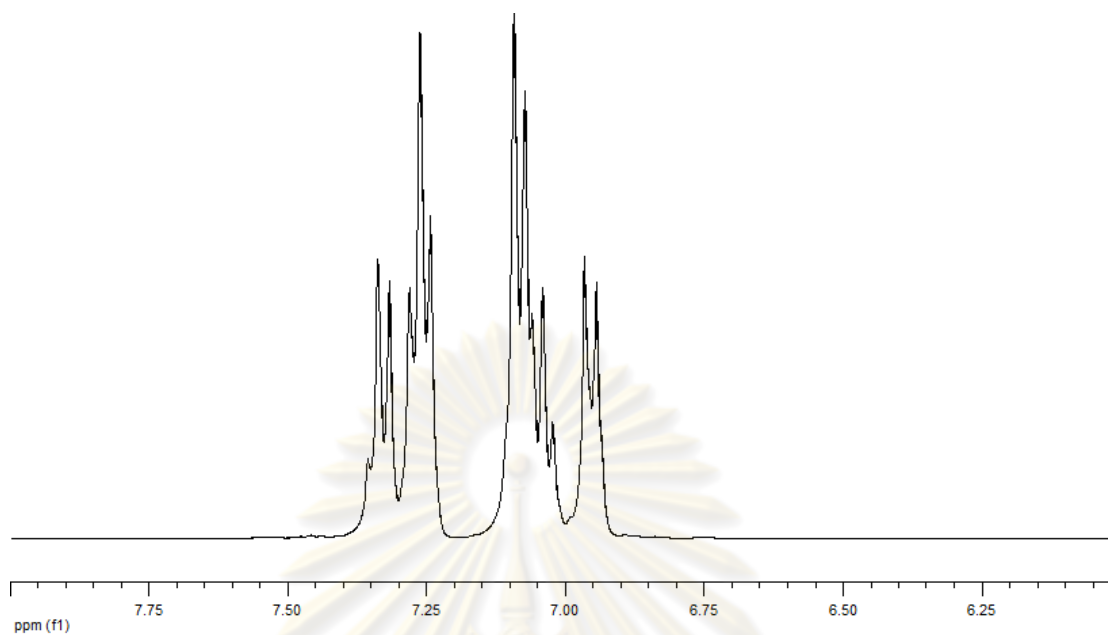**Figure 10** ^{13}C-NMR spectrum of 1,2-bis(chloroacetoxy)ethane **(10)**

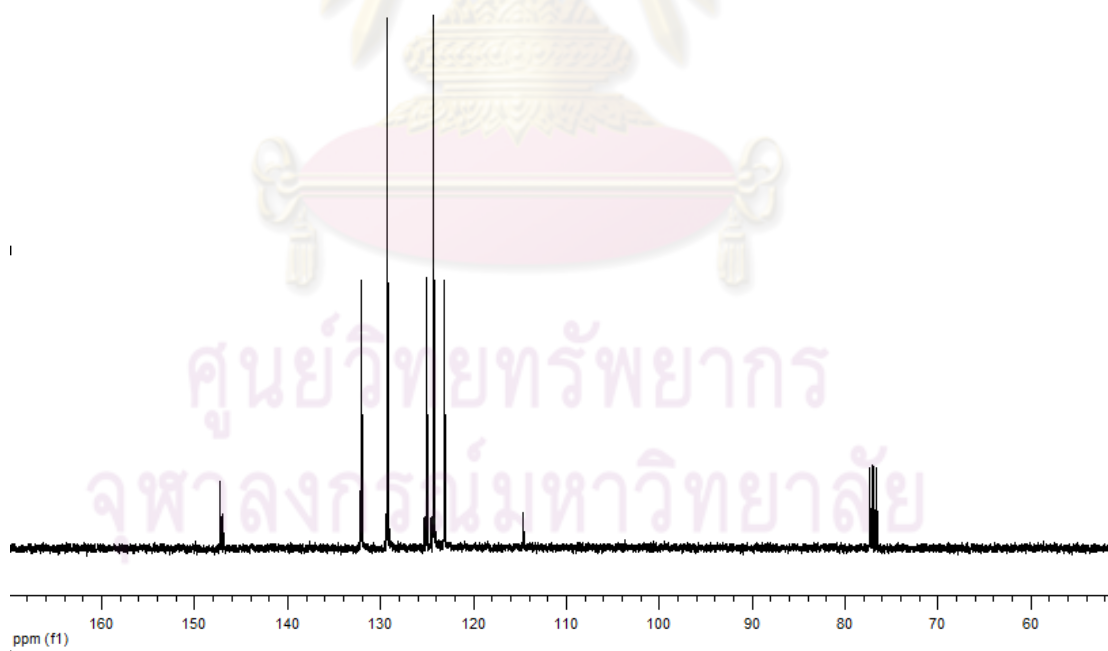**Figure 11** ^{1}H-NMR spectrum of 4-bromo-*N*,*N*-diphenylaniline (**11**)

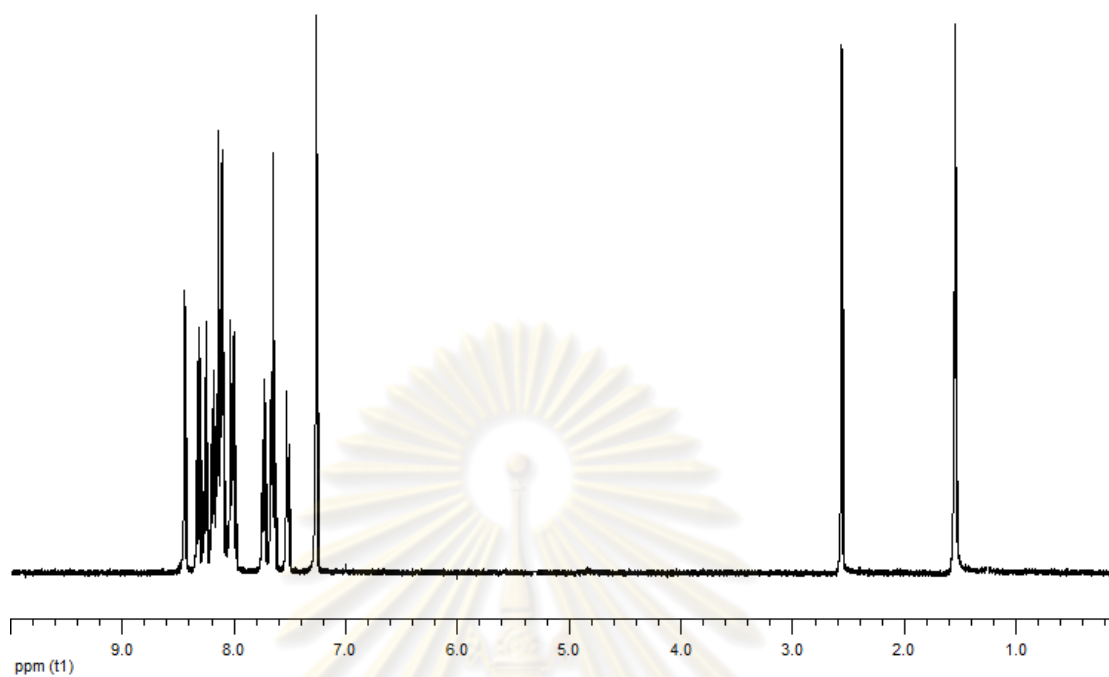**Figure 12** ^{13}C-NMR spectrum of 4-bromo-*N*,*N*-diphenylaniline (**11**)

Figure 13 ^{1}H-NMR spectrum of 3,6-di(pyren-1-yl)-9-*p*-tolyl-9*H*-carbazole (**2PCT**)
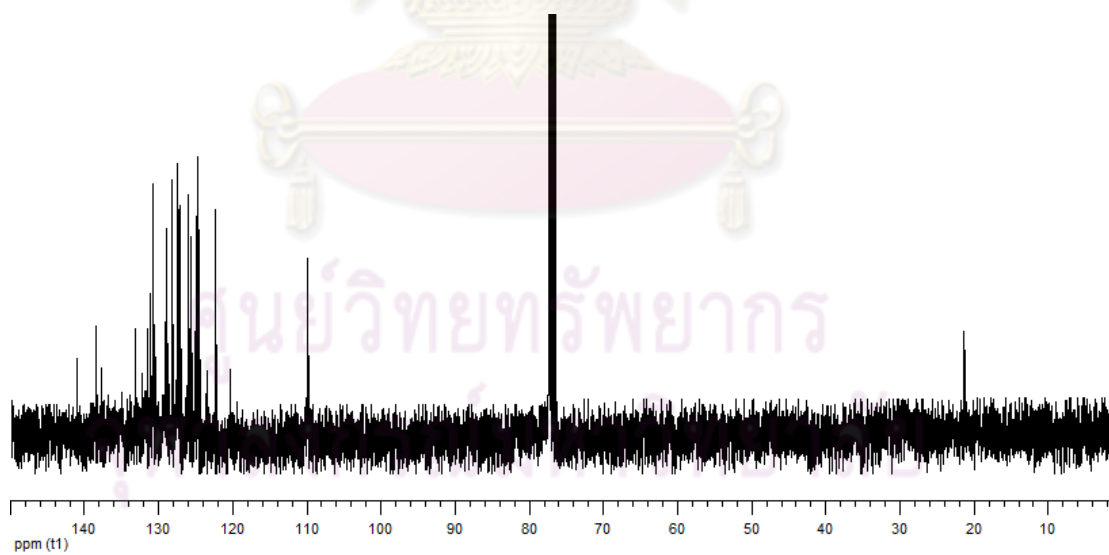
Figure 14 ^{13}C-NMR spectrum of 3,6-di(pyren-1-yl)-9-*p*-tolyl-9*H*-carbazole (**2PCT**)
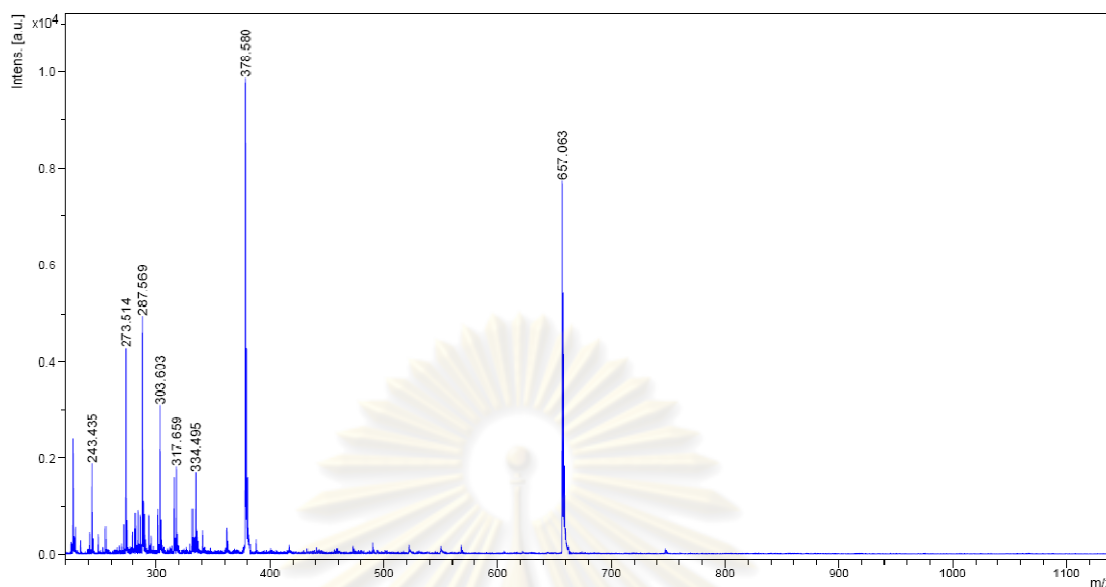
Figure 15 Mass spectrum of 3,6-di(pyren-1-yl)-9-*p*-tolyl-9*H*-carbazole **(2PCT)**

Figure 16 Elemental analysis data of 3,6-di(pyren-1-yl)-9-*p*-tolyl-9*H*-carbazole
(2PCT)
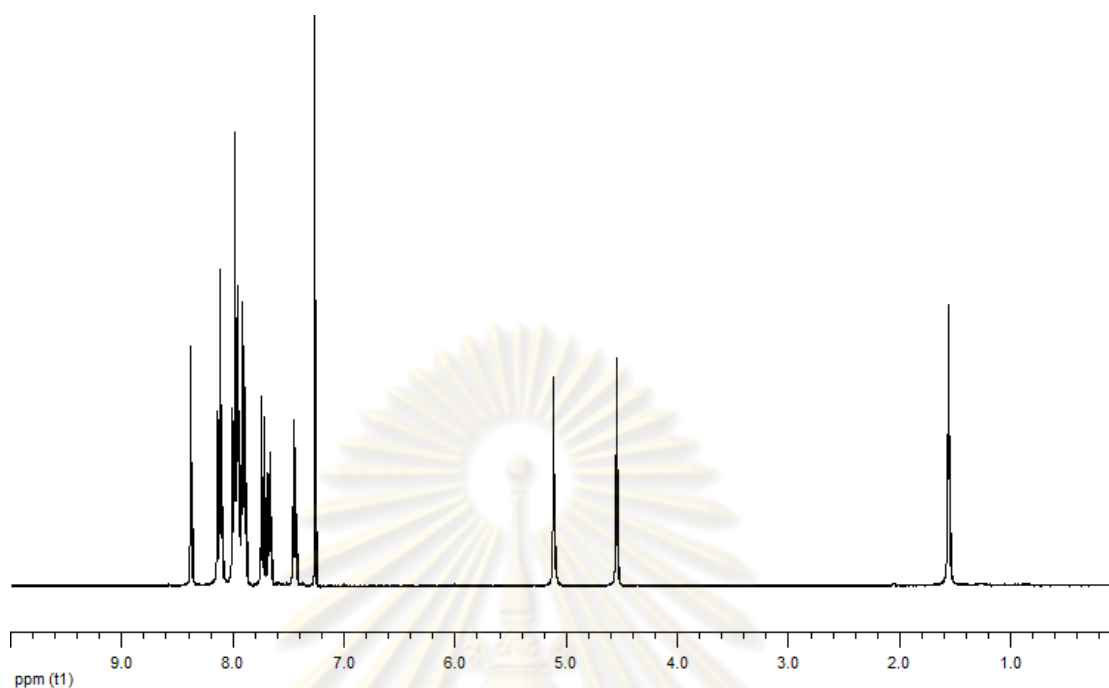
Figure 17 ¹H-NMR spectrum of Ethane-1,2-diyl bis(2-(3,6-di(pyren-1-yl)-9-*H*-carbazol-9-yl)acetate) **(4P2C)**
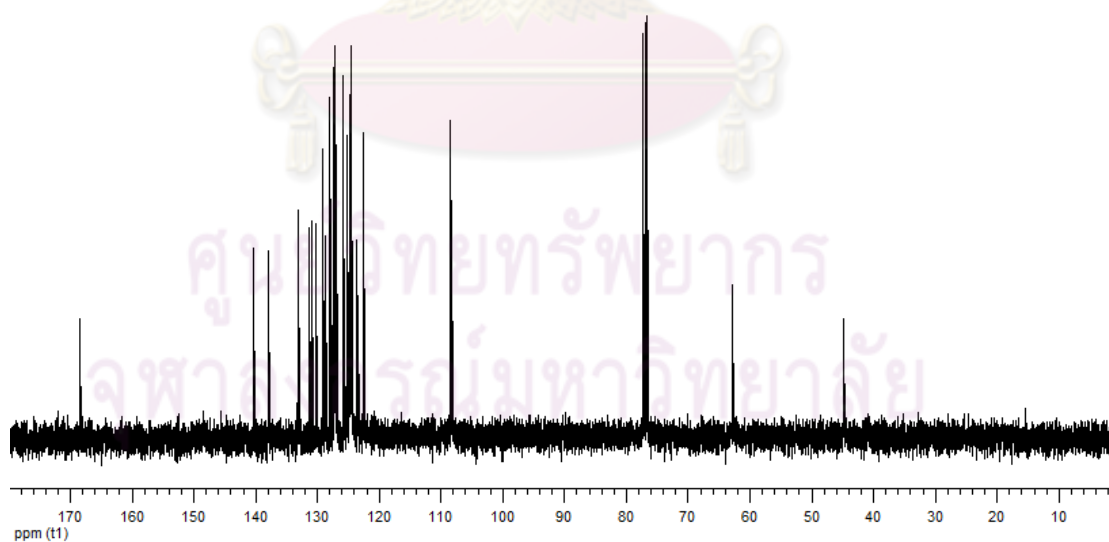

Figure 18 ¹³C-NMR spectrum of Ethane-1,2-diyl bis(2-(3,6-di(pyren-1-yl)-9-*H*-carbazol-9-yl)acetate) **(4P2C)**
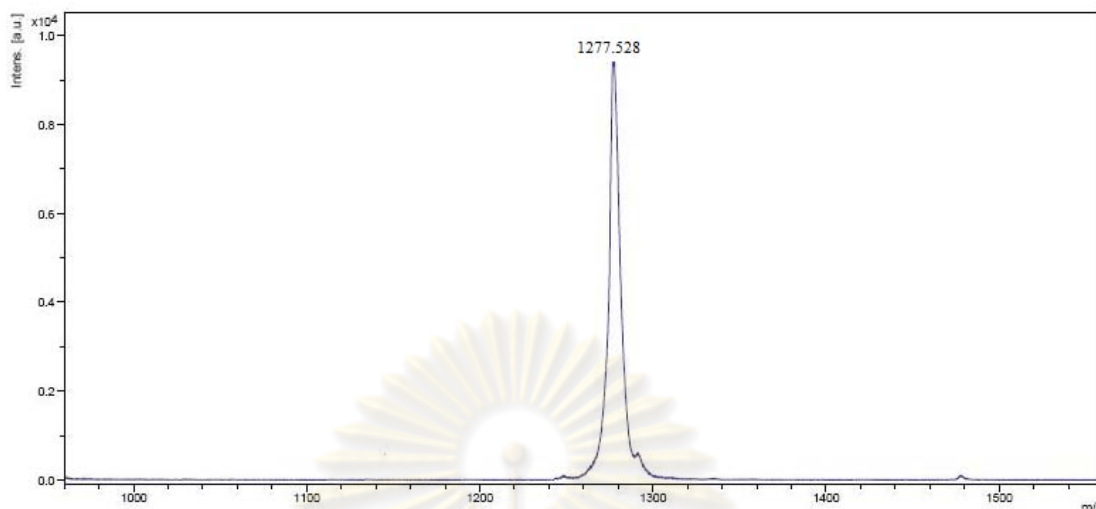
Figure 19 Mass spectrum of Ethane-1,2-diyl bis(2-(3,6-di(pyren-1-yl)-9-*H*-carbazol-9-yl)acetate) **(4P2C)**

```
DATE 23 07 09      TIME 15 36 37      OPERATOR ID YUI

     ID TK III 5A1     WEIGHT 1.086

                                   SIGNALS

                                   ZR 9698
     CARBON 88.58%                 NR 9809
     HYDROGEN 3.96%                CR 22795
     NITROGEN 2.11%                HR 24519
```

Figure 20 Elemental analysis data of Ethane-1,2-diyl bis(2-(3,6-di(pyren-1-yl)-9-*H*-carbazol-9-yl)acetate) **(4P2C)**
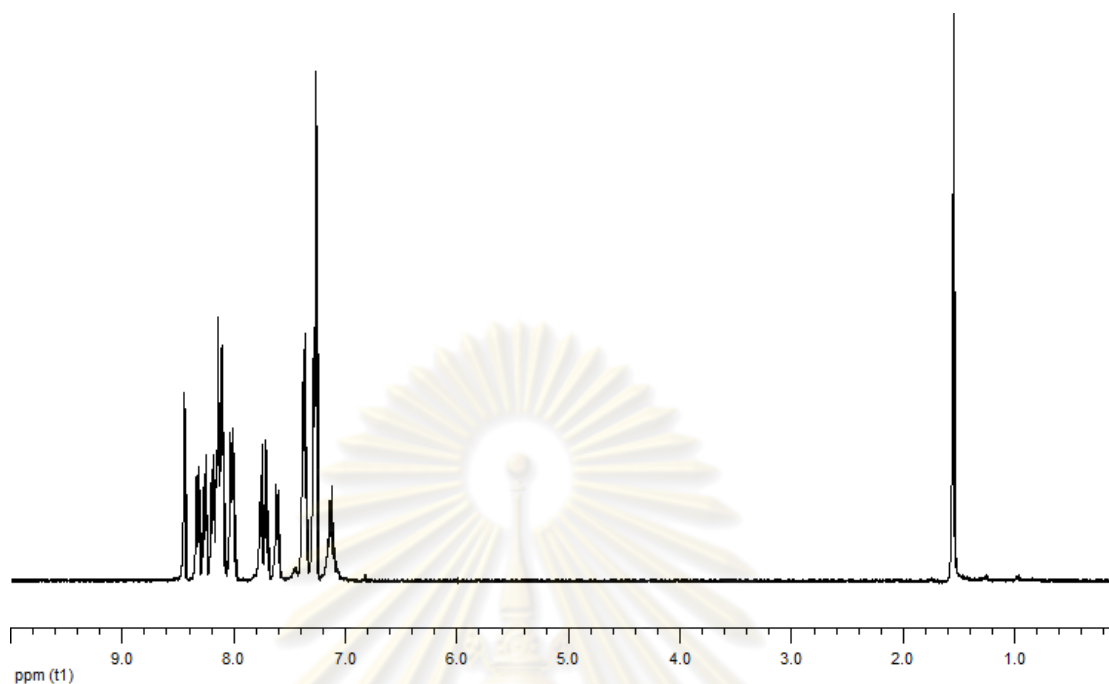
Figure 21 ^{1}H-NMR spectrum of 4-(3,6-di(pyren-1-yl)-9*H*-carbazol-9-yl)-*N,N*-diphenylaniline **(2PCP)**
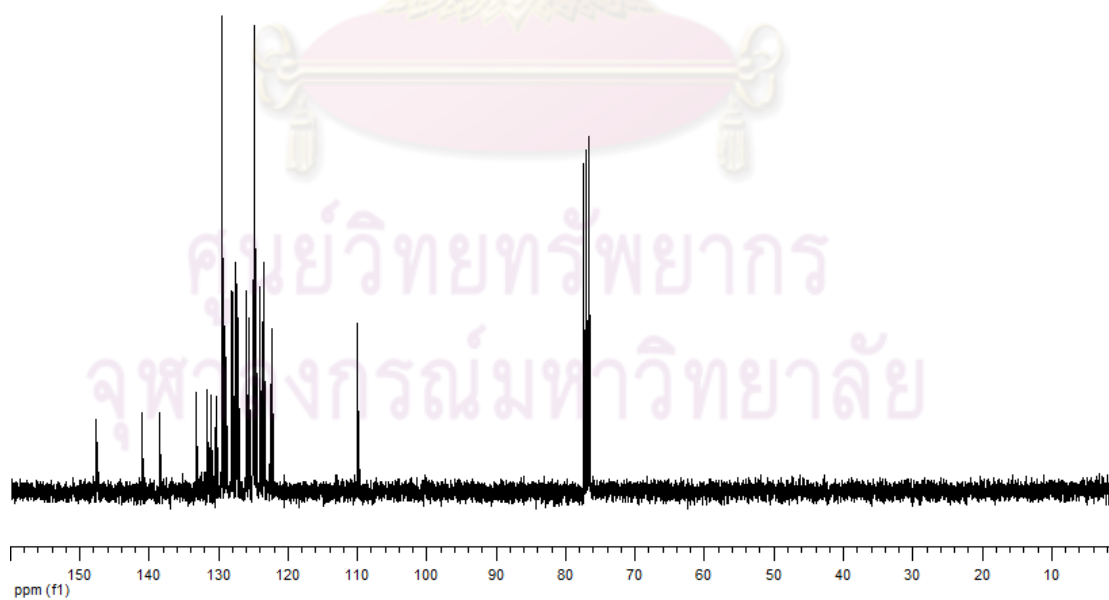

Figure 22 ^{13}C-NMR spectrum of 4-(3,6-di(pyren-1-yl)-9*H*-carbazol-9-yl)-*N,N*-diphenylaniline **(2PCP)**
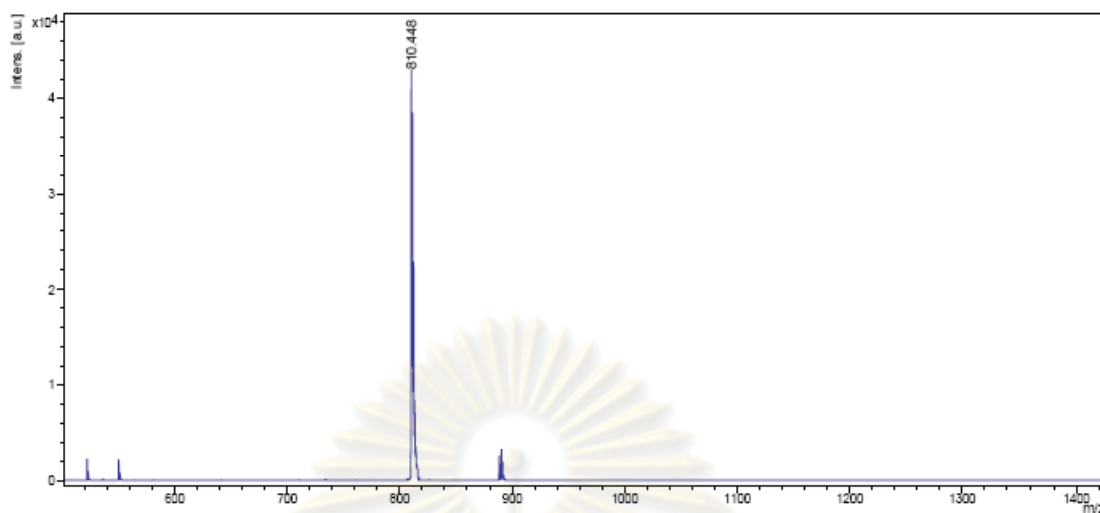
Figure 23 Mass spectrum of 4-(3,6-di(pyren-1-yl)-9*H*-carbazol-9-yl)-*N,N*-diphenylaniline **(2PCP)**

Figure 24 Elemental analysis data of 4-(3,6-di(pyren-1-yl)-9*H*-carbazol-9-yl)-*N,N*-diphenylaniline **(2PCP)**

VITAE

Mr. Trakool Kumchoo was born on May 29, 1982 in Uttaradit, Thailand. He got a Bachelor's Degree of Science in Chemistry from Chiang Mai University in 2004. He was working at Union frozen product company and Sunco and Riotex polymer company. After that, he started his a Master's Degree in Petrochemistry and Polymer Science program at Chulalongkorn University. During he had presented "Synthesis of novel luminescent starburst compounds containing pyrene and carbazole" in Pure and Applied Chemistry International Conference (PACCON 2009), "Synthesis of blue light –emitting dipyrenyl carbazole derivatives" in 6th International Symposium on Advance Material in Asia-Pacific Rim (6th ISAMAP) by poster presentation and "Synthesis of blue light-emitting dipyrenyl carbazole derivatives" in Pure and Applied Chemistry International Conference (PACCON 2010) by oral presentation.

His address is 99 Moo 5, Soi 5, Srichaowang Road, Muang, Uttaradit, 53000 Thailand, Tel. 089-7723329.